Electronic Supporting Information (ESI)

C-H Amidation and Amination of Arenes and Heteroarenes with Amide and Amine using Cu-MnO as a Reusable Catalyst under Mild Condition

Harshvardhan Singh, Chiranjit Sen, Eringathodi Suresh, Asit B. Panda and Subhash C. Ghosh**

Central Salt and Marine Chemicals Research Institute (CSIR-CSMCRI), G.B. Marg, Bhavnagar 364002, Gujarat, India, and Academy of Scientific and Innovative Research (AcSIR), Ghaziabad 201002. E-mail: scghosh@csmcri.res.in

Contents

1. Synthesis and Characterization results of Cu-MnO catalysts:

The catalyst was synthesized based on ethylene glycol mediated preparation of Mn-carbonate precursor followed by calcination to MnO_2. Then, the Cu-MnO catalyst was synthesized through impregnation of Cu on MnO_2 by deposition precipitation method using Cu-acetate followed by calcination under 5%H_2 in N_2 flow at 350ºC/6h in. XRD pattern of the synthesized 5%Cu-MnO catalyst evidenced the presence of distinct diffraction peaks, ascribed to the face-centered cubic MnO phase (manganosite, JCPDS Card 00-075-1090). In addition to the intense peaks, the very low intense peak at $2\theta = 43.7°$ was also observed. The low intense peal is attributed to the (111) plane of cubic metallic Cu. Thus, the XRD results imply the reduction of Mn^{4+} to Mn^{2+} and Cu^{2+} to Cu^0 during calcination in 5%H_2 in N_2, a reducing environment. Large area SEM image evidenced the formation of quite uniform spherical morphology. Corresponding high-magnified image evidenced that the individual spheres are made of individual small particles. Respective low magnified TEM images also evidenced the presence of spherical microstructures made of very small particles. TEM image also evidenced that the formed spheres are porous. Respective magnified images showed the presence of nanoparticles with a size range of 15-20 nm and the pores are nothing but the inter-particle pores. HRTEM image indicates the presence of distinct fringes with inter planer distance of 0.26 nm, corresponds to the (111) plane of face-centred cubic MnO (JCPDS Card 00-075-1090). In the HRTEM image some odd lattice fringe (other than 0.26 nm) was observed in the wall of larger particle. Detailed investigation explores the inter-planer distance is 0.21 nm, corresponds to the (001) plane of cubic metallic copper. Thus, TEM image confirmed the formation of highly crystalline 15-20 nm MnO with very small Cu nanoparticle on the surface. Elemental mapping

of the synthesized catalyst evidenced uniform

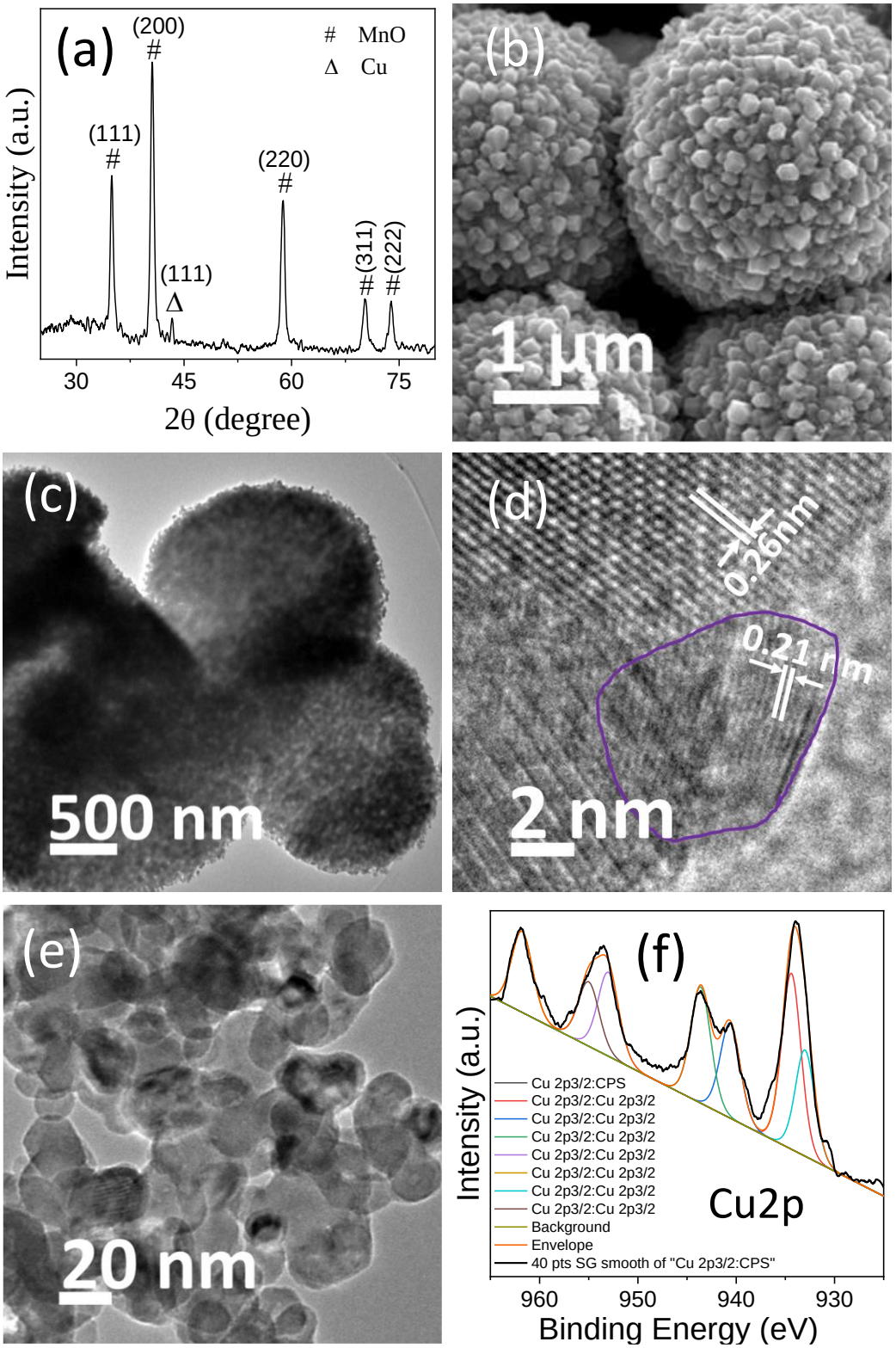

Figure S1: (a) XRD pattern of synthesized Cu-MnO, (b) SEM, (c) TEM, (d-e) HRTEM images of Cu-MnO catalyst, and (f) core level Cu2p XPS distribution of Cu on MnO spheres.

A detailed elemental state was further investigated by X-ray photoelectron (XPS) analysis. The survey spectrum evidenced the presence of both Mn and Cu. Best Gaussian fitted Cu2p spectrum evidenced presence of distinguishable several peaks in the region of 925– 970 eV. Among these identifiable peaks, the peaks at 930.7 and 951.6 eV is recognized as either Cu0 or Cu1+. However, the presence of a distinct Cu-LMM signal at 568.2 eV confirmed that both the mentioned peaks at 930.7 and 951.6 eV are for Cu0. Another set of peaks at 933.06 and 953.3 eV along with spin splitting peak at 961.11 eV can be recognized to Cu2+. Two satellite peaks of Cu at has also been observed in 938–945 eV region. Two peaks at 640.3 eV and 651.9 eV having energy gap of 11.6 eV for Mn 2p and peaks at 81.82 and 88.20 eV with energy gap of 6.3 eV also confirmed the presence of Mn2+. Thus, catalyst characterization results confirmed the formation of porous MnO spheres having uniformly dispersed Cu0 and Cu2+ species.

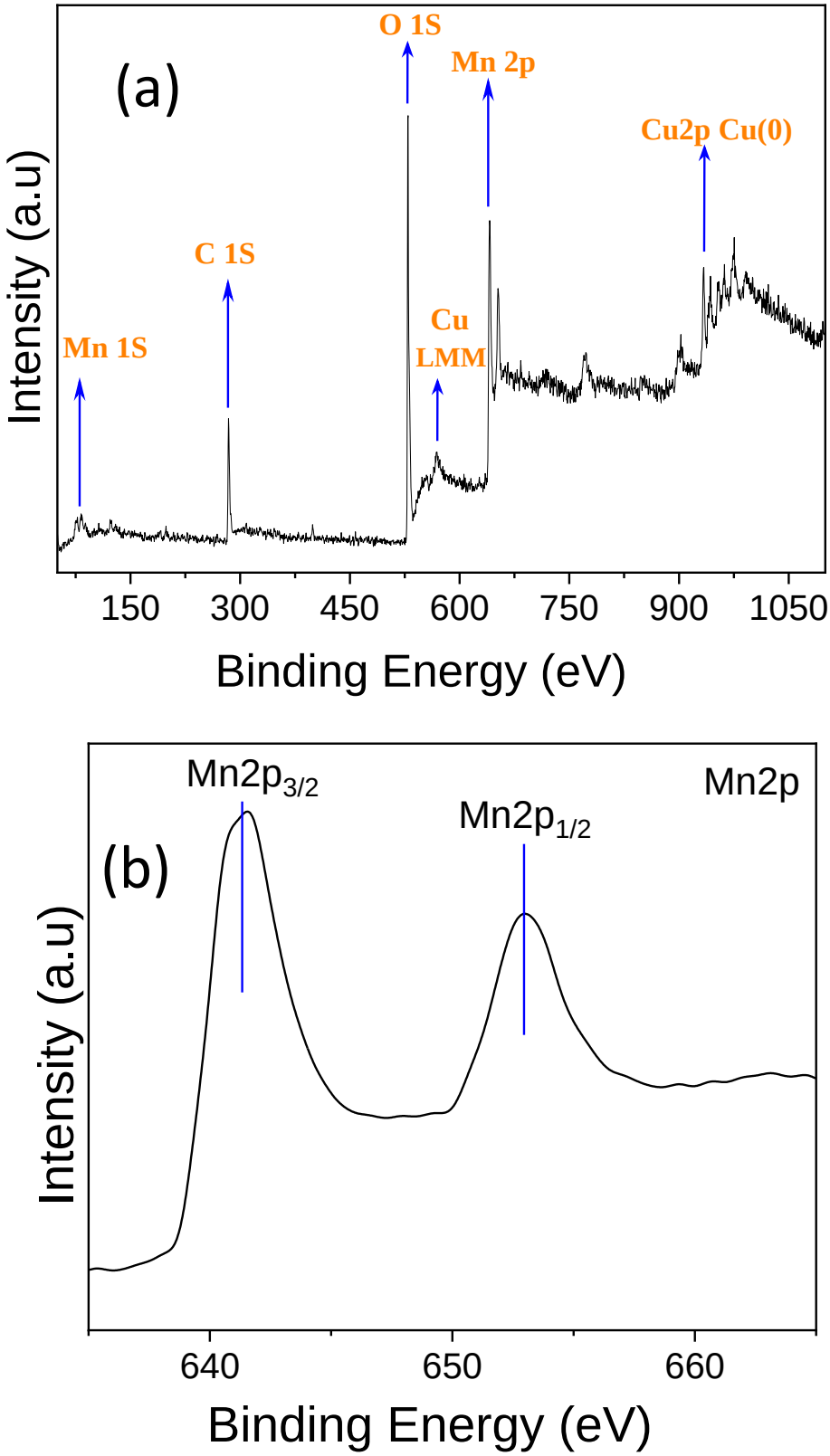

Figure S2: XPS spectra of 5% Cu-MnO

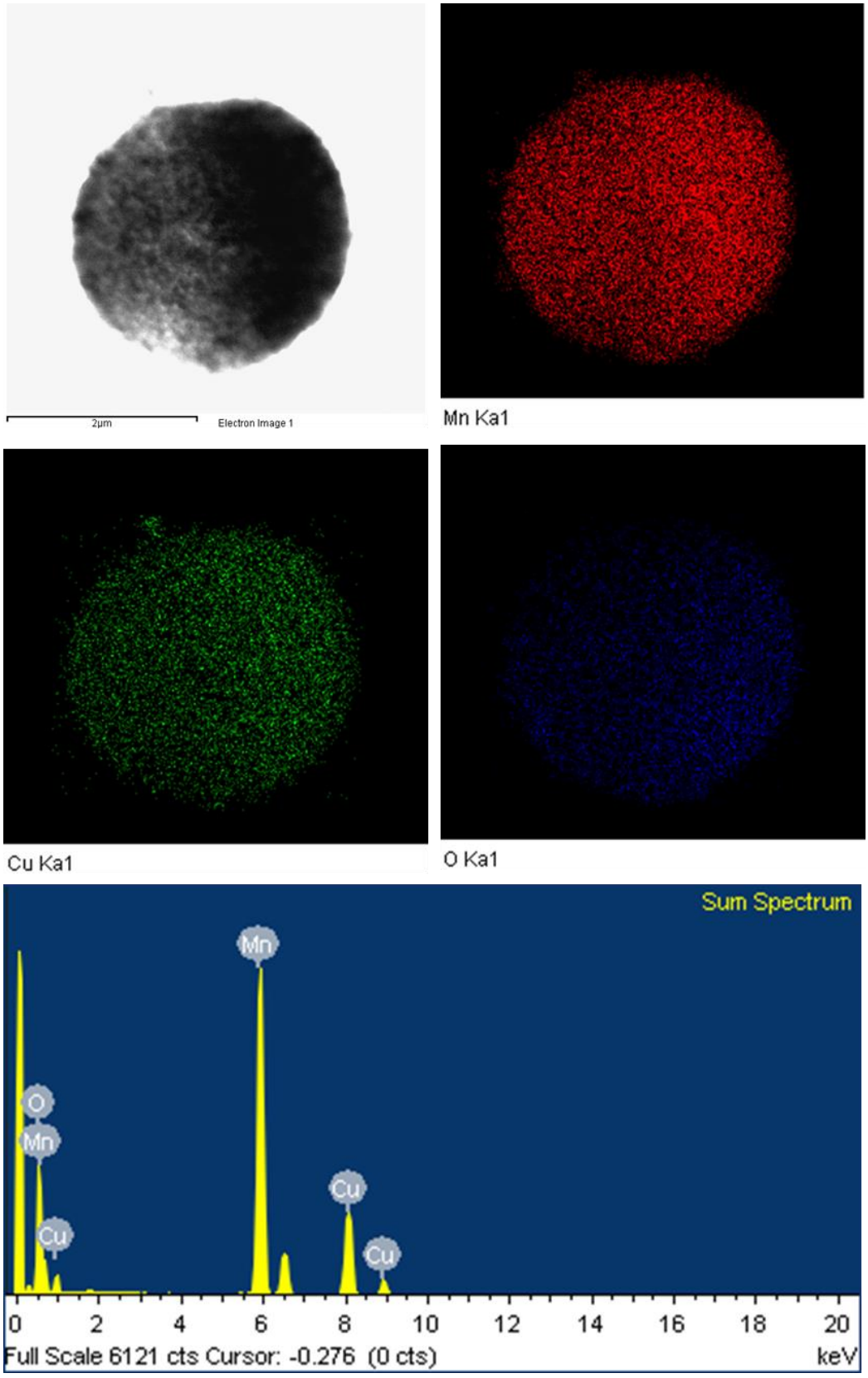

Figure S3: EDS SEM images of the synthesized 5% Cu-MnO catalyst, showed the homogeneous distribution of Copper on the manganese oxide surface

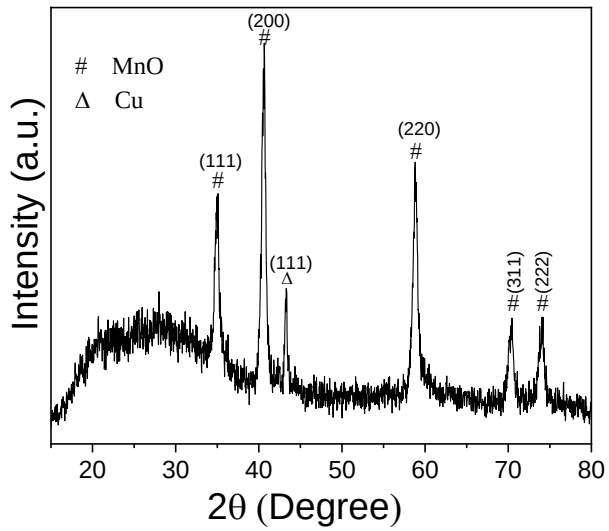

Figure S4: XRD pattern of re-used catalyst evidenced that no distinct change in the crystal structure of MnO took place. However, the peak intensity of Cu was increased, most probably due to the particle growth of metallic Cu during cycling. The broad hump in the 2θ range of 20-30 due to the adsorbed carbonaceous organic substrates.

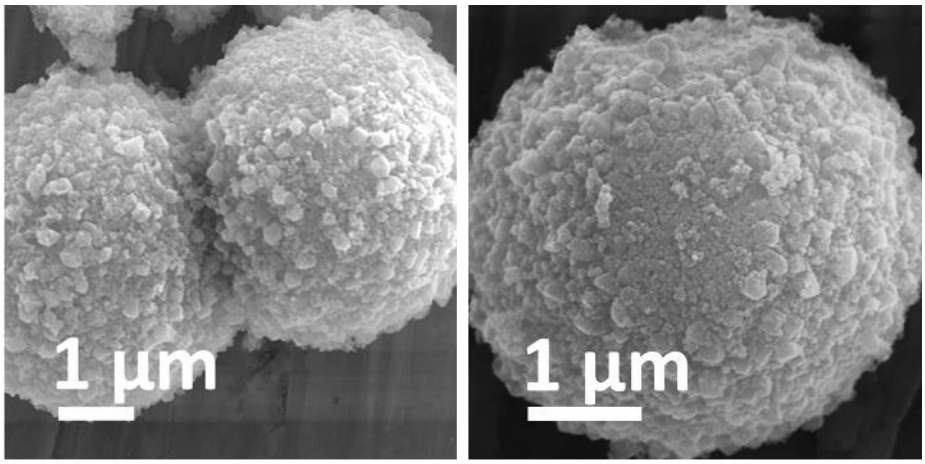

Figure S5: SEM images of the reused catalyst

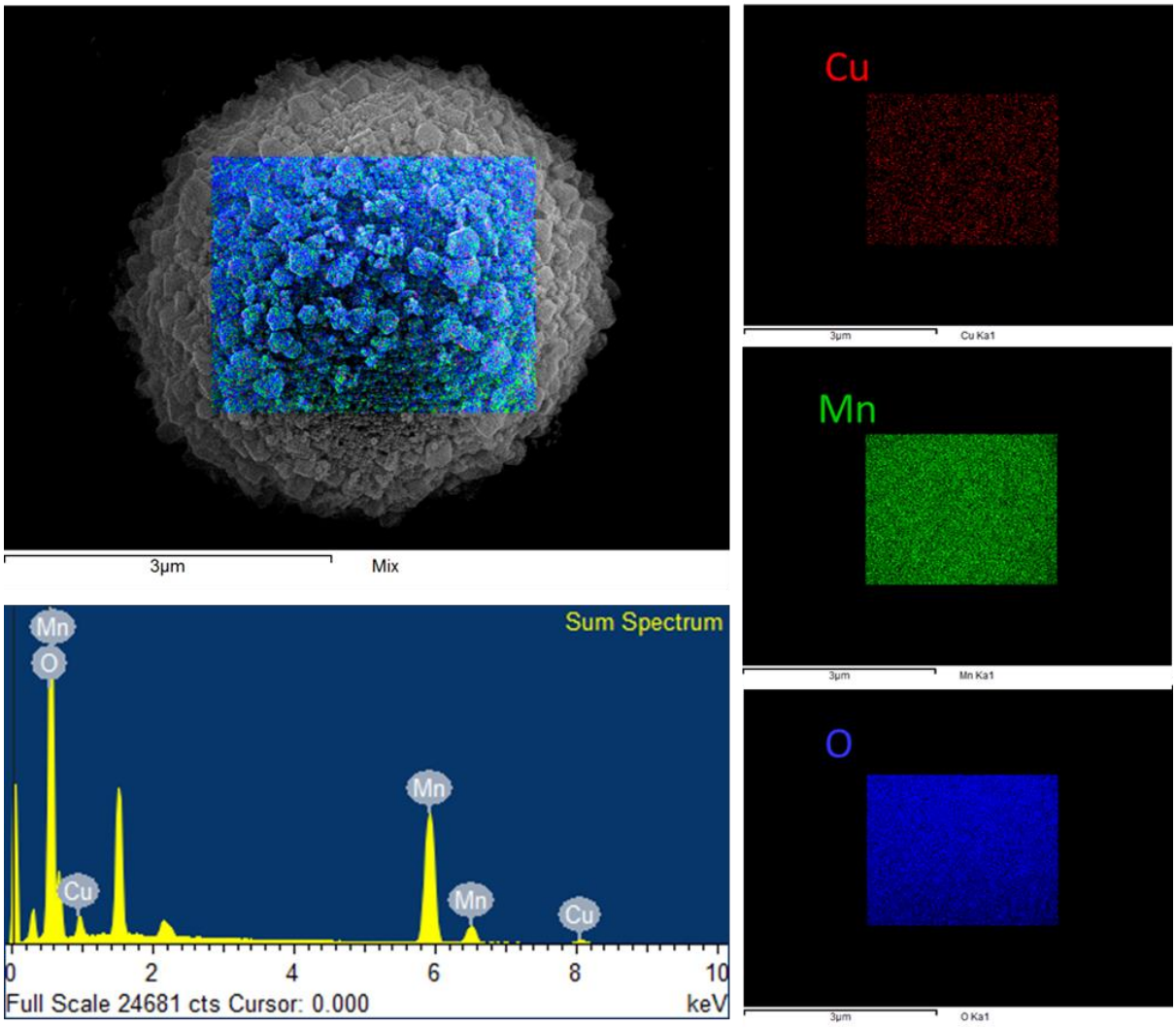

Figure S6: EDS SEM images of the reused 5% Cu-MnO catalyst, showed homogeneous distribution of Copper on manganese oxide surface after the reaction

2. KIE experiments

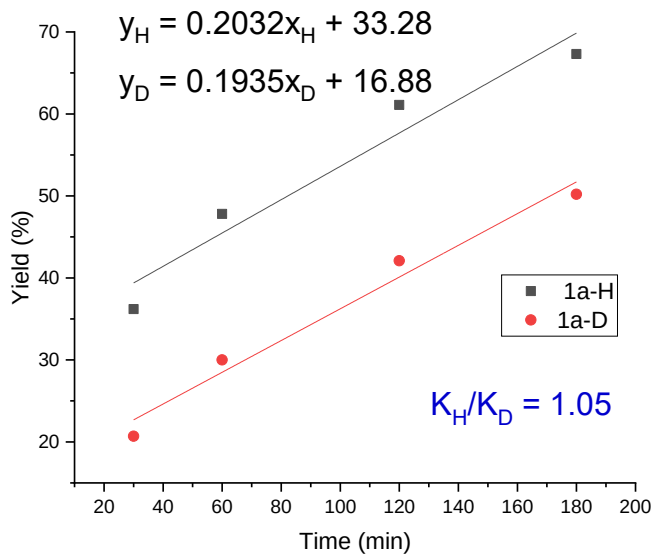

Figure S7. Determination of KIE by independent parallel experiments with **1a** and deuterated **1a**

Table S1: Reaction optimization

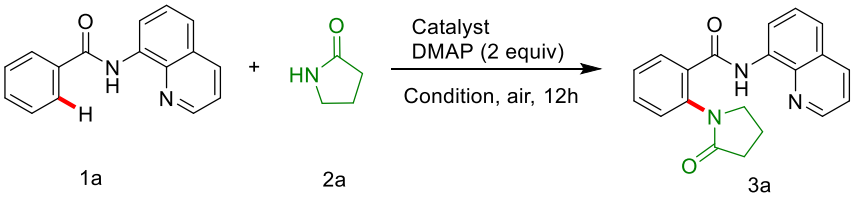

Entry	Catalyst	Base	Solvent	Temp. (°C)	Yield (%)[b]
1	5%CuMnO	DMAP	DMSO	120	94
2	5%CuMnO	DMAP	DMSO	120	48[c]
3	5%CuMnO	K_2CO_3	DMSO	120	35
4	5%CuMnO	Na_2CO_3	DMSO	120	45
5	5%CuMnO	Et_3N	DMSO	120	38

[a]reaction conditions: 1a (0.2 mmol), 2a (0.3 mmol, 1.5 equiv), Cu-MnO catalyst 25 mg (7.8 mol% Cu), DMAP (2 equiv.), in 1 mL solvent, air, at 120 °C for 12h; [b]isolated yield; [c] under N_2 atmosphere

3. ^{1}H and ^{13}C NMR spectral copies of amidation and amination:

2-(2-oxopyrrodin-1-yl)-N-(quinoline-8-yl)benzamide (3a):

^{1}H NMR (600 MHz, $CDCl_3$)

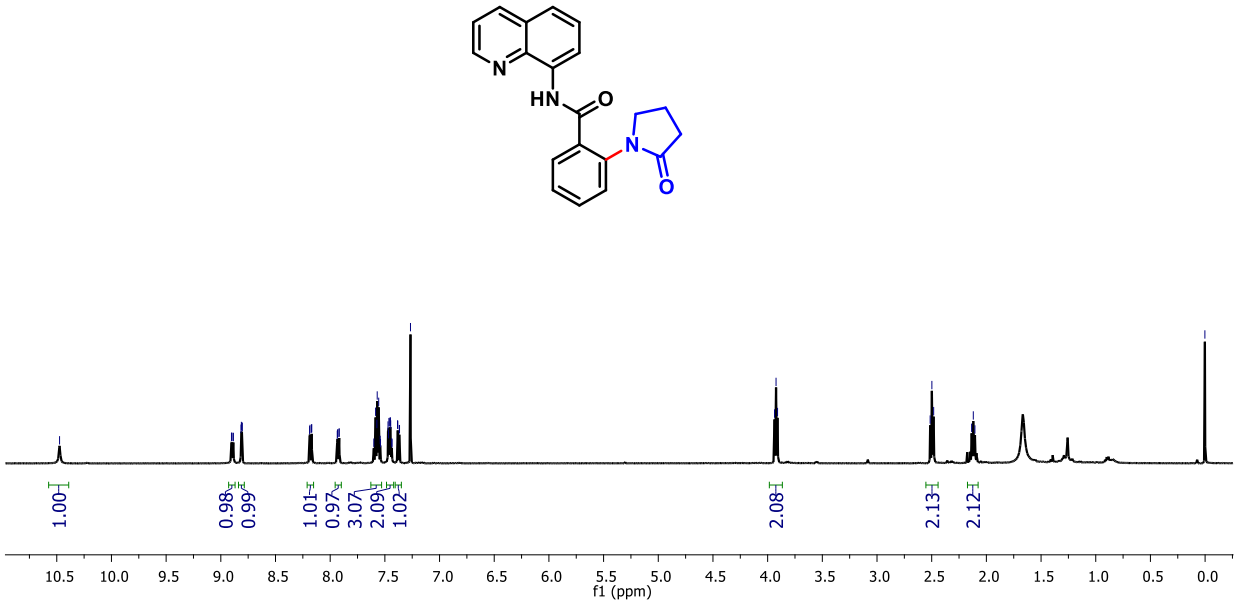

^{13}C{^{1}H} NMR (151 MHz, $CDCl_3$)

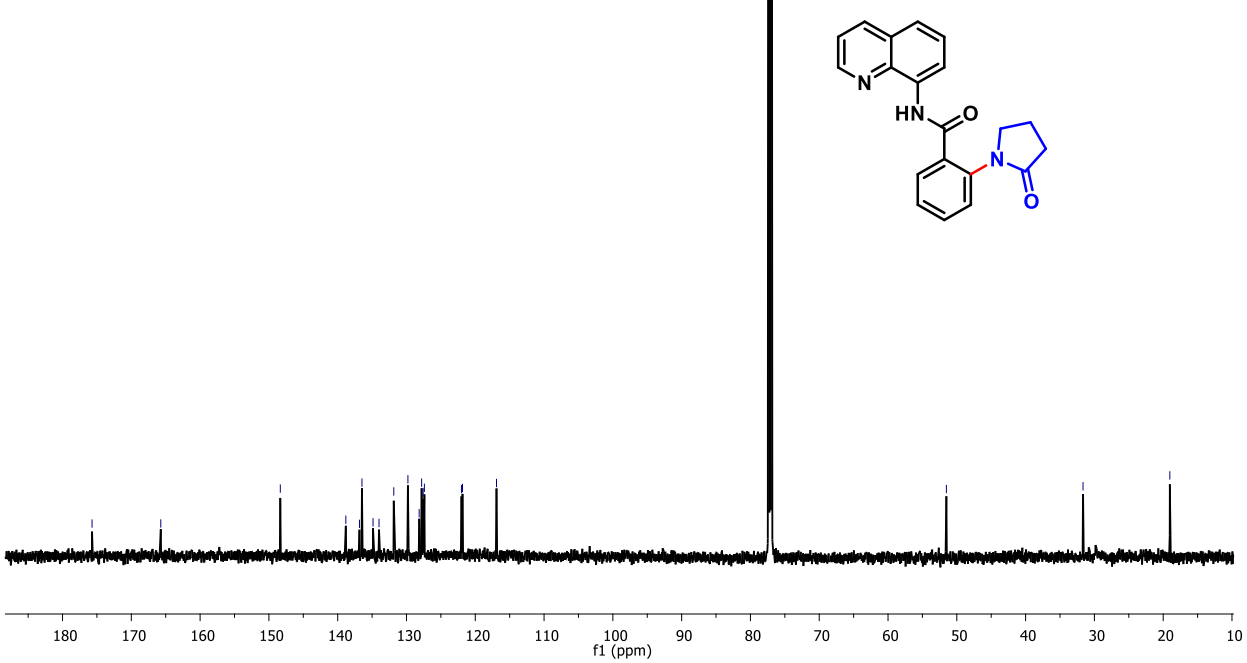

4-methoxy-2-(2-oxopyrrolidin91-yl)-N-(quinoline-8-yl)benzamide (3b):

^{1}H NMR (500 MHz, $CDCl_3$)

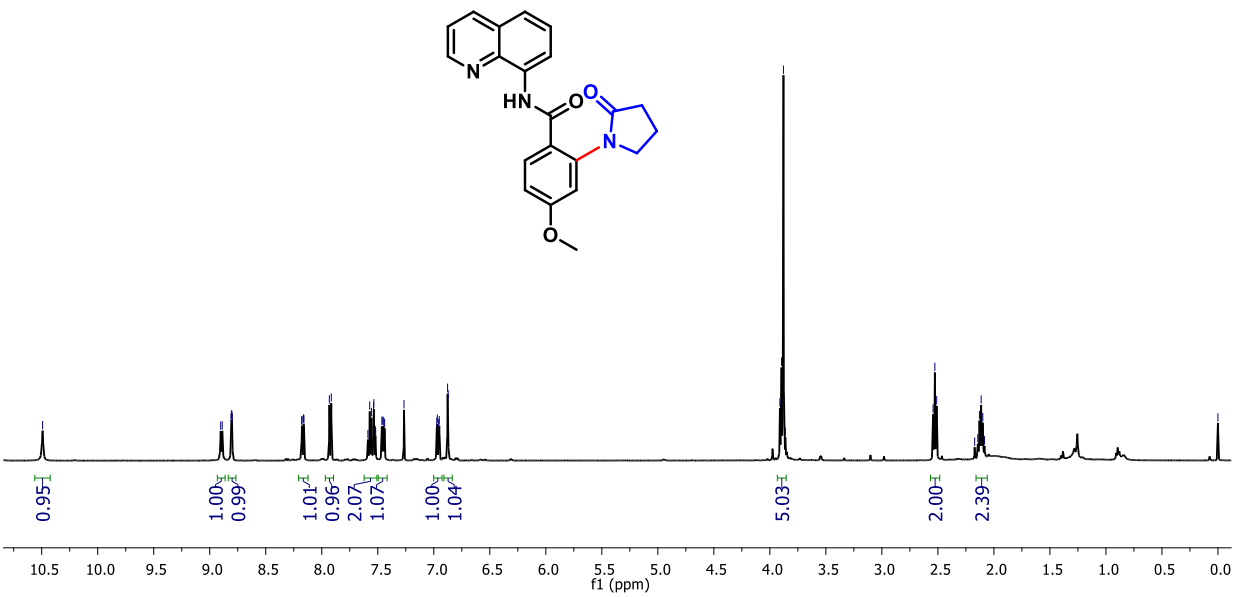

^{13}C{^{1}H} NMR (126 MHz, $CDCl_3$)

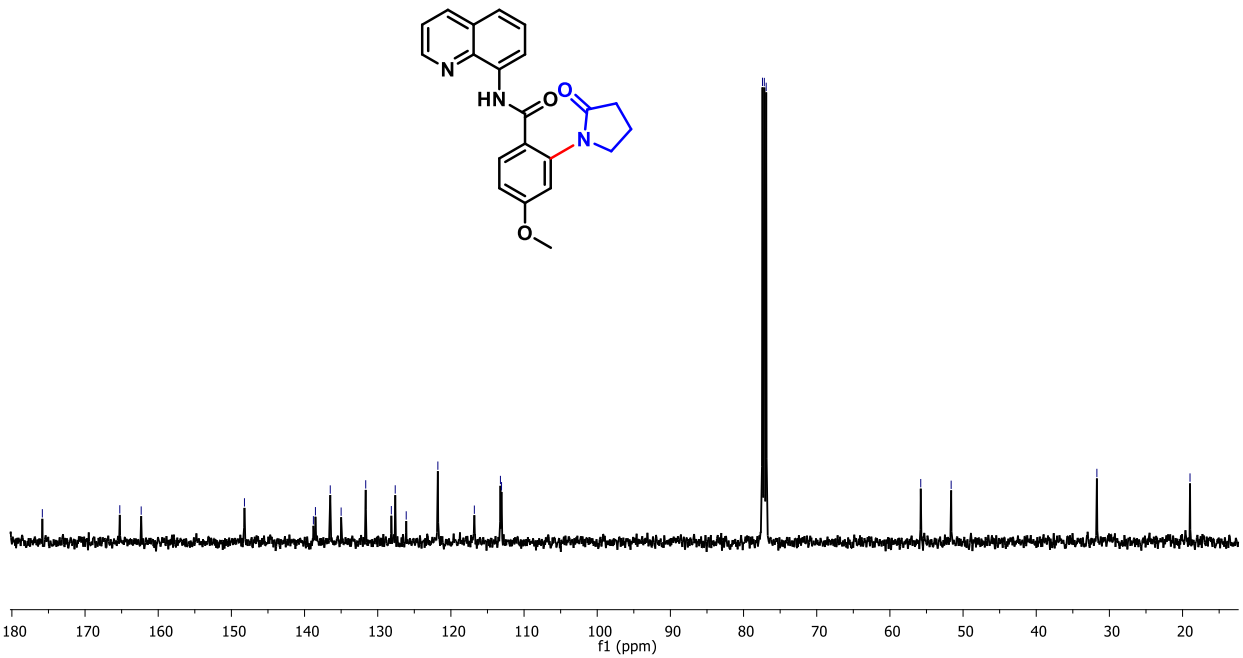

2-(2-oxopyrrodin-1-yl)-N-(quinoline-8-yl)-4-(trifluoromethyl)benzamide (3c):

^{1}H NMR (600 MHz, $CDCl_3$)

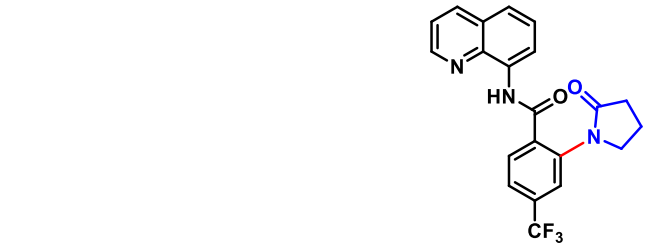

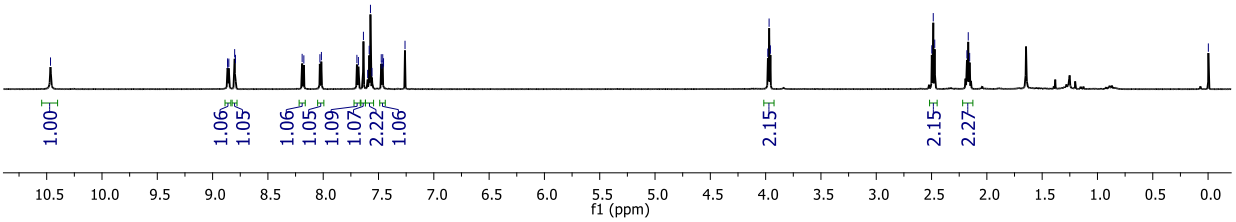

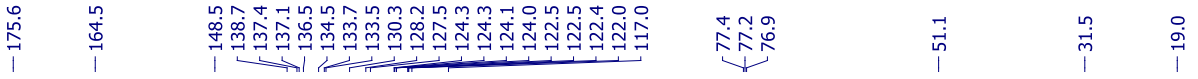

^{13}C{^{1}H} NMR (151 MHz, $CDCl_3$)

^{19}F NMR (565 MHz, $CDCl_3$)

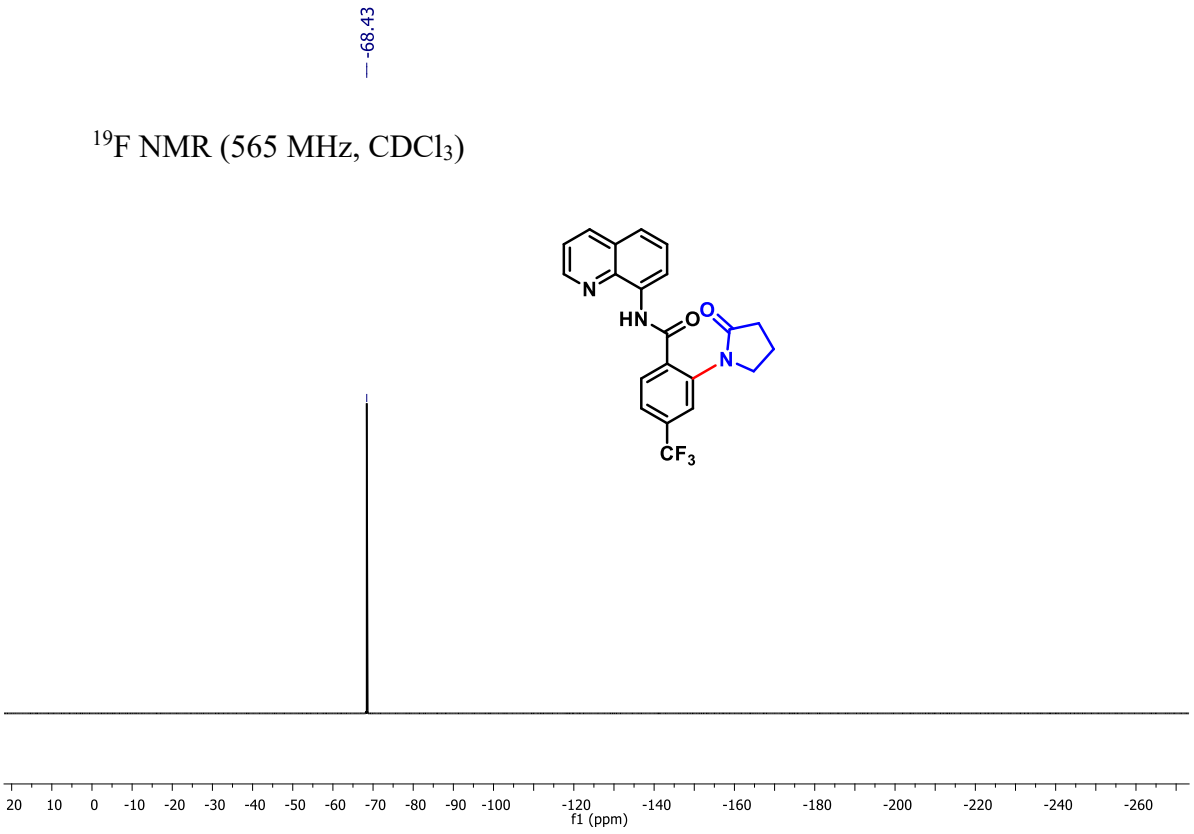

4-Iodo-6-(2-oxopyrrodin-1-yl)-N-(quinoline-8-yl)benzamide (3d):

^{1}H NMR (600 MHz, $CDCl_3$)

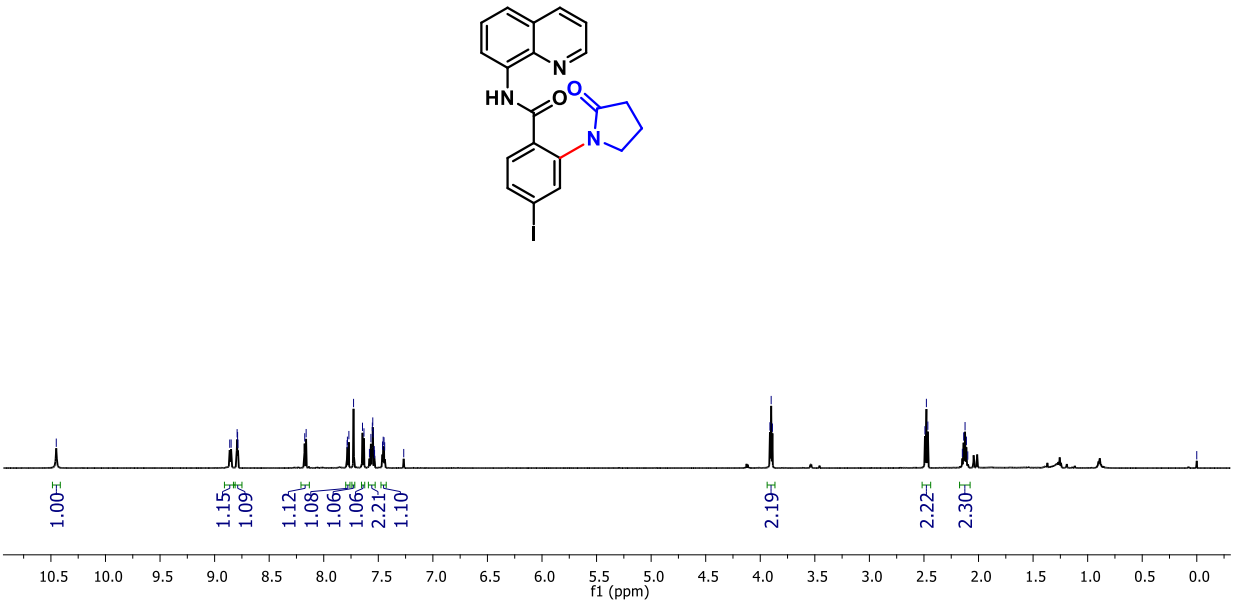

^{13}C{^{1}H} NMR (151 MHz, $CDCl_3$)

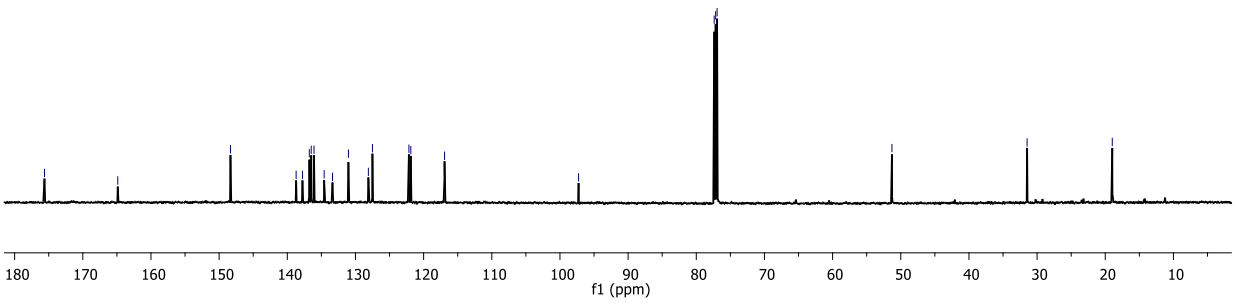

5-methyl-2-(2-oxopyrrodin-1-yl)-N-(quinoline-8-yl)benzamide (3e):

^{1}H NMR (500 MHz, $CDCl_3$)

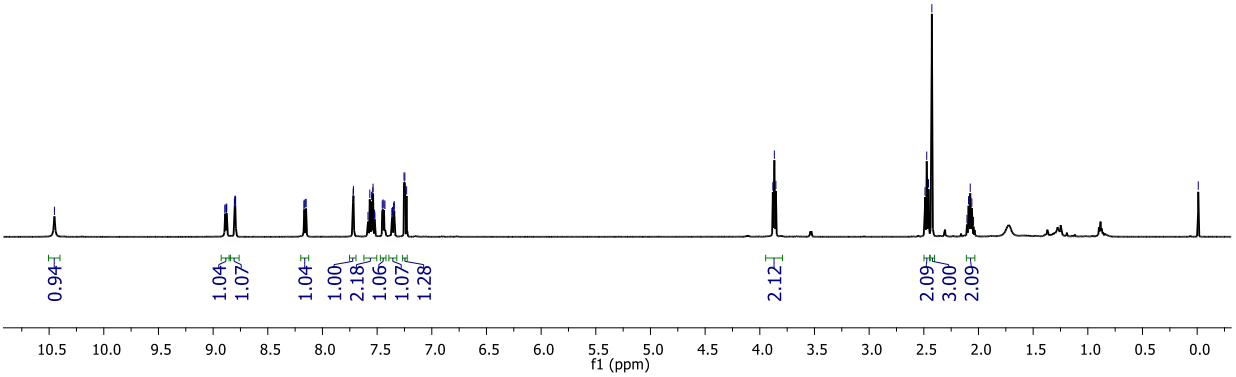

^{13}C{^{1}H} NMR (126 MHz, $CDCl_3$)

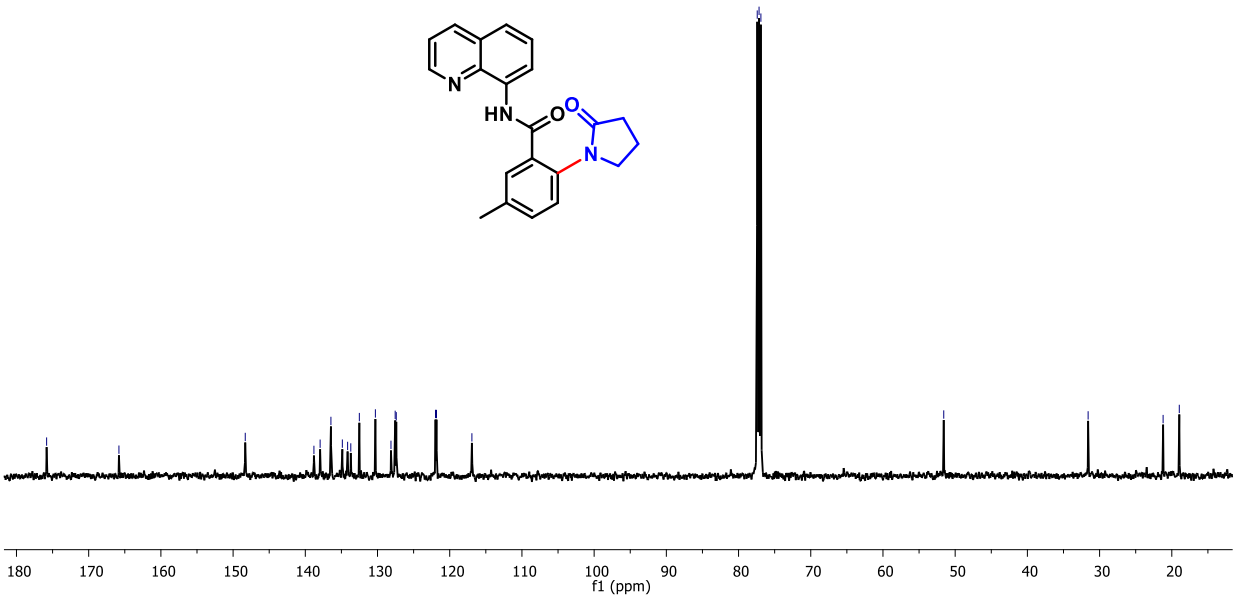

2-fluoro-6-(2-oxopyrrodin-1-yl)-N-(quinoline-8-yl)benzamide (3f):

^{1}H NMR (600 MHz, $CDCl_3$)

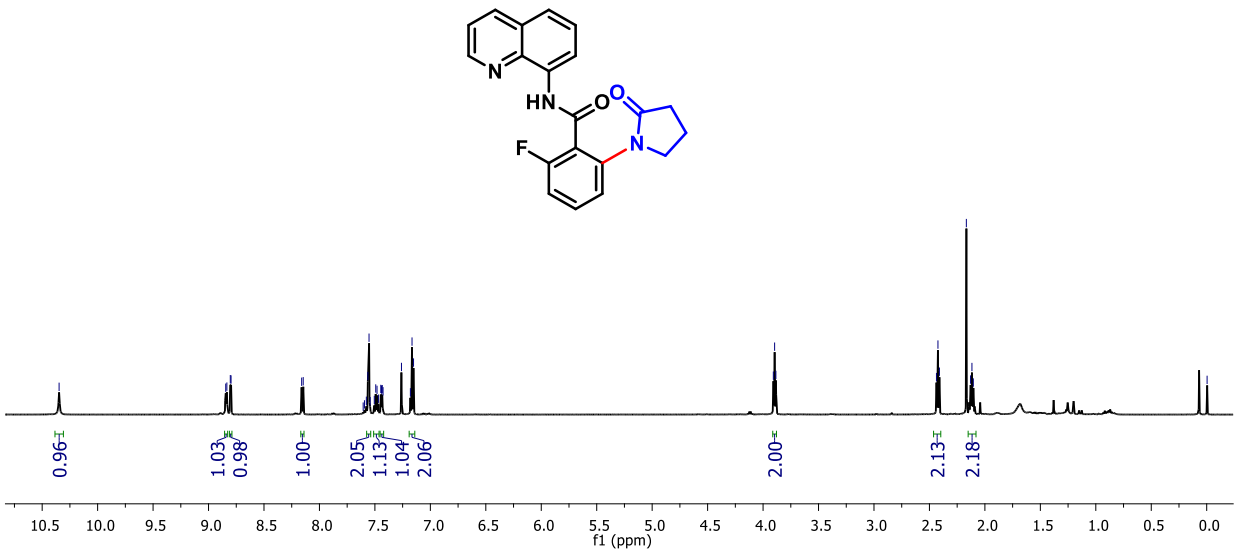

^{13}C{^{1}H} NMR (151 MHz, $CDCl_3$)

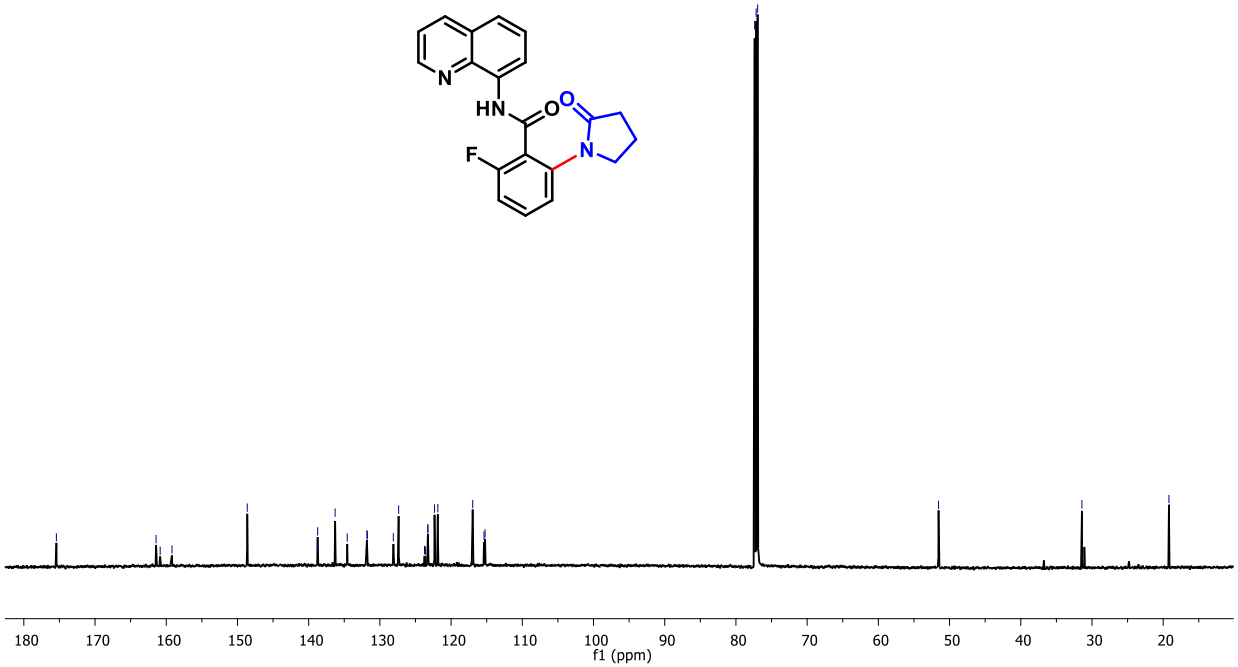

^{19}F NMR (565 MHz, $CDCl_3$)

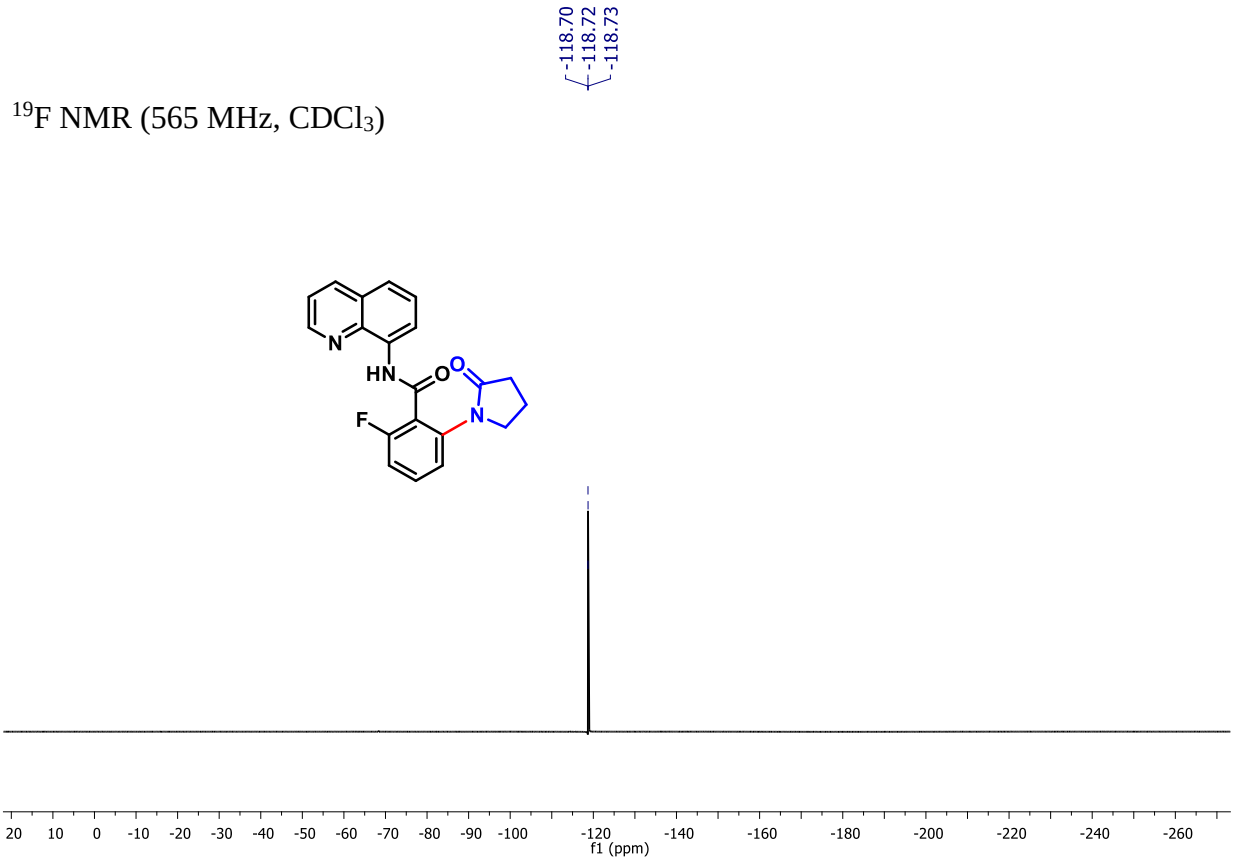

N-(2-methylquinoline-8-yl)-2-(2-oxopyrrodin-1-yl)benzamide (3g):

^{1}H NMR (600 MHz, $CDCl_3$)

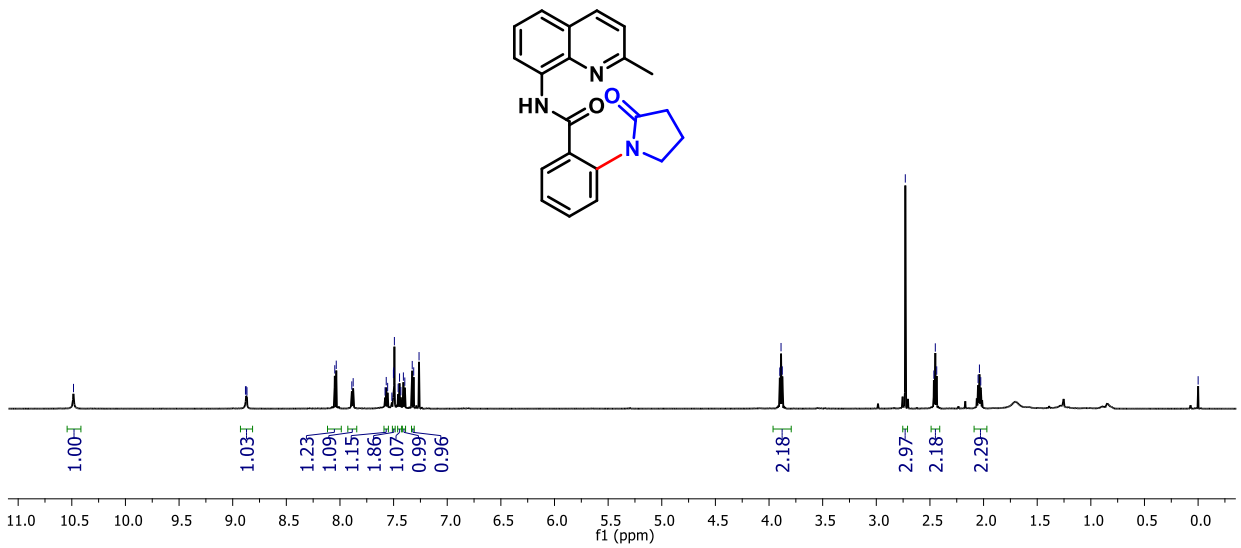

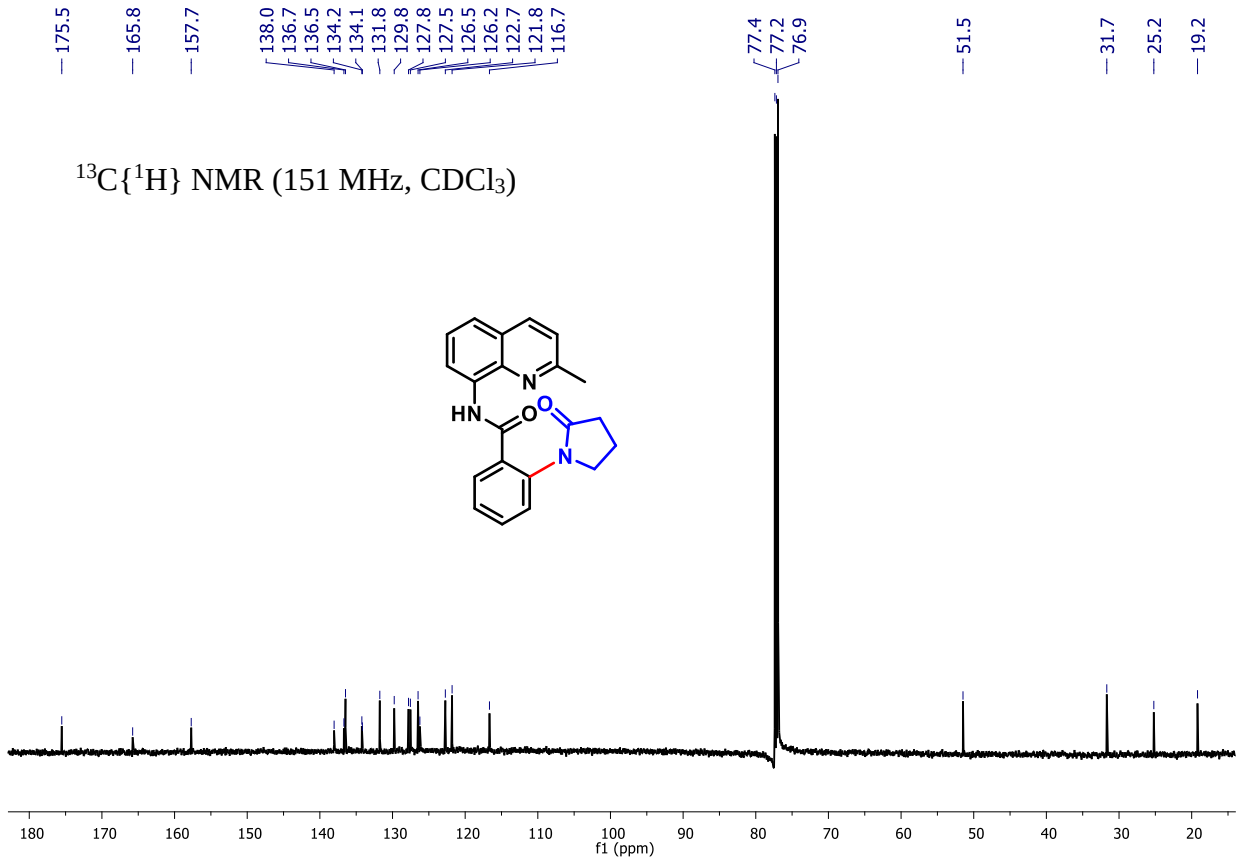

^{13}C{^{1}H} NMR (151 MHz, $CDCl_3$)

N-(5-chloroquinoline-8-yl)-2-(2-oxopyrrodin-1-yl)benzamide (3h):

^{1}H NMR (600 MHz, $CDCl_3$)

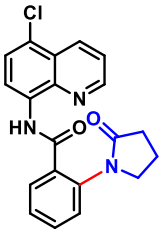

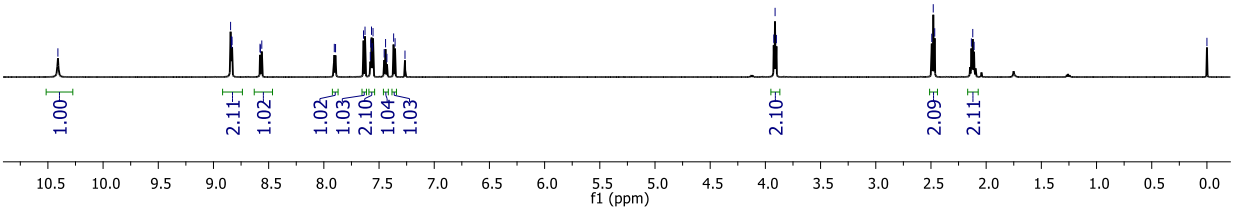

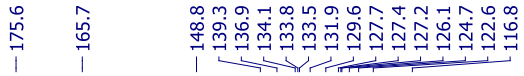

^{13}C{^{1}H} NMR (151 MHz, $CDCl_3$)

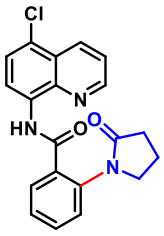

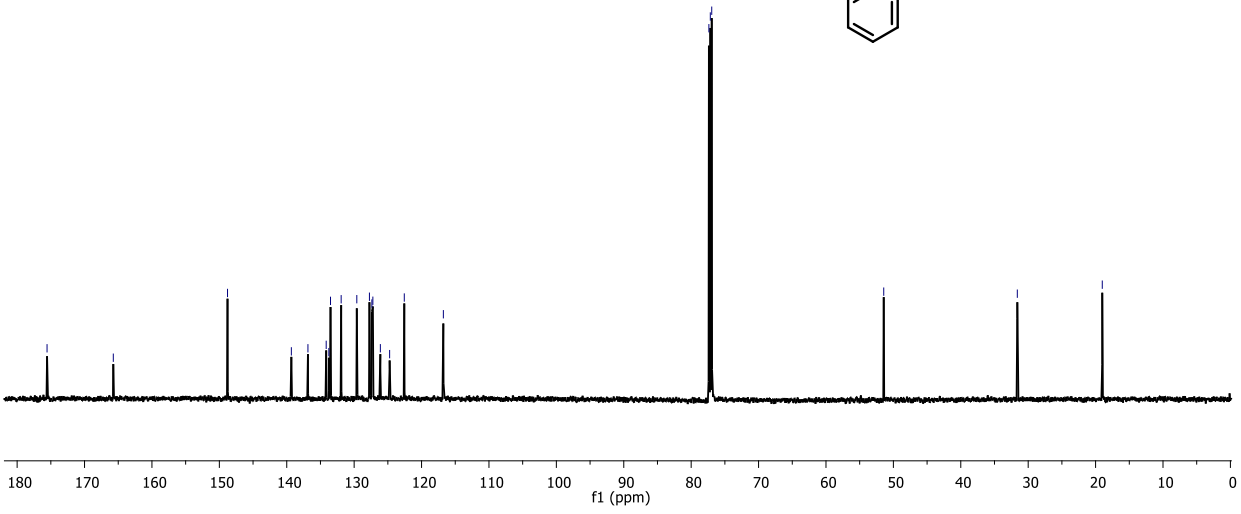

N-(6-methoxyquinolin-8-yl)-2-(2-oxopyrrolidin-1-yl-)benzamide (3i):

^{1}H NMR (500 MHz, $CDCl_3$)

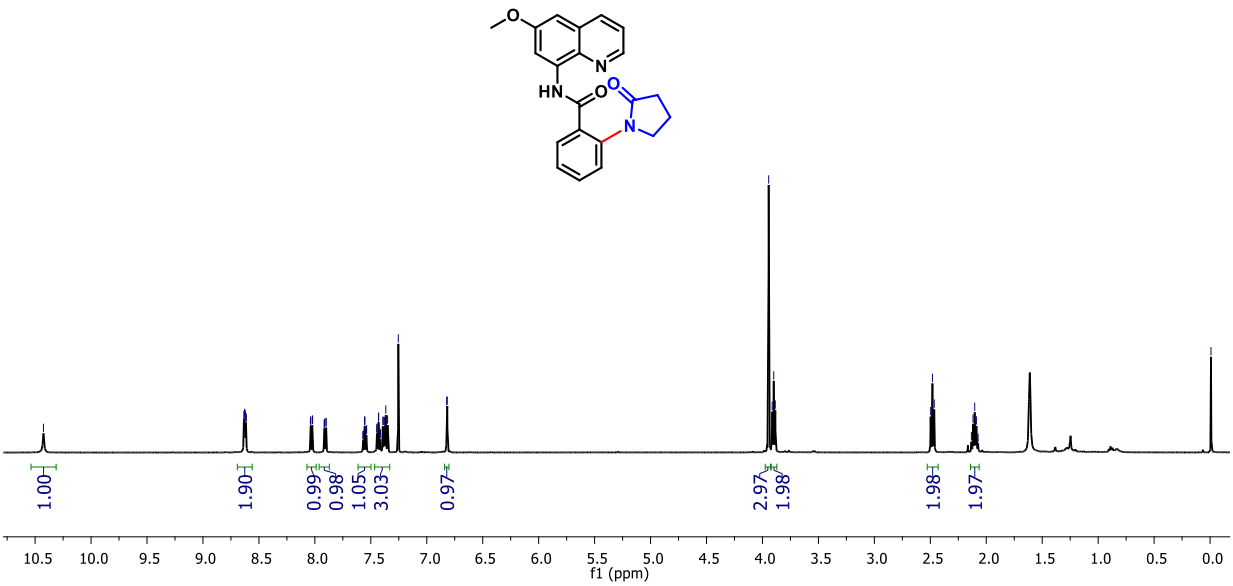

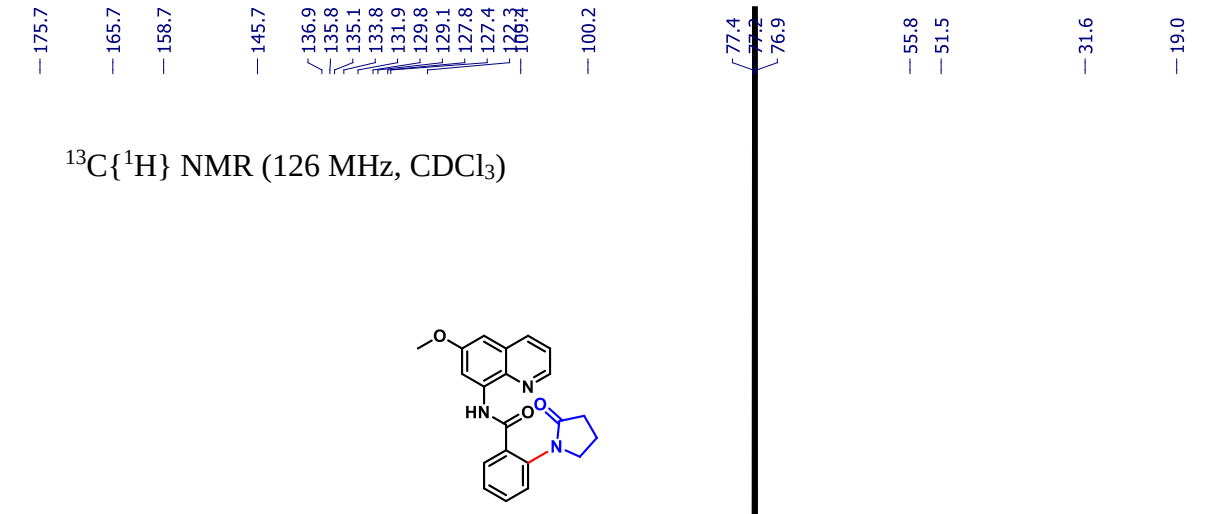

^{13}C{^{1}H} NMR (126 MHz, $CDCl_3$)

2-fluoro-6-(2-oxopyrrodin-1-yl)-N-(quinoline-8-yl)benzamide (3j):

^{1}H NMR (600 MHz, $CDCl_3$)

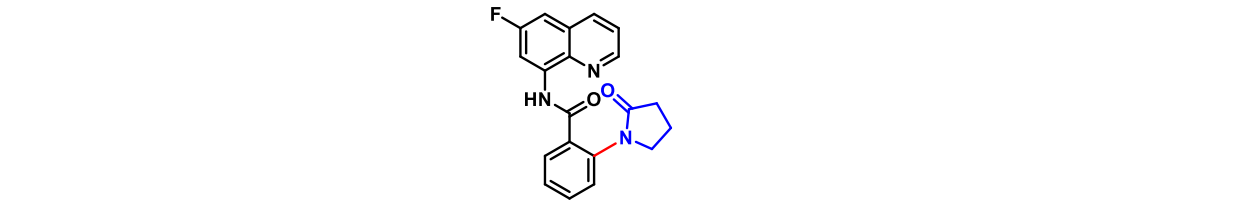

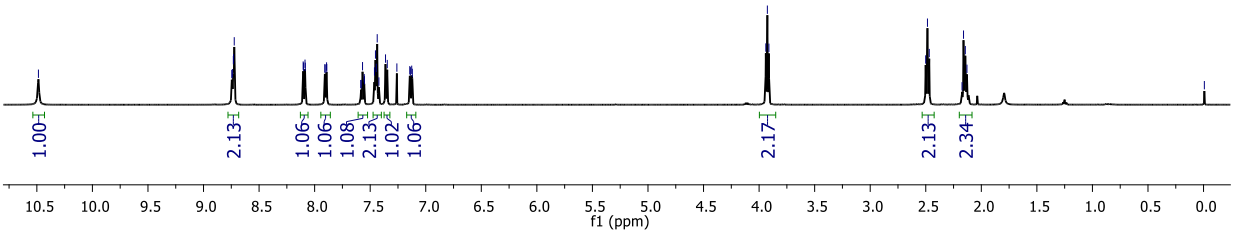

^{13}C{^{1}H} NMR (151 MHz, $CDCl_3$)

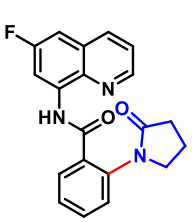

-114.79
-114.81
-114.82

^{19}F NMR (565 MHz, $CDCl_3$)

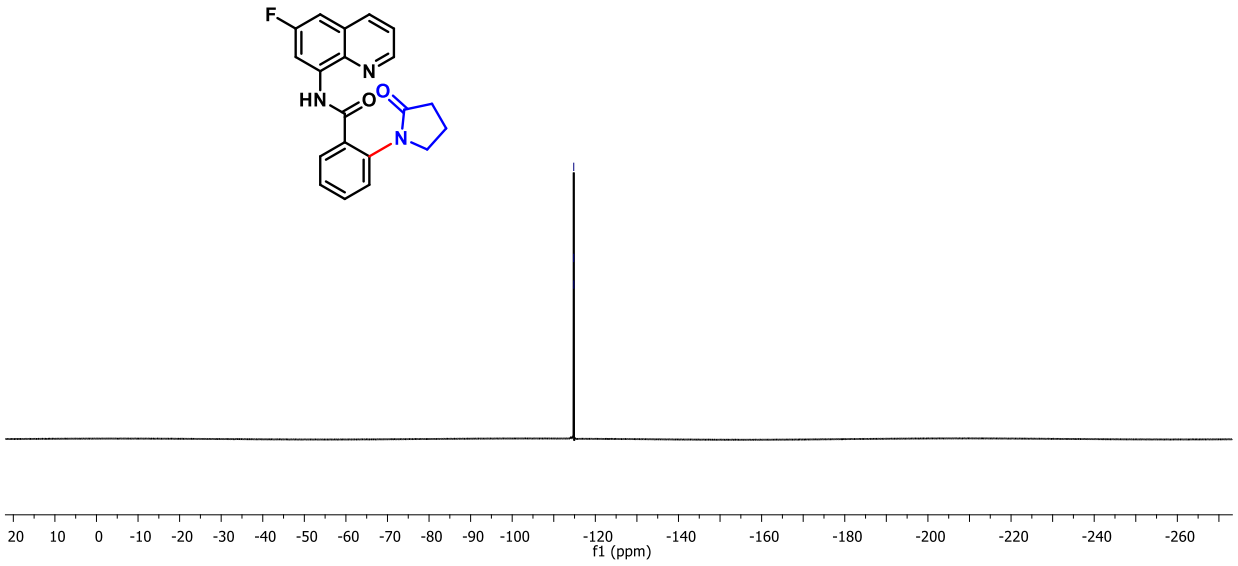

2-(2-oxopyrrodin-1-yl)-N-(quinoline-8-yl)-1naphthamide (3k):

^{1}H NMR (500 MHz, $CDCl_3$)

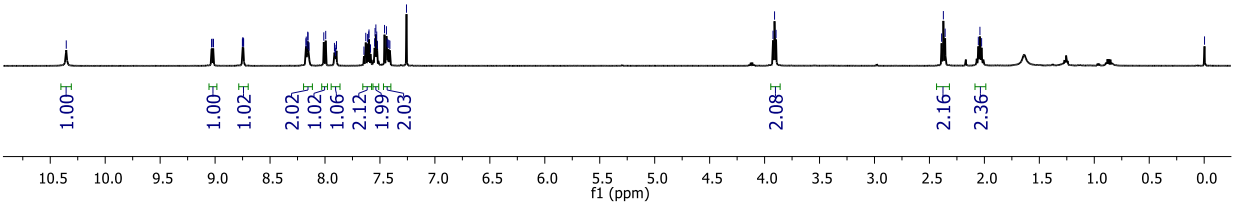

^{13}C{^{1}H} NMR (126 MHz, $CDCl_3$)

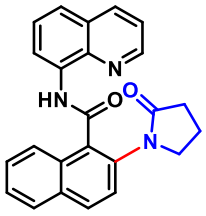

2-(2-oxopiperidin-1-yl)-N-(quinoline-8-yl)benzamide (3l):

^{1}H NMR (500 MHz, $CDCl_3$)

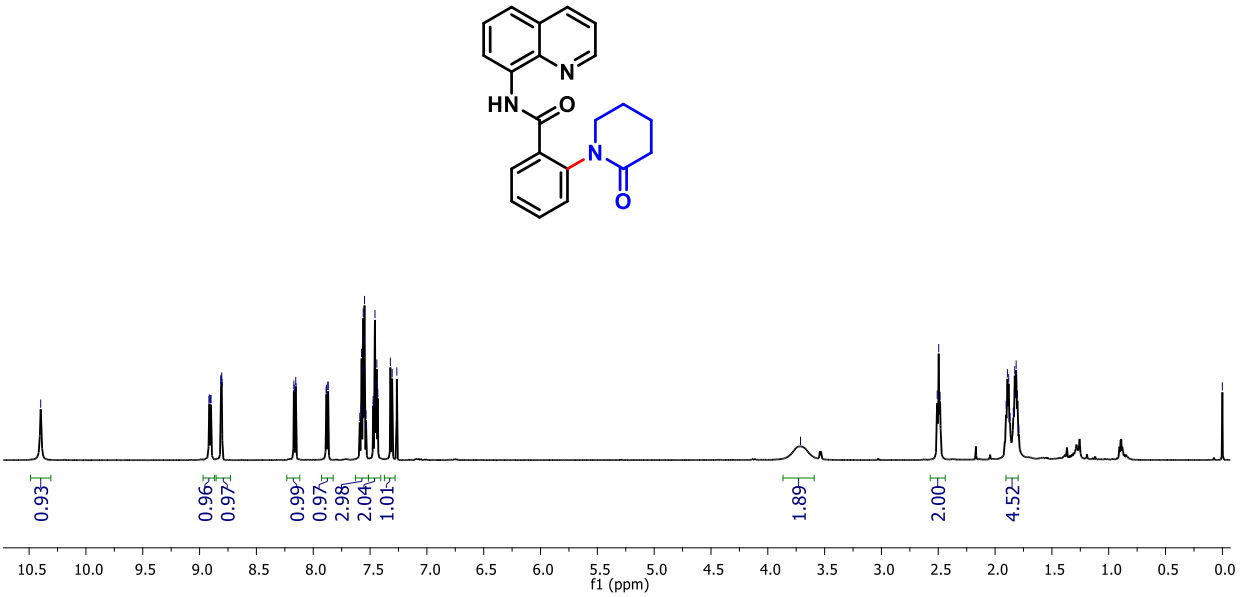

^{13}C{^{1}H} NMR (126 MHz, $CDCl_3$)

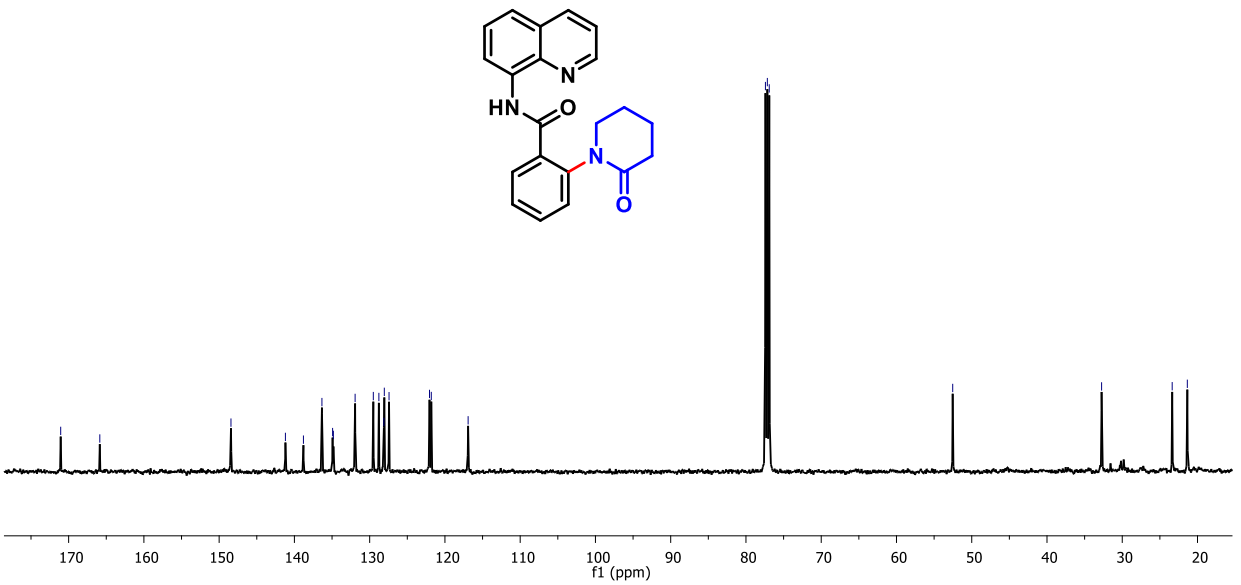

2-(2-oxopiperidin-1-yl)-N-(quinoline-8-yl)-4-(trifluoromethyl)benzamide (3m):

^{1}H NMR (500 MHz, $CDCl_3$)

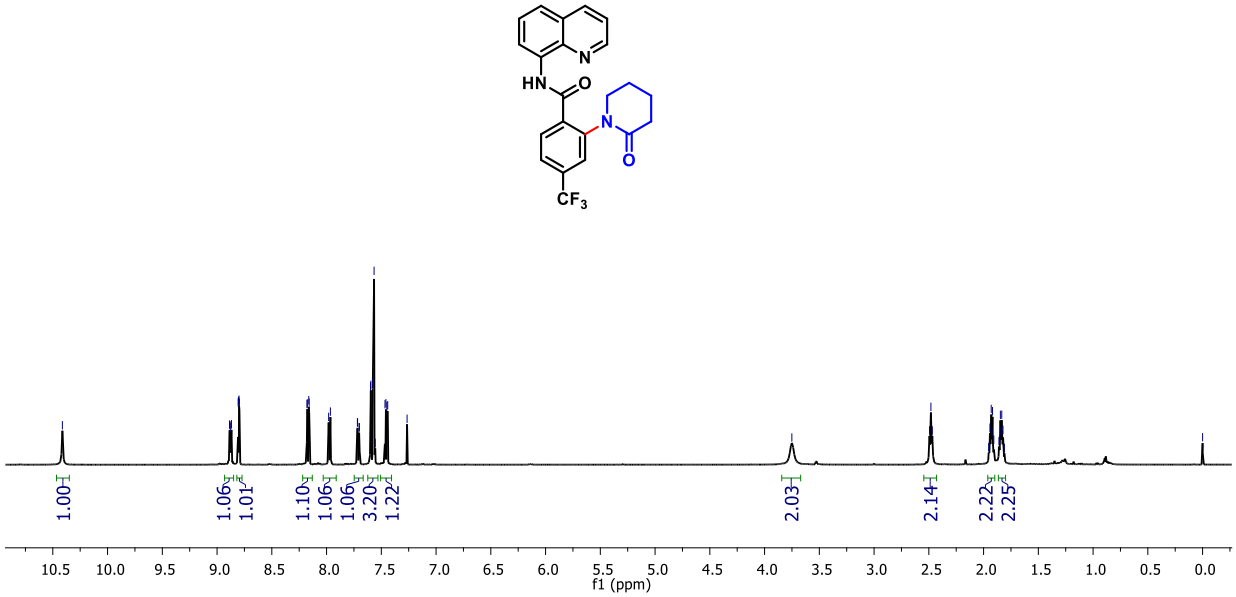

^{13}C{^{1}H} NMR (126 MHz, $CDCl_3$)

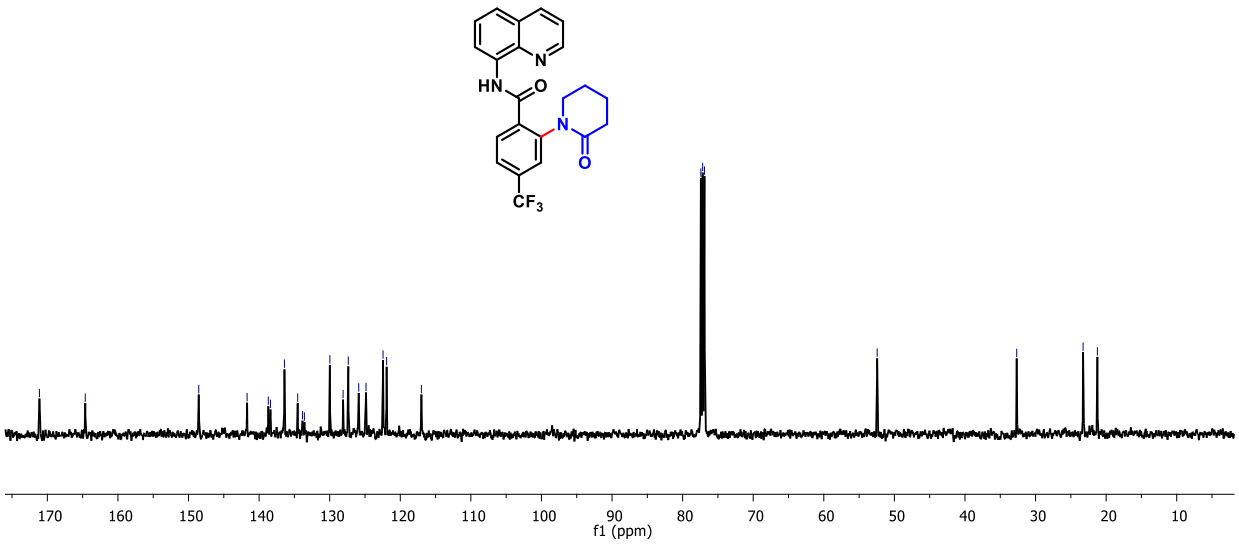

^{19}F NMR (565 MHz, $CDCl_3$)

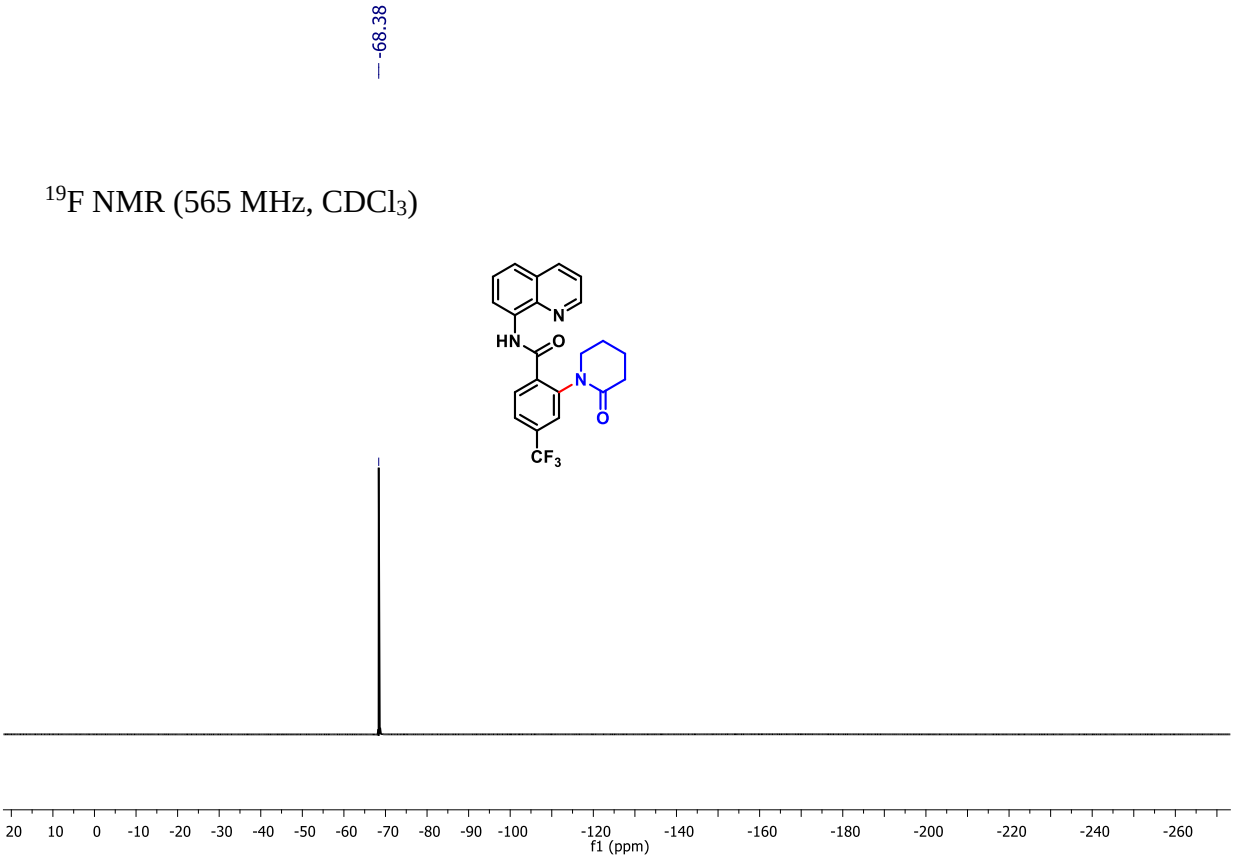

2-(2-oxoazepan-1-yl)-N-(quinoline-8-yl)benzamide (3n):

^{1}H NMR (600 MHz, $CDCl_3$)

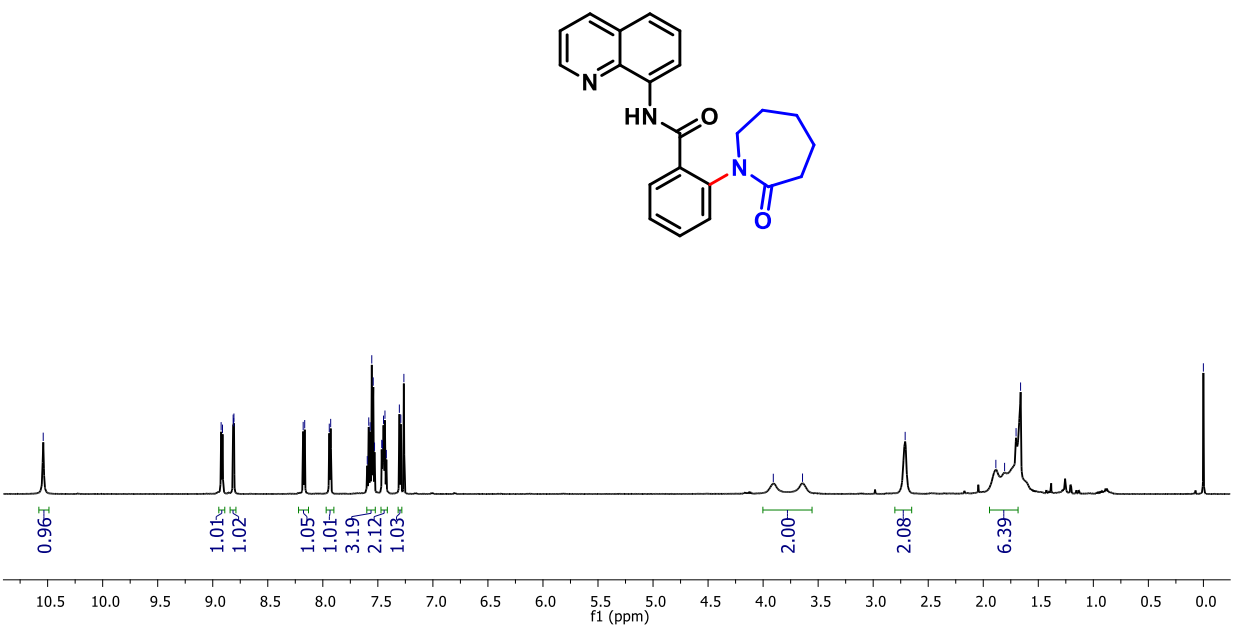

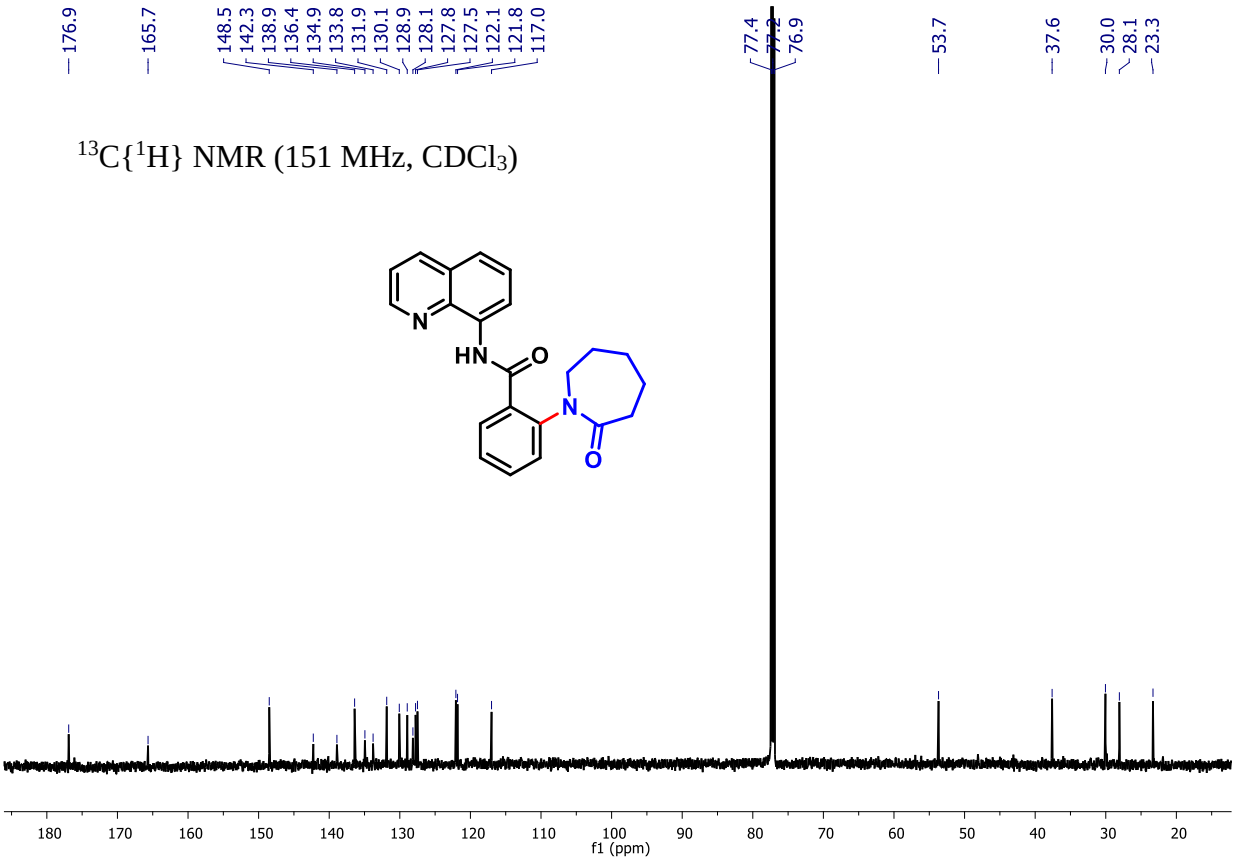

^{13}C{^{1}H} NMR (151 MHz, $CDCl_3$)

4-methoxy-2-(2-oxoazepan-1-yl)-N-(quinoline-8-yl)benzamide (3o):

^{1}H NMR (600 MHz, $CDCl_3$)

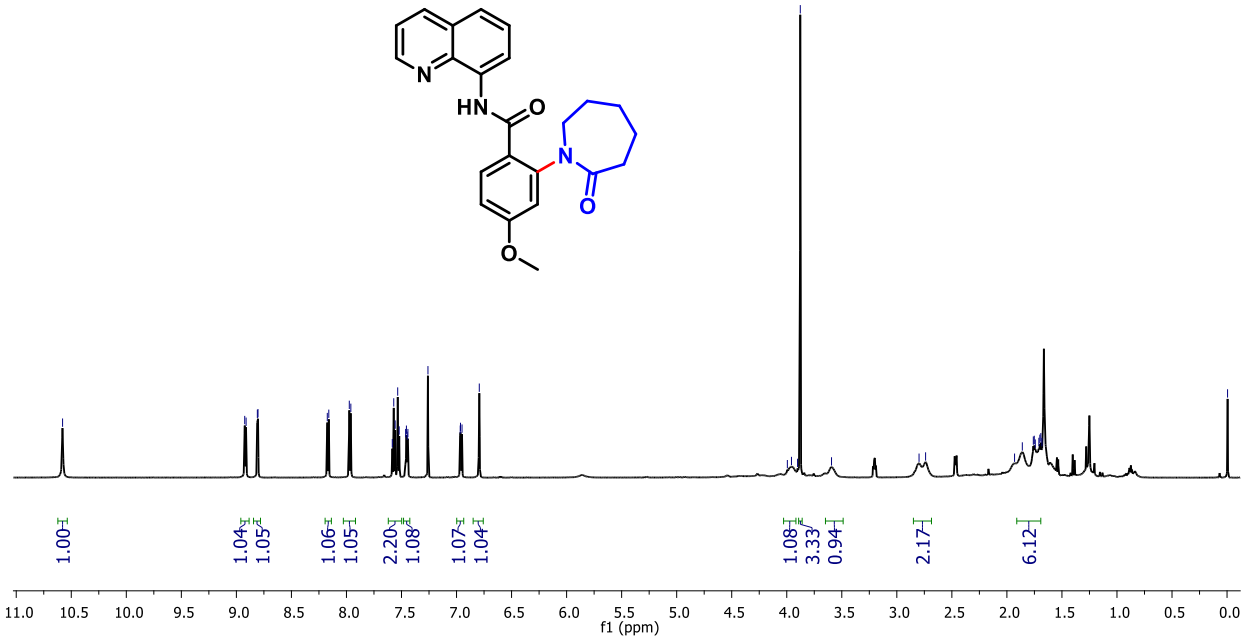

^{13}C{^{1}H} NMR (151 MHz, $CDCl_3$)

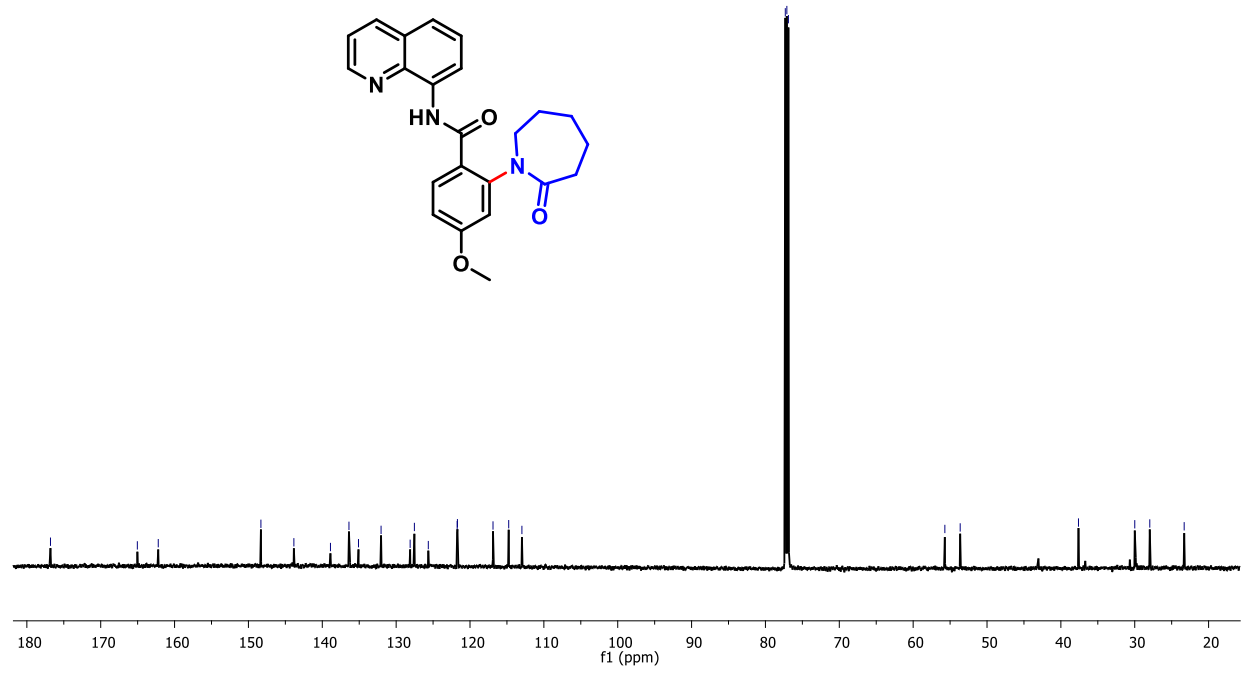

2-(2-oxoazepan-1-yl)-N-(quinoline-8-yl)-1-naphthamide (3p):

^{1}H NMR (600 MHz, $CDCl_3$)

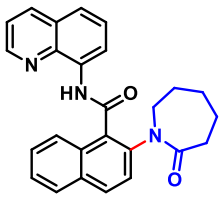

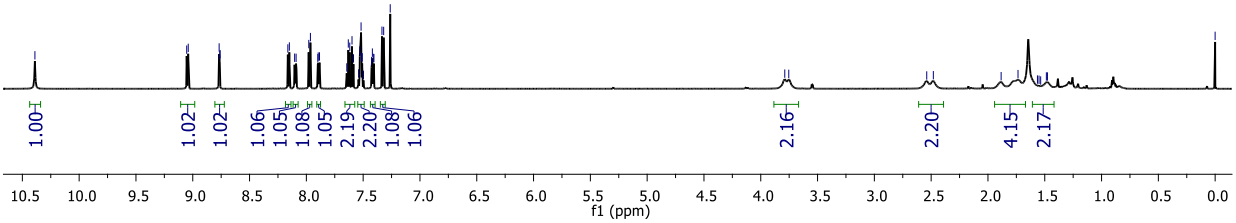

^{13}C{^{1}H} NMR (151 MHz, $CDCl_3$)

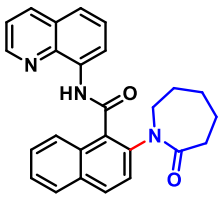

3-(2-oxopyrrodin-1-yl)-N-(quinoline-8-yl)thiophene-2-carboxamide (3q):

^{1}H NMR (500 MHz, $CDCl_3$)

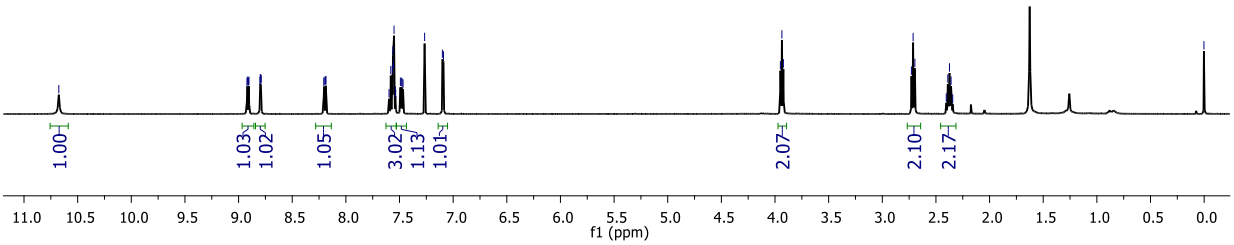

^{13}C{^{1}H} NMR (126 MHz, $CDCl_3$)

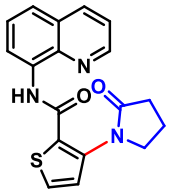

3-(2-oxopiperidin-1-yl)-N-(quinoline-8-yl)thiophene-2-carboxamide (3r):

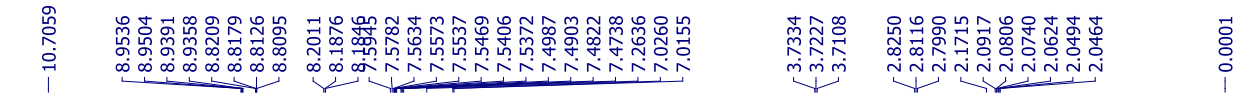

^{1}H NMR (500 MHz, $CDCl_3$)

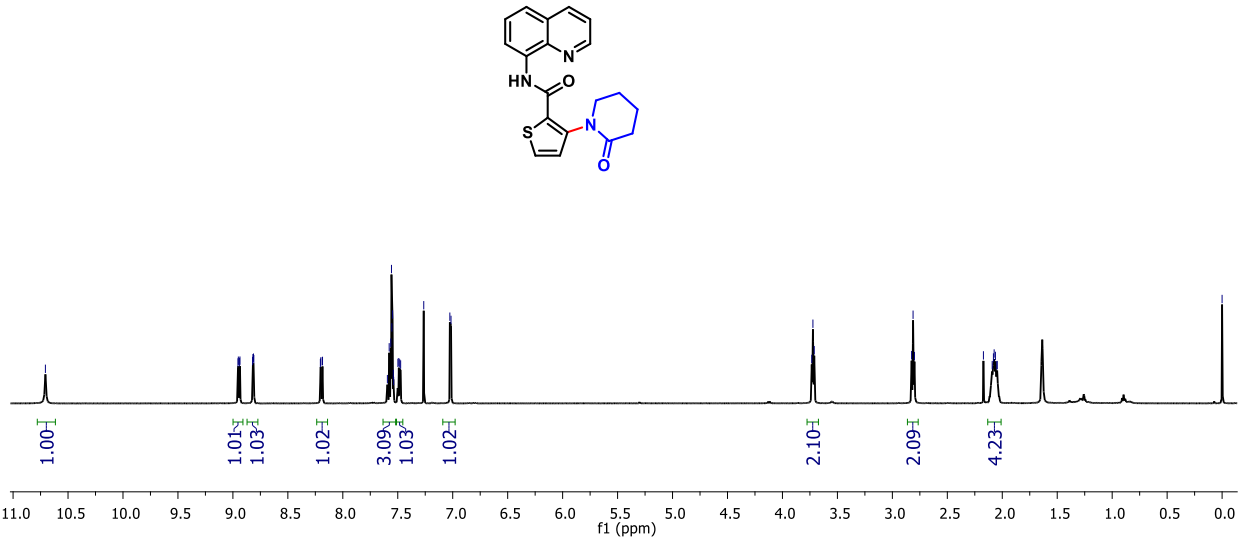

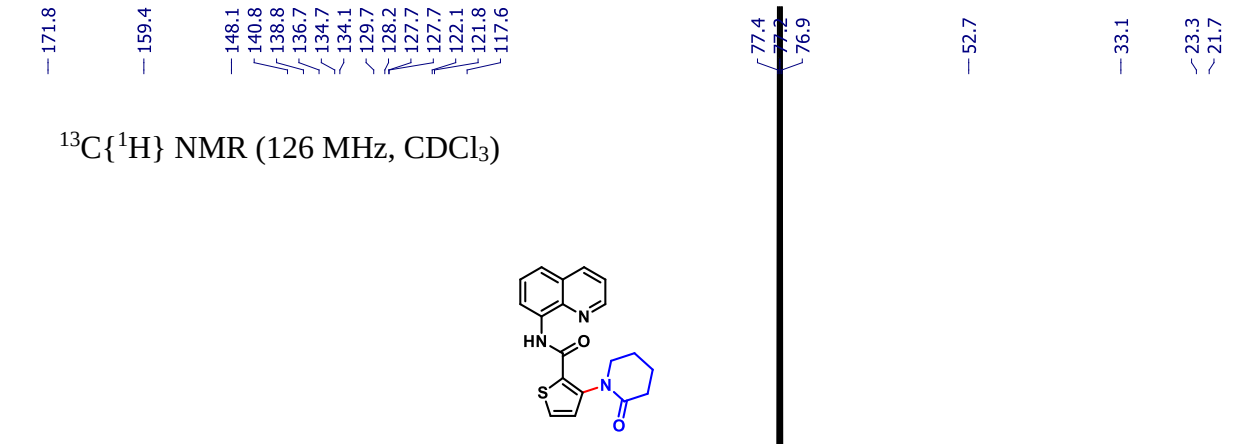

^{13}C{^{1}H} NMR (126 MHz, $CDCl_3$)

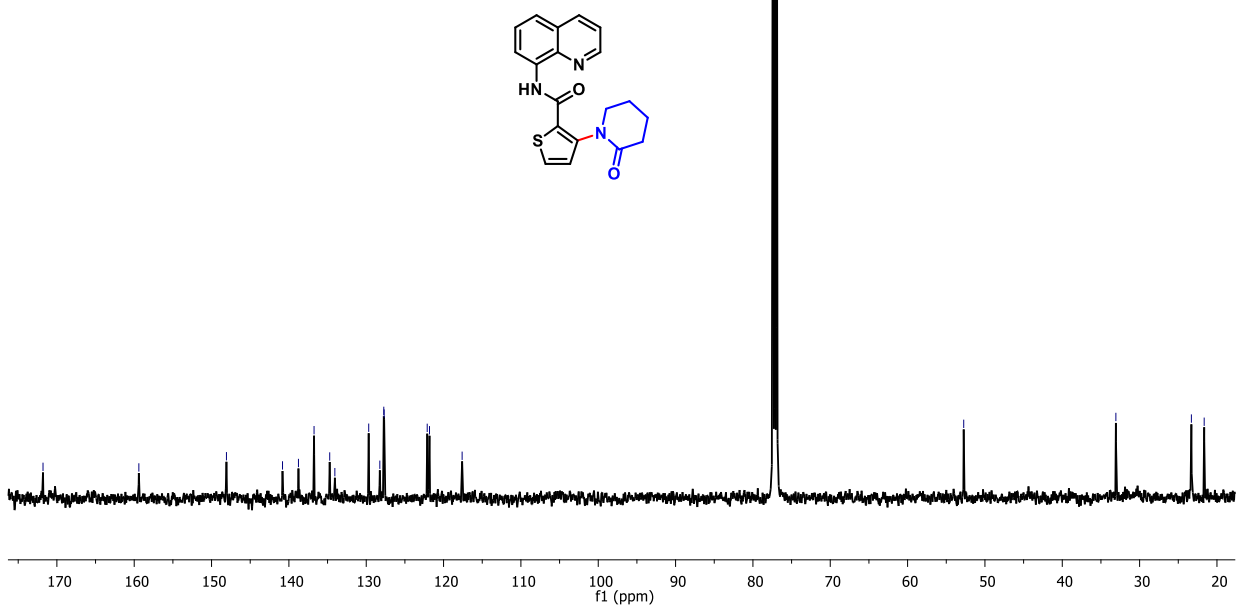

3-(2-oxoazepan-1-yl)-N-(quinoline-8-yl)thiophene-2-carboxamide (3s):

^{1}H NMR (600 MHz, $CDCl_3$)

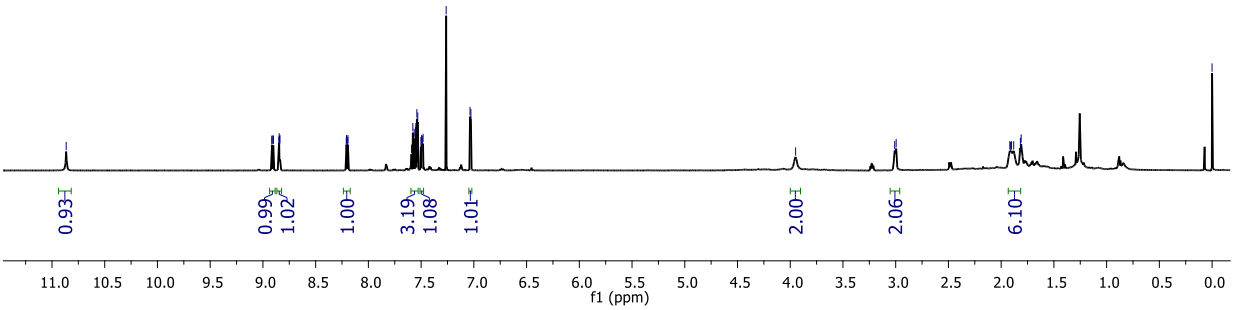

^{13}C{^{1}H} NMR (151 MHz, $CDCl_3$)

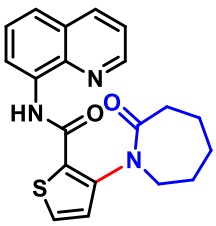

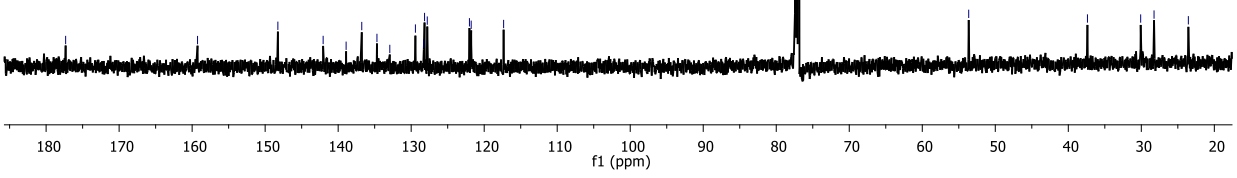

2-(4-methylpiperidin-1-yl)-N-(quinolin-8-yl)benzamide (5a):

^{1}H NMR (600 MHz, $CDCl_3$)

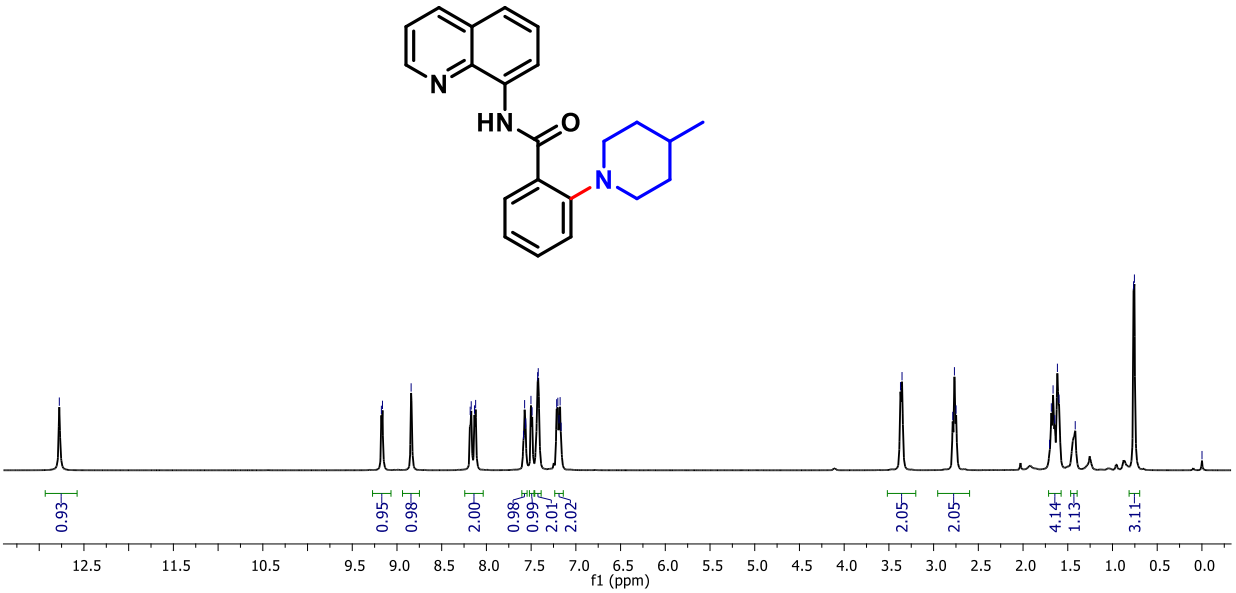

^{13}C{^{1}H} NMR (151 MHz, $CDCl_3$)

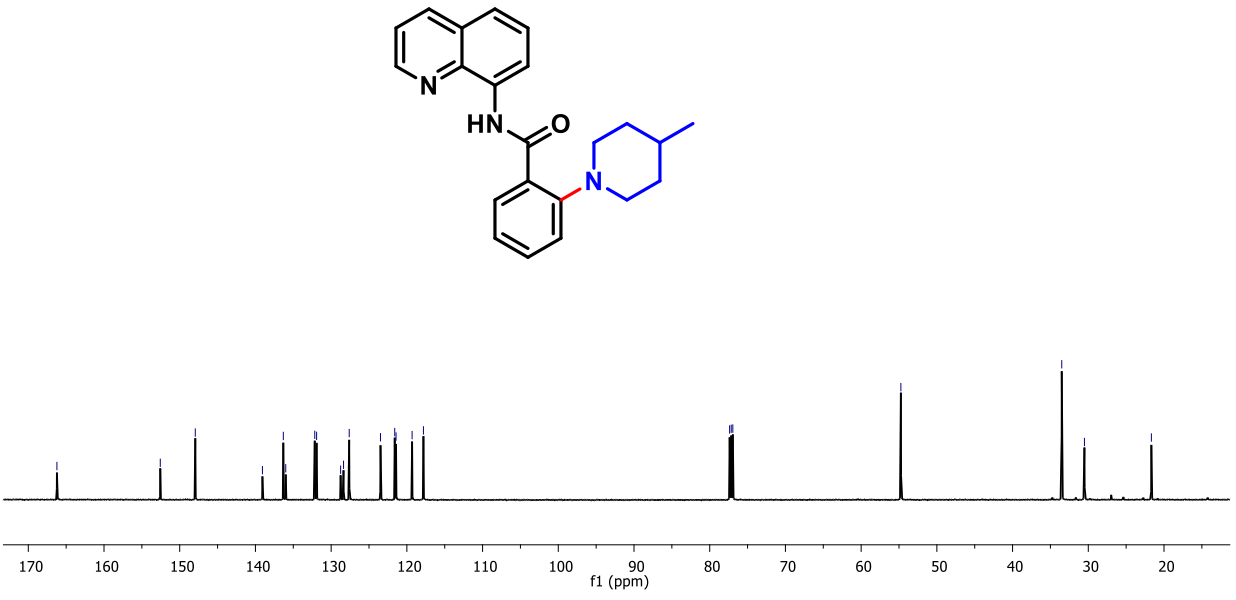

4-methoxy-2-(4-methylpiperidin-1-yl)-N-(quinolin-8-yl)benzamide (5b):

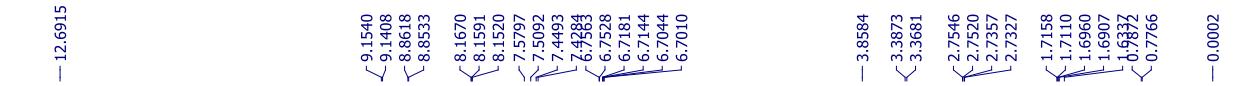

^{1}H NMR (600 MHz, $CDCl_3$)

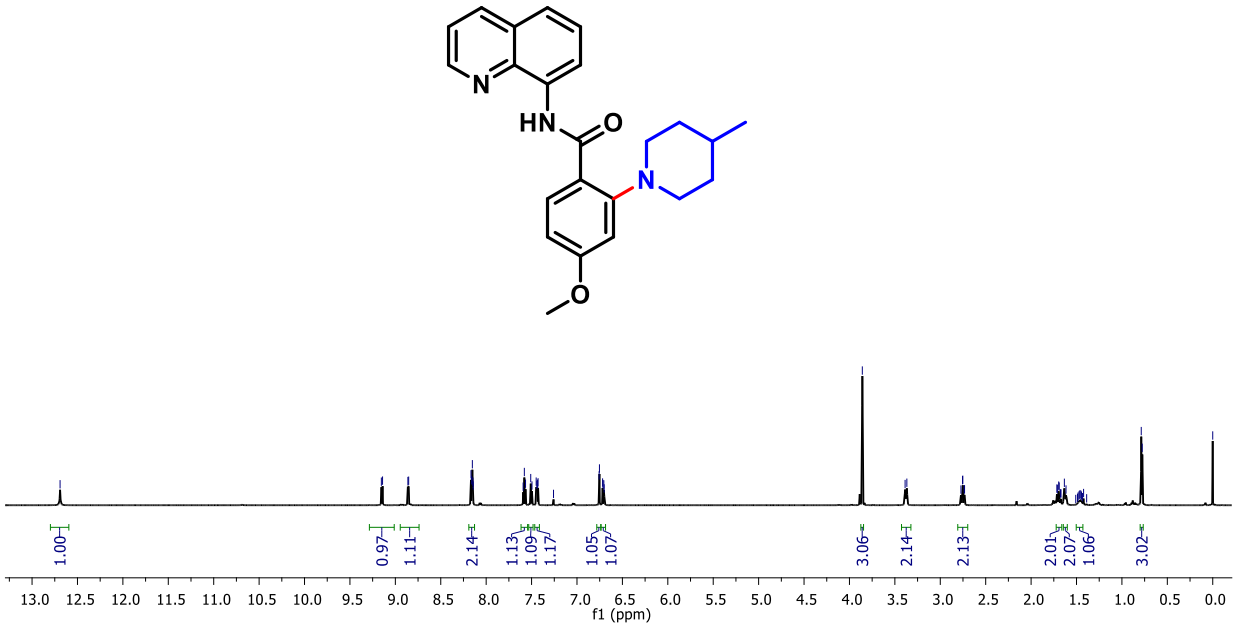

^{13}C{^{1}H} NMR (151 MHz, $CDCl_3$)

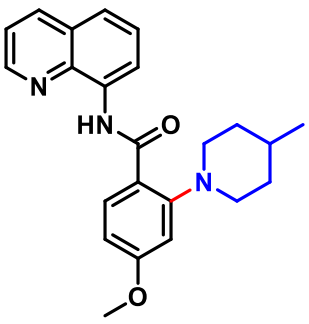

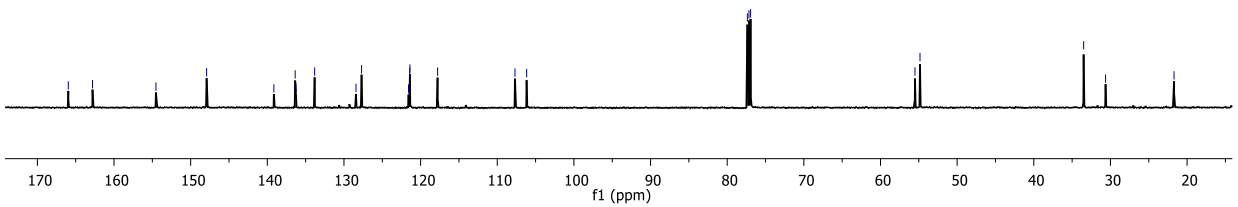

4-chloro-2-(4-methylpiperidin-1-yl)-N-(quinolin-8-yl)benzamide (5c):

^{1}H NMR (600 MHz, $CDCl_3$)

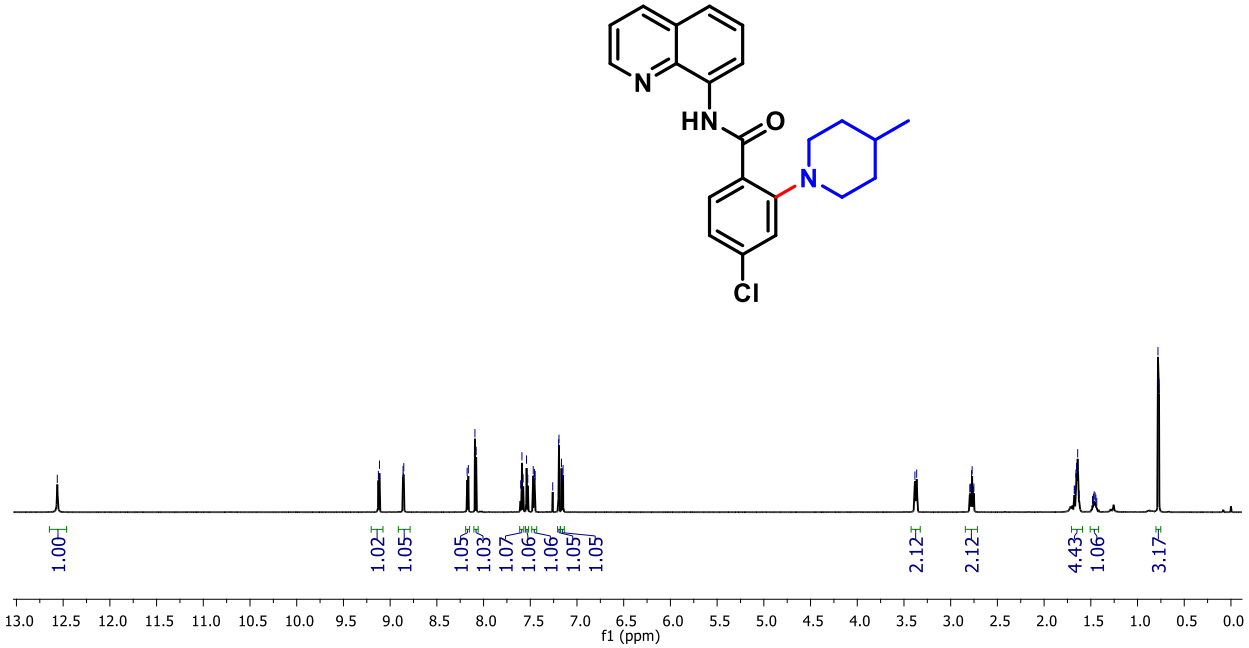

^{13}C{^{1}H} NMR (151 MHz, $CDCl_3$)

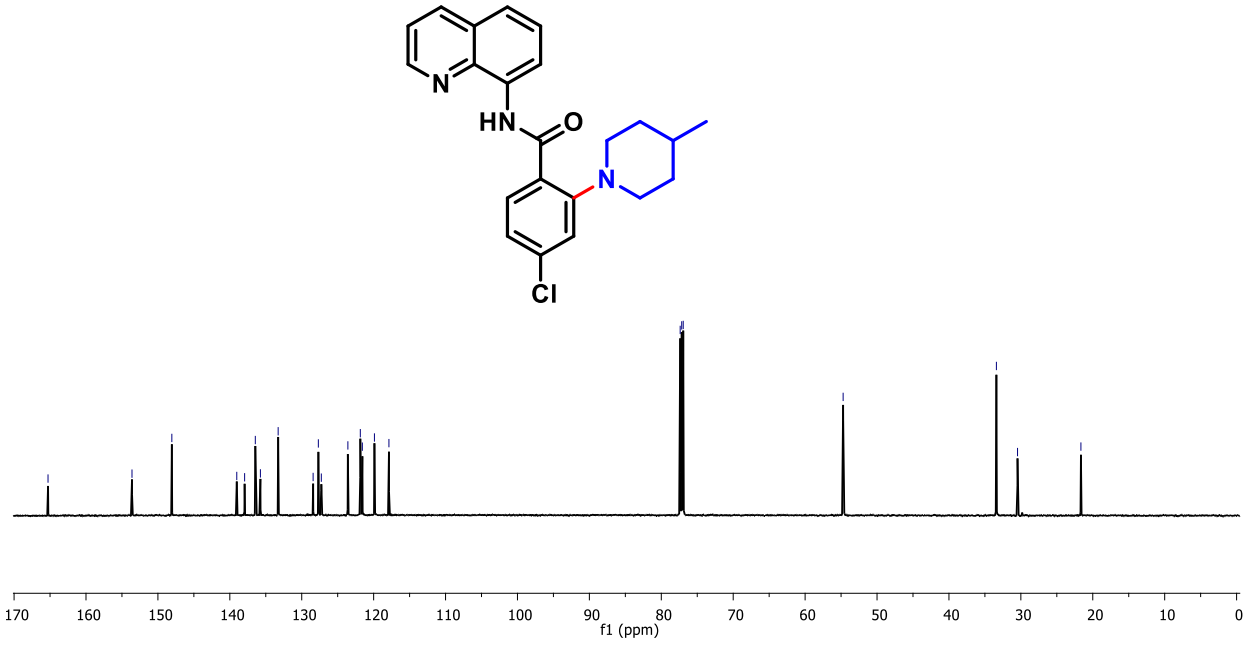

4-fluoro-2-(4-methylpiperidin-1-yl)-N-(quinolin-8-yl)benzamide (5d):

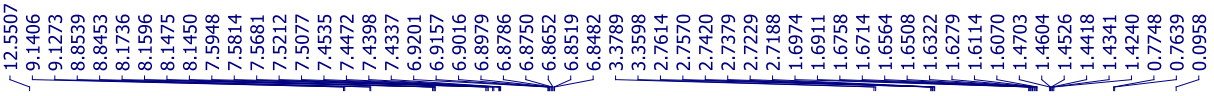

^{1}H NMR (600 MHz, $CDCl_3$)

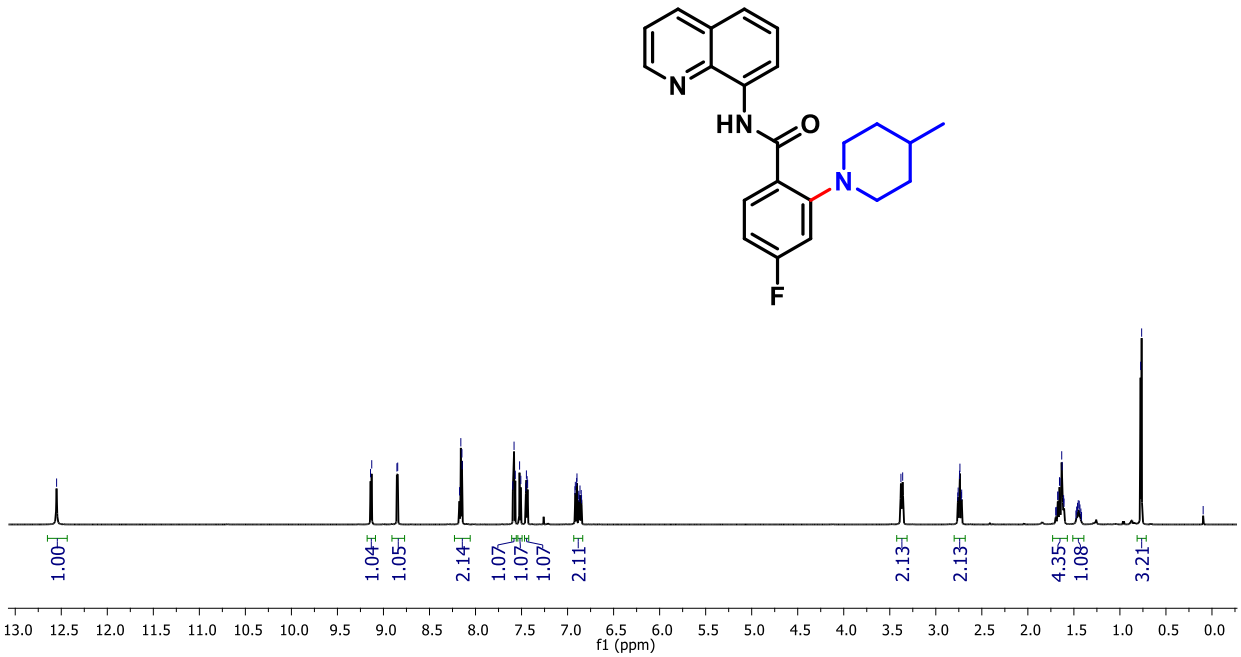

^{13}C{^{1}H} NMR (151 MHz, $CDCl_3$)

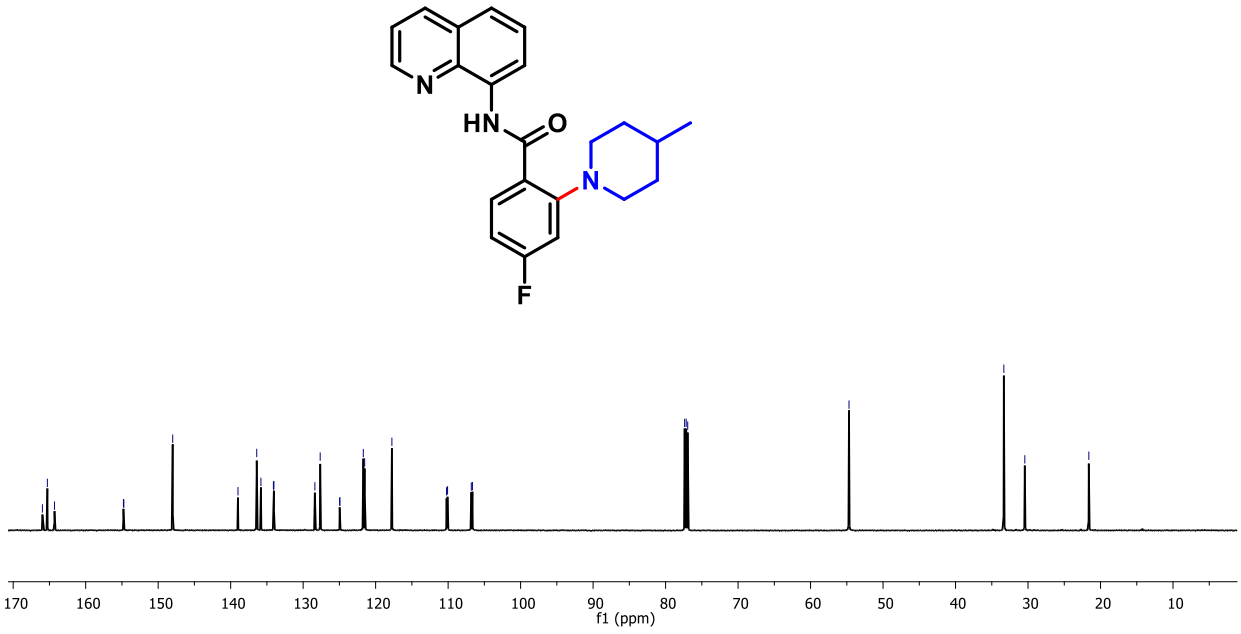

-113.65
-113.67
-113.68
-113.69

^{19}F NMR (565 MHz, $CDCl_3$)

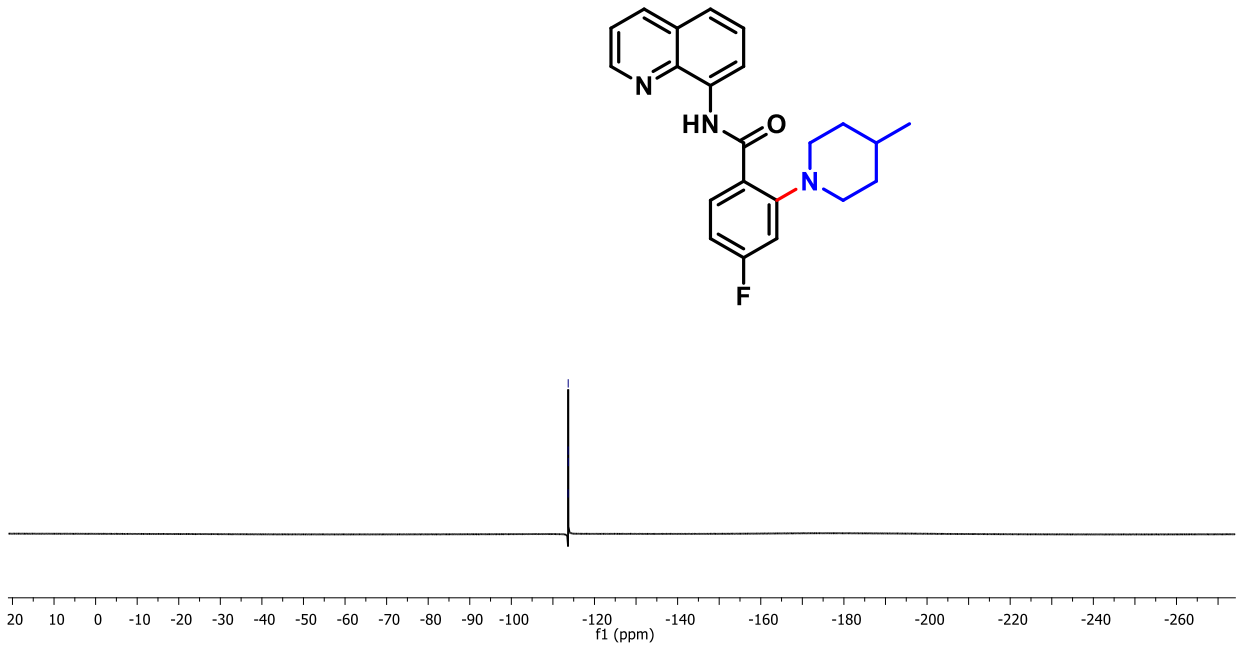

4-trifluoromethyl-2-(4-methylpiperidin-1-yl)-N-(quinolin-8-yl)benzamide (5e):

^{1}H NMR (600 MHz, $CDCl_3$)

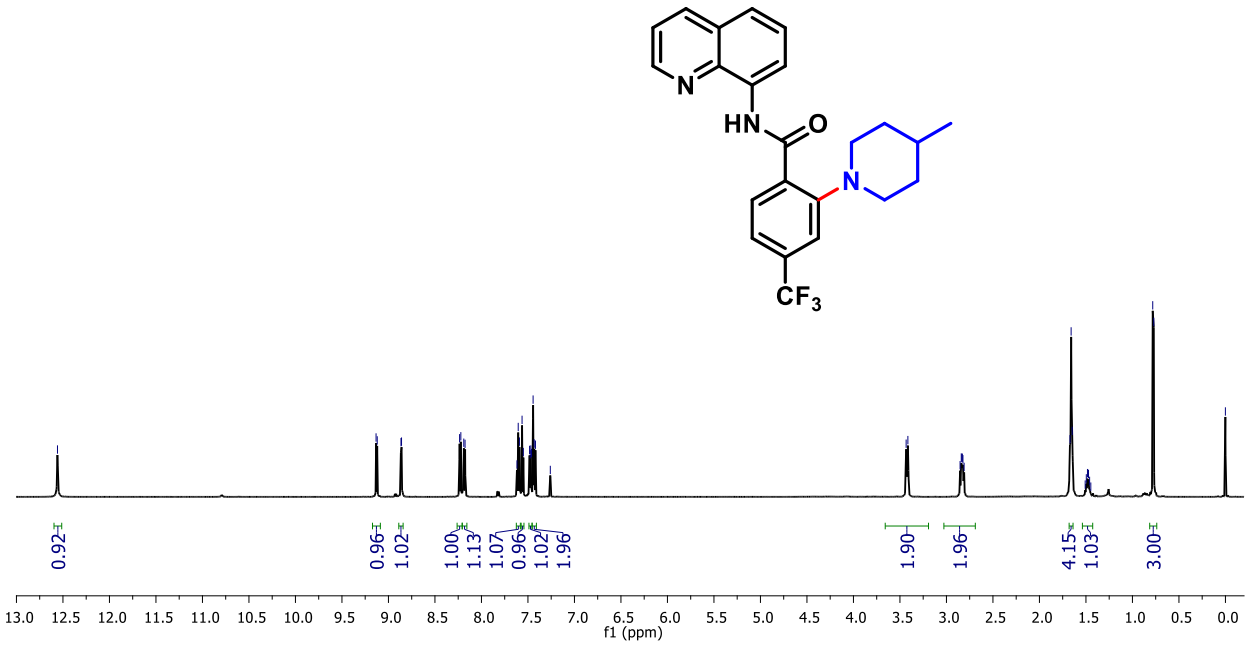

^{13}C{^{1}H} NMR (151 MHz, $CDCl_3$)

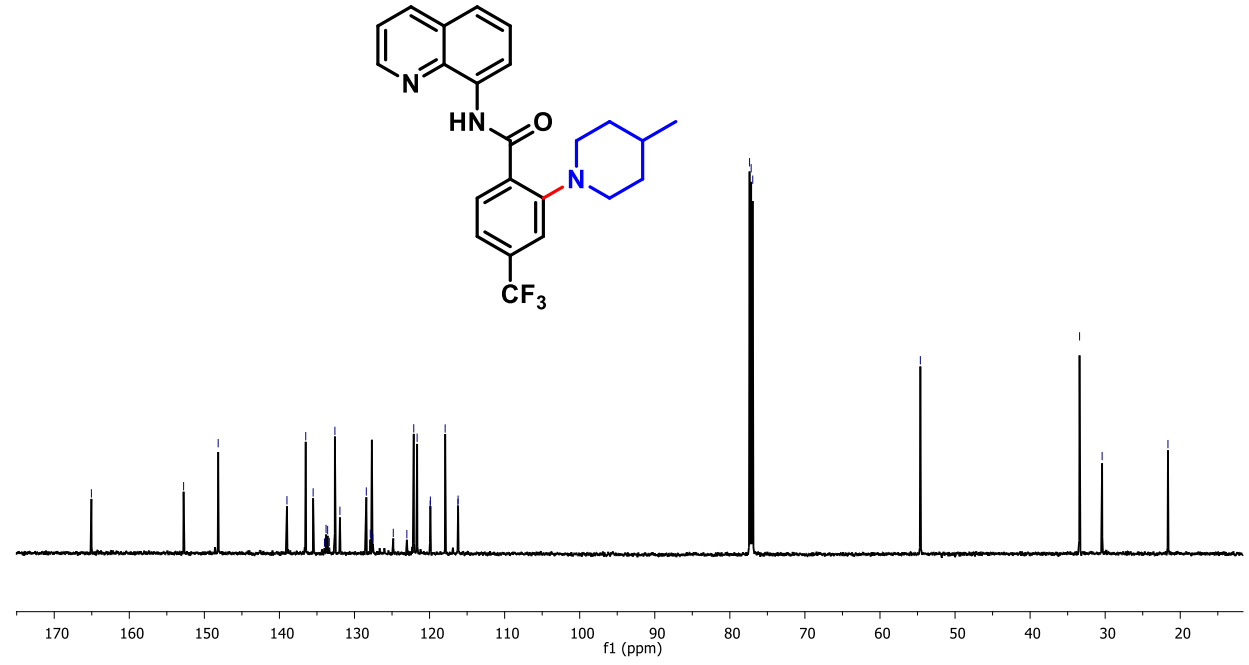

^{19}F NMR (565 MHz, $CDCl_3$)

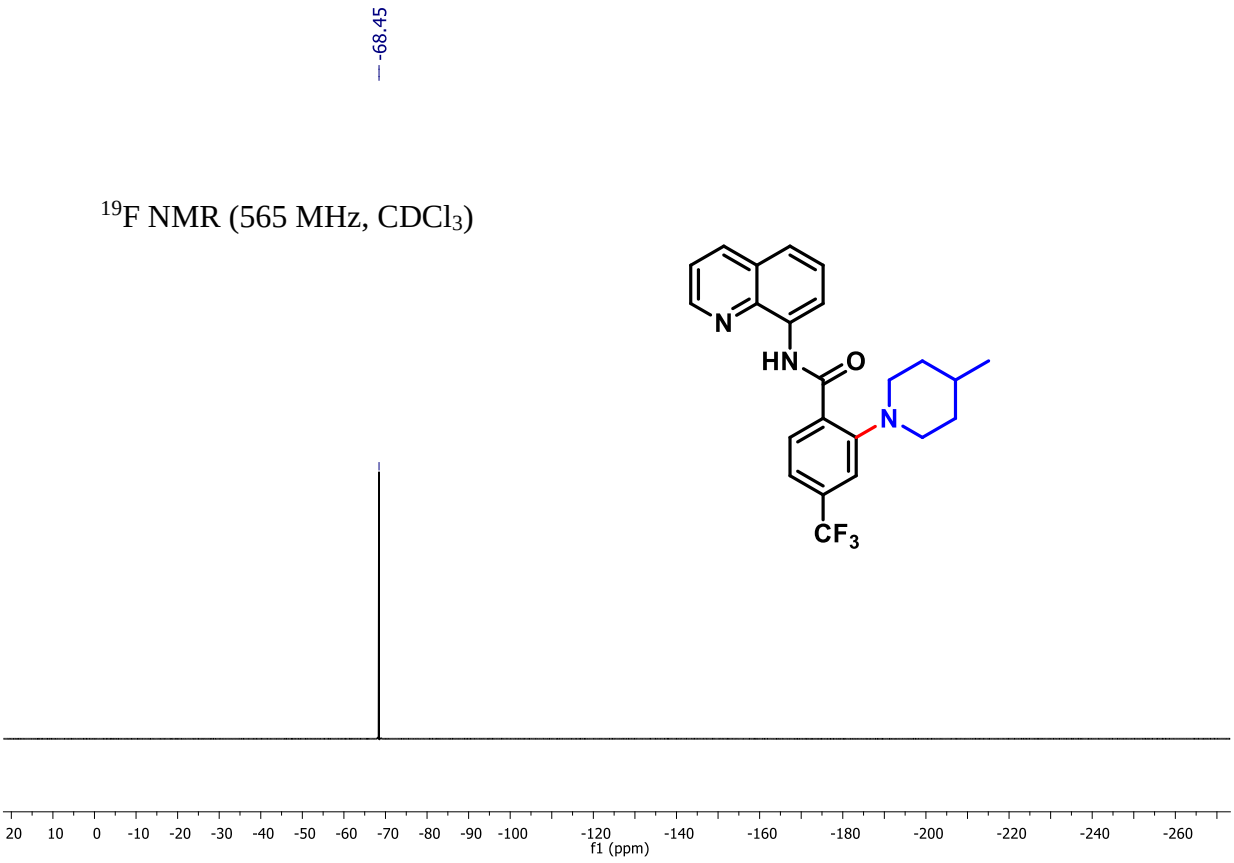

2-(4-phenylpiperidin-1-yl)-N-(quinolin-8-yl)benzamide (5f):

^{1}H NMR (600 MHz, $CDCl_3$)

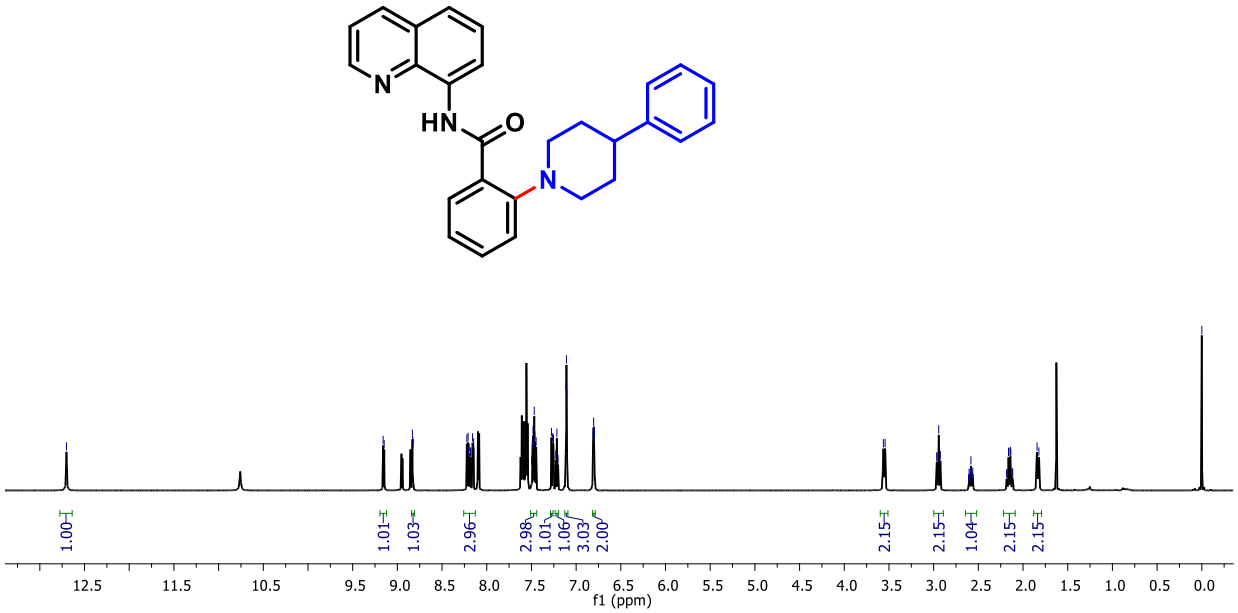

^{13}C{^{1}H} NMR (151 MHz, $CDCl_3$)

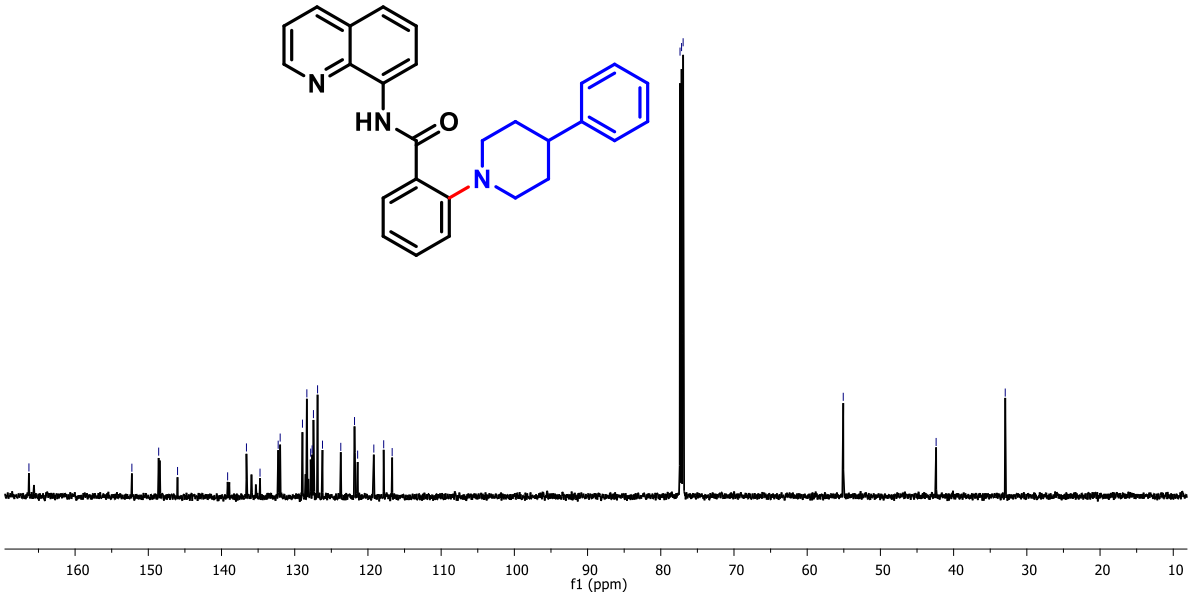

4-methoxy-2-(4-phenylpiperidin-1-yl)-N-(quinolin-8-yl)benzamide (5g):

^{1}H NMR (600 MHz, $CDCl_3$)

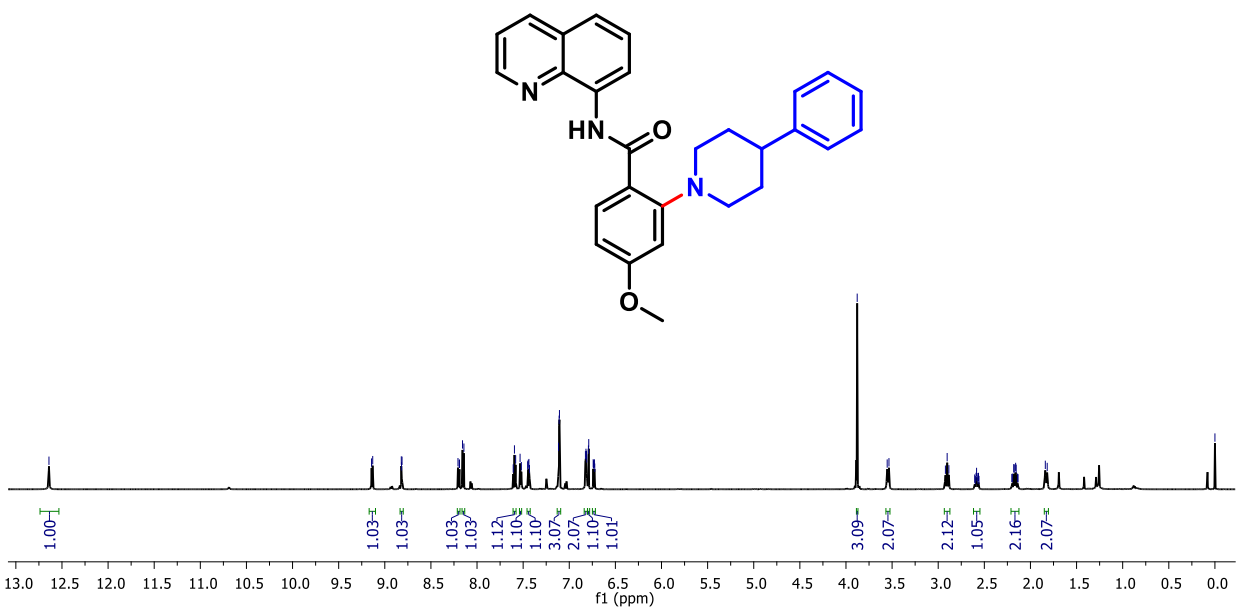

^{13}C{^{1}H} NMR (151 MHz, $CDCl_3$)

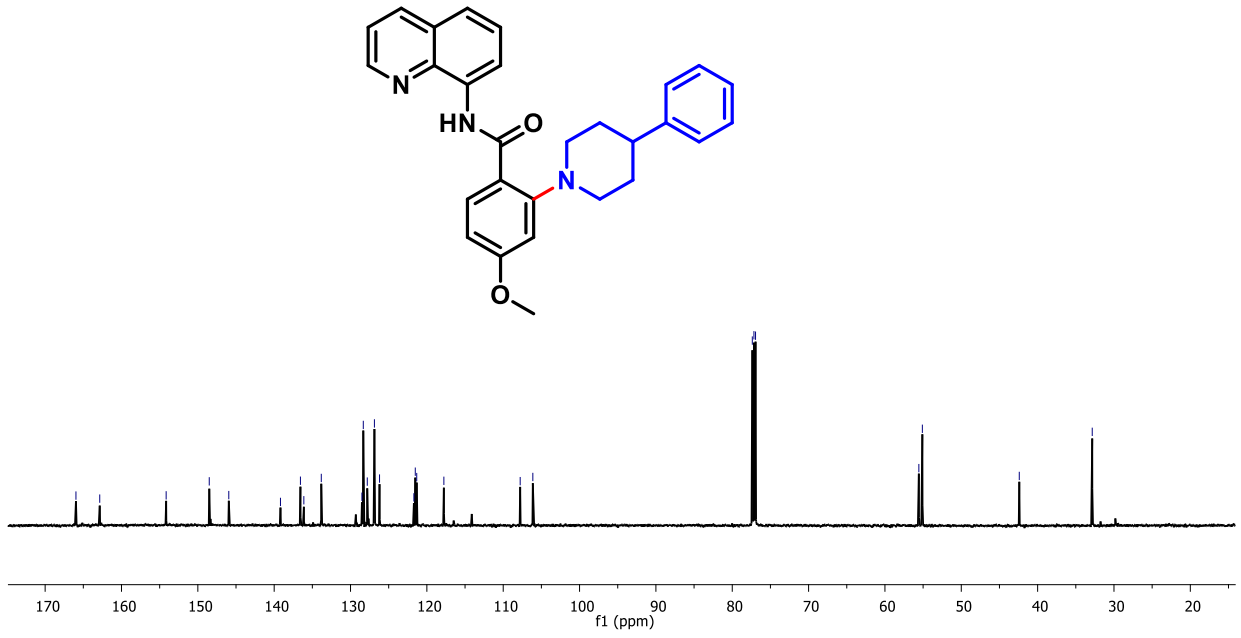

4-chloro-2-(4-phenylpiperidin-1-yl)-N-(quinolin-8-yl) benzamide (5h):

^{1}H NMR (600 MHz, $CDCl_3$)

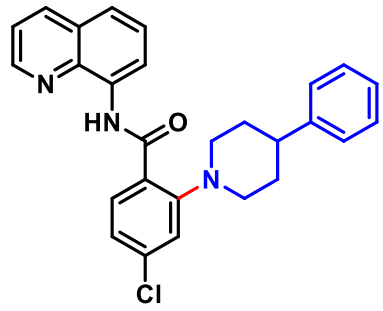

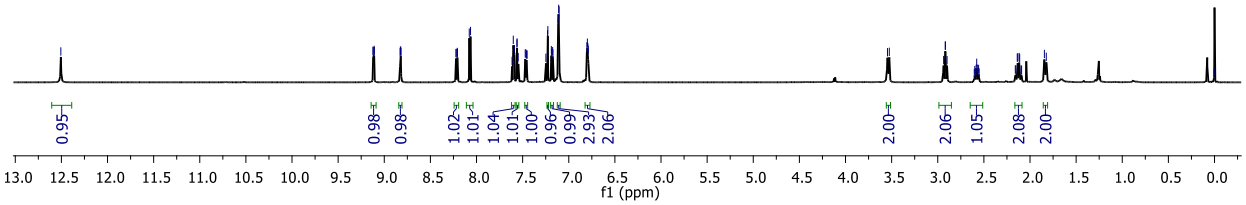

^{13}C{^{1}H} NMR (151 MHz, $CDCl_3$)

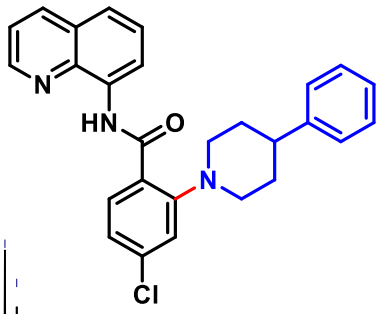

5-methyl-2-(4-methylpiperidin-1-yl)-N-(quinolin-8-yl)benzamide (5i):

^{1}H NMR (600 MHz, $CDCl_3$)

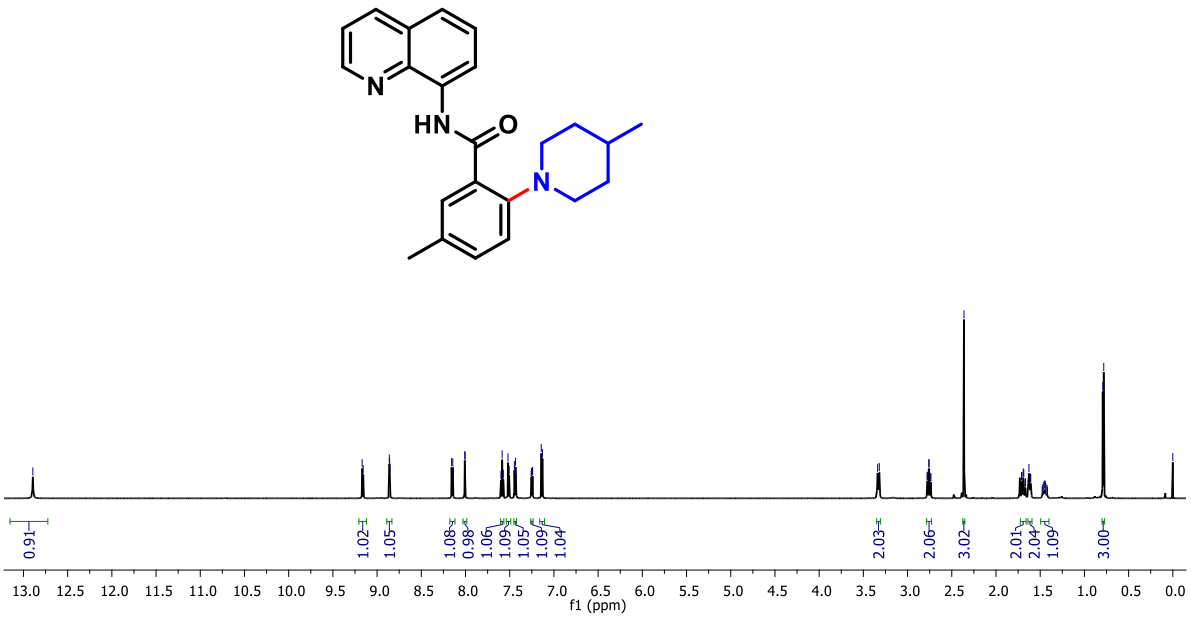

^{13}C{^{1}H} NMR (151 MHz, $CDCl_3$)

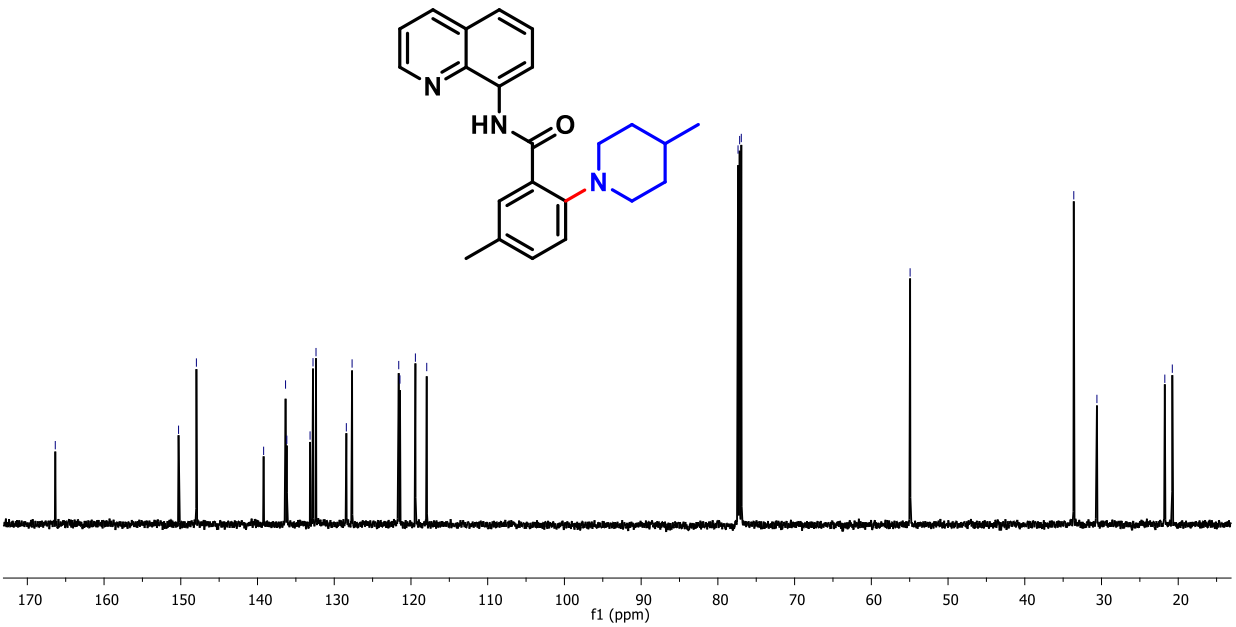

2-morpholino-N-(quinolin-8-yl)benzamide (5j)

^{1}H NMR (600 MHz, $CDCl_3$)

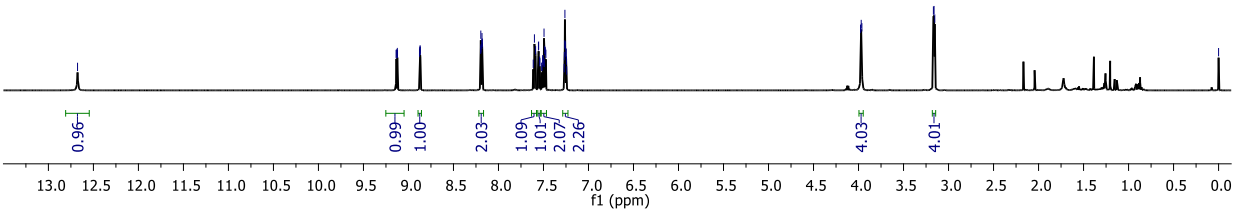

^{13}C{^{1}H} NMR (151 MHz, $CDCl_3$)

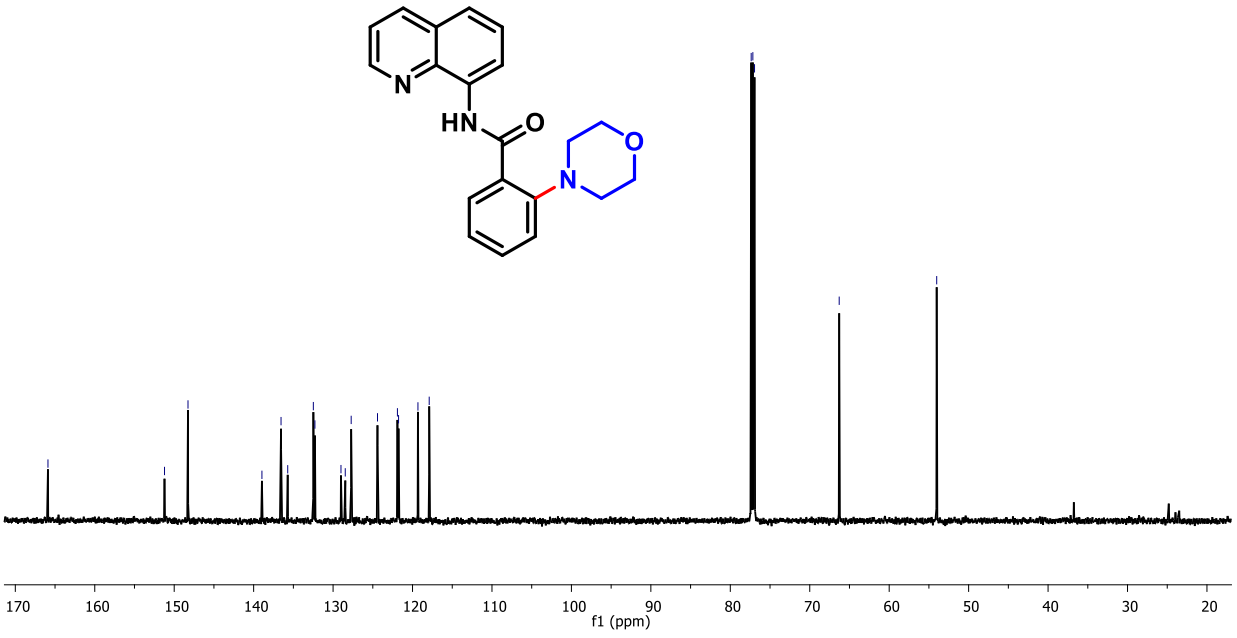

4-methyl-2-morpholino-N-(quinolin-8-yl)benzamide (5k)

^{1}H NMR (600 MHz, $CDCl_3$)

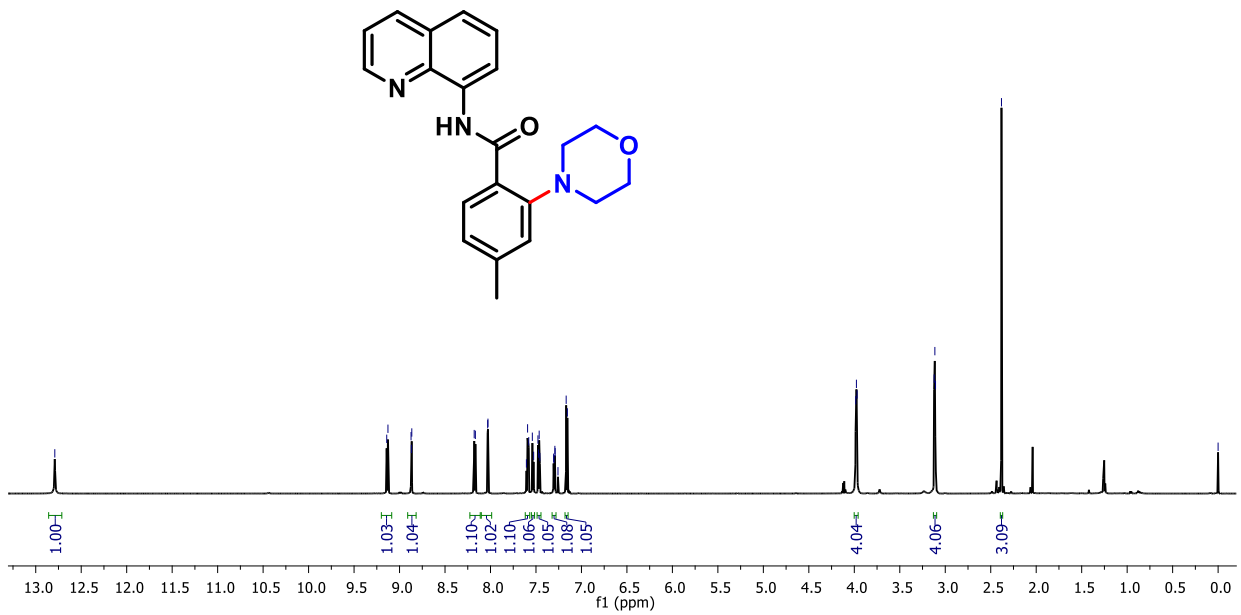

^{13}C{^{1}H} NMR (151 MHz, $CDCl_3$)

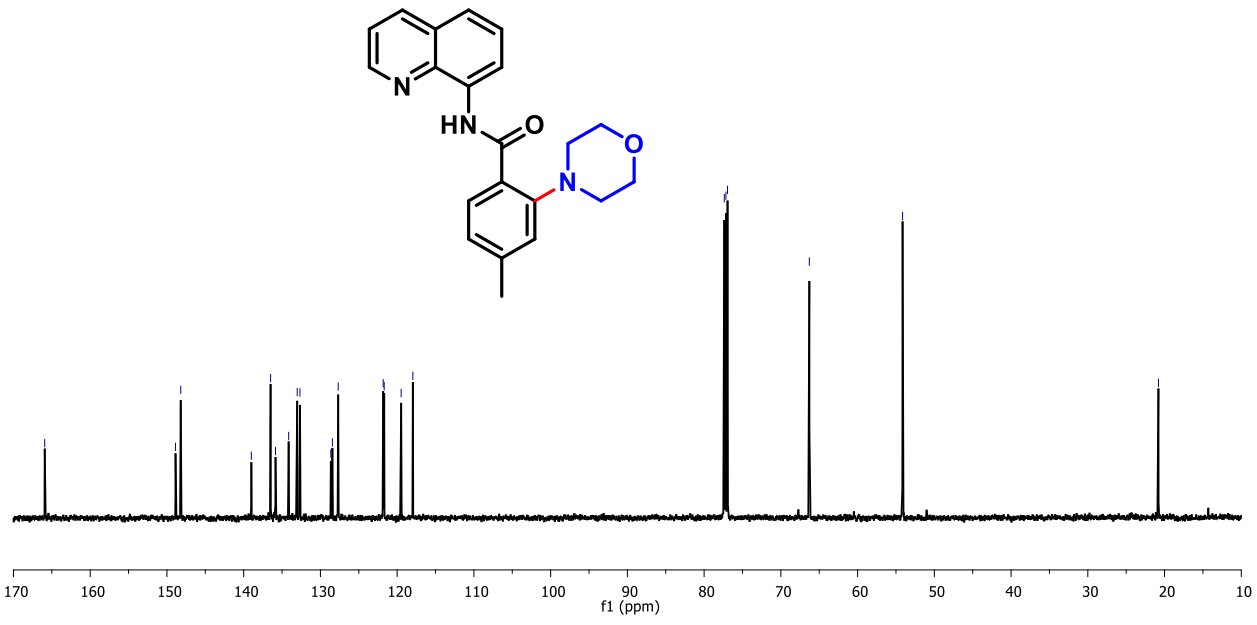

4-fluoro-2-morpholino-N-(quinolin-8-yl)benzamide (5l)

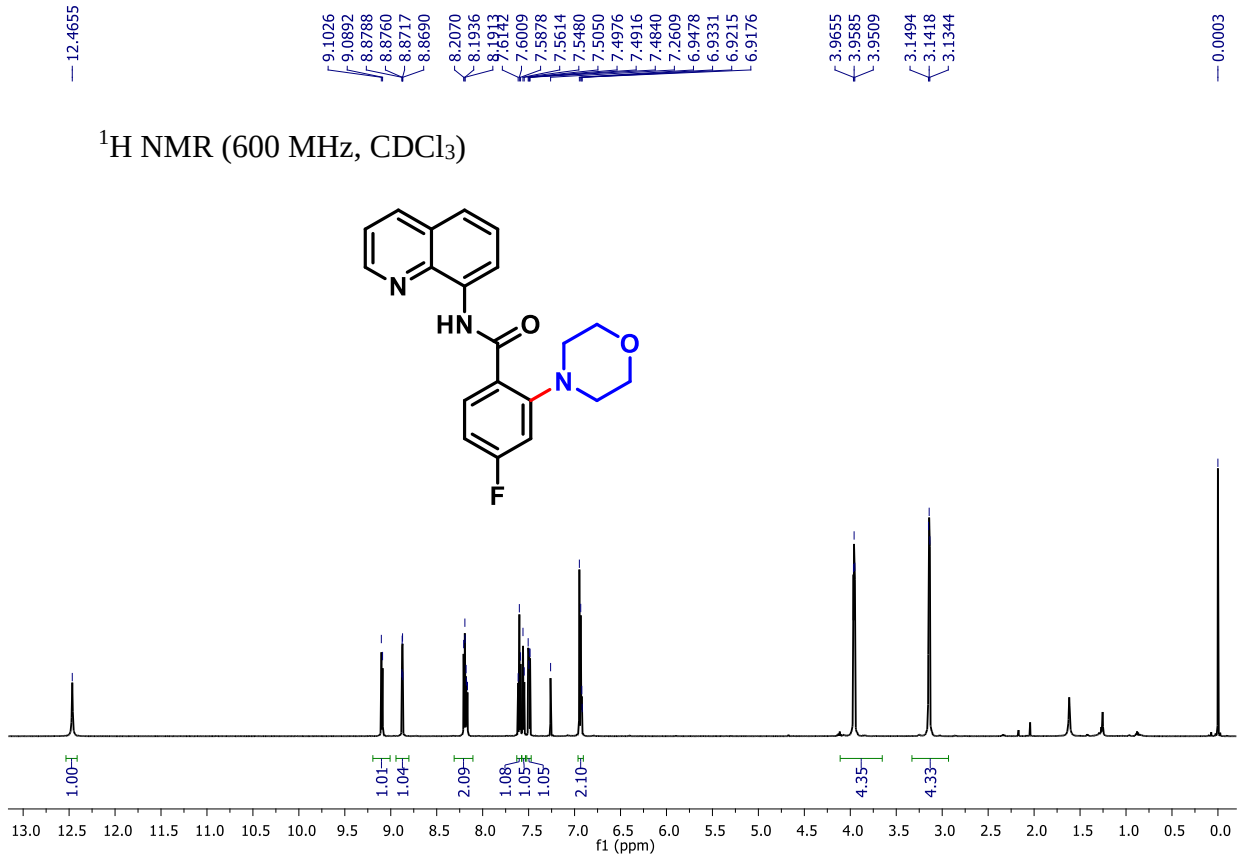

^{1}H NMR (600 MHz, $CDCl_3$)

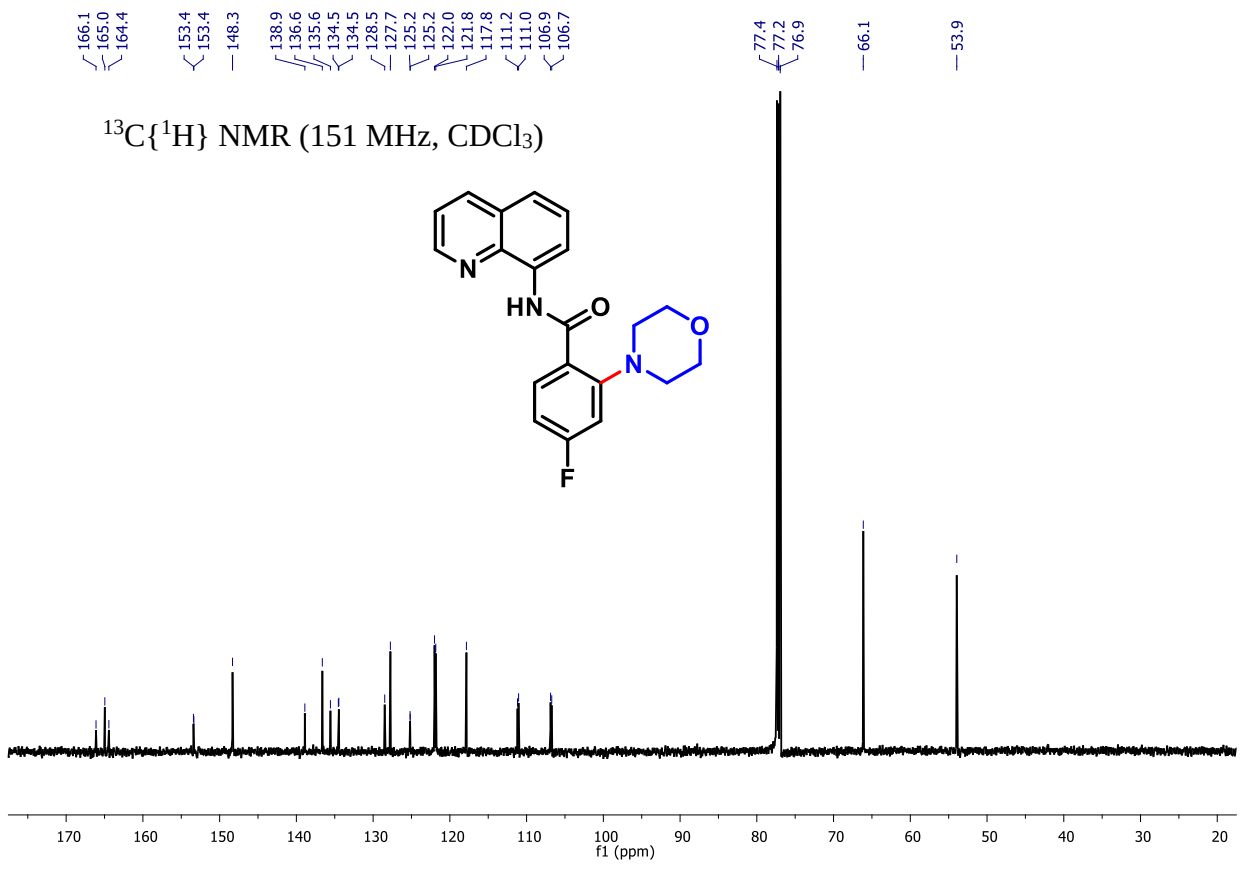

^{13}C{^{1}H} NMR (151 MHz, $CDCl_3$)

^{19}F NMR (565 MHz, $CDCl_3$)

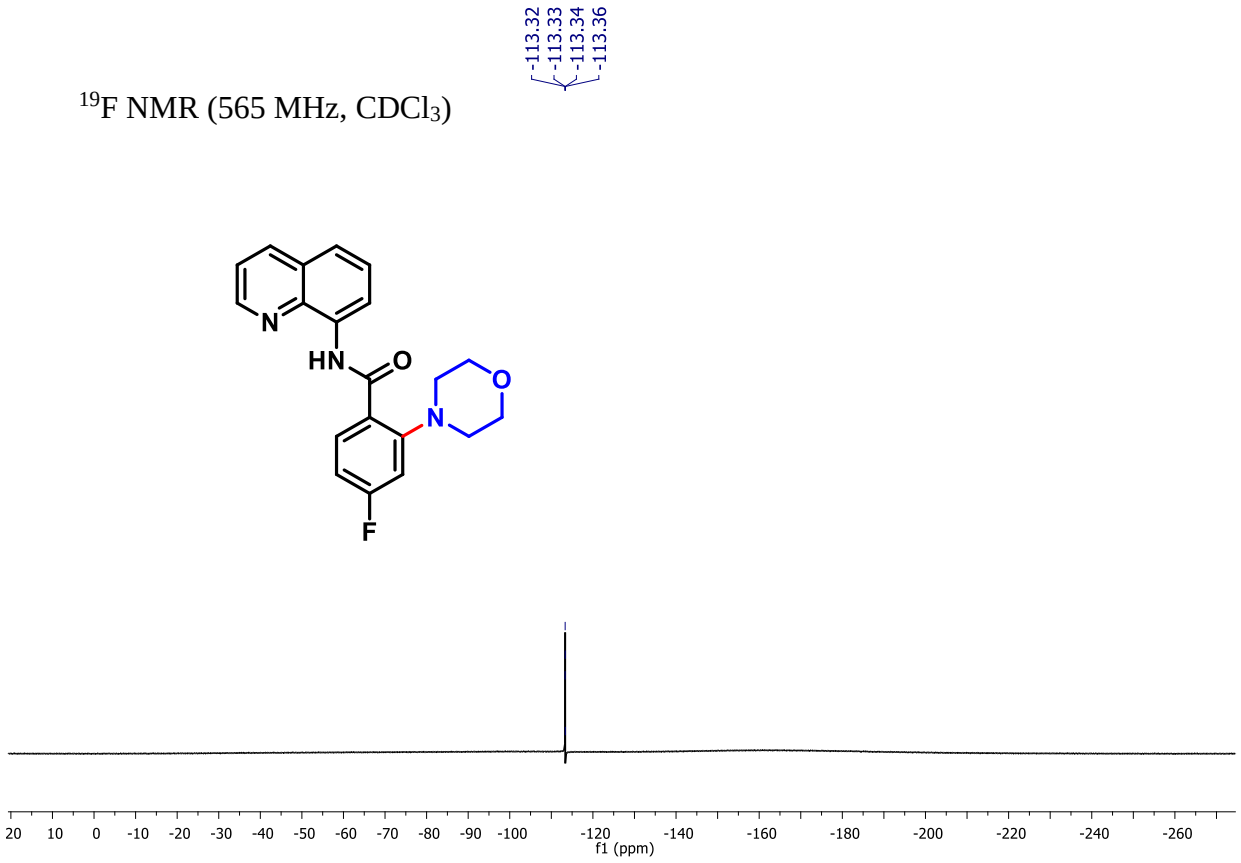

4-methoxy-2-morpholino-N-(quinolin-8-yl)benzamide (5m):

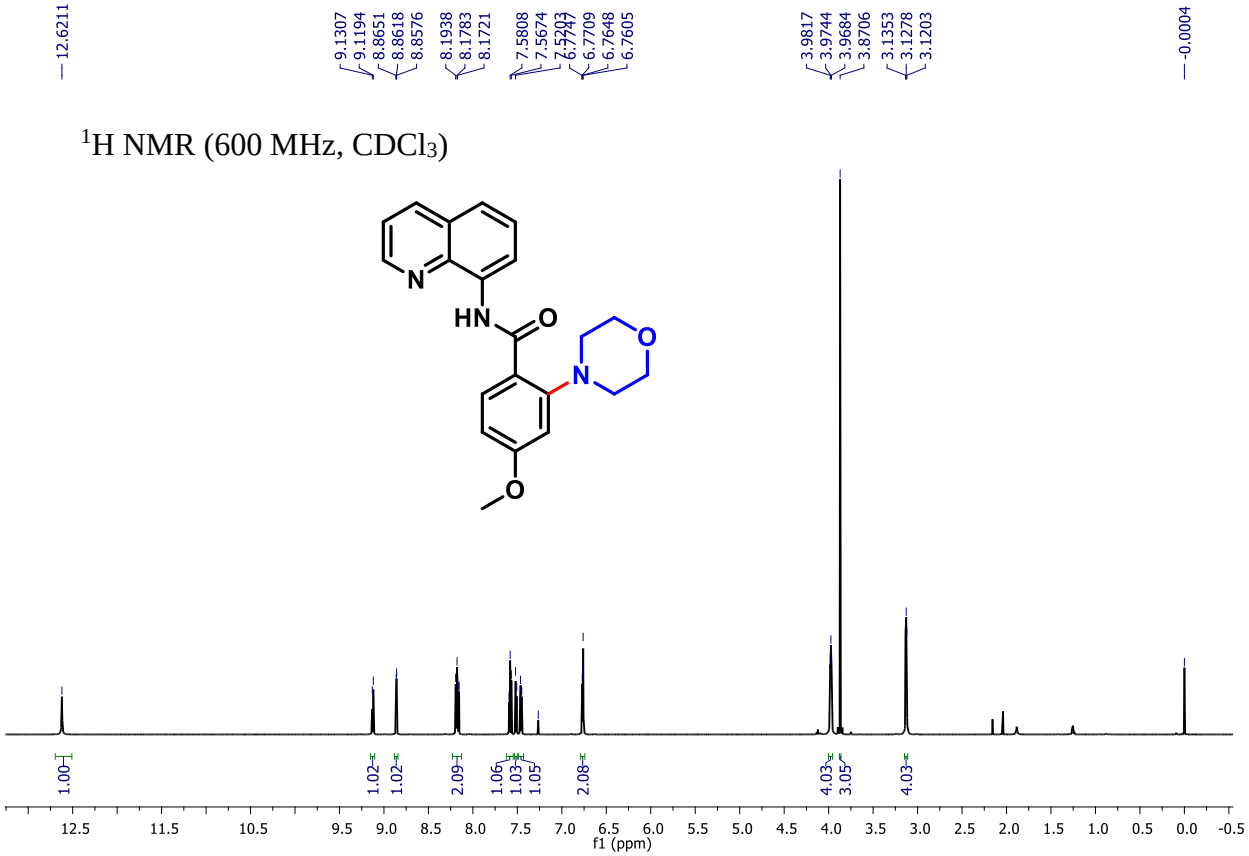

^{1}H NMR (600 MHz, $CDCl_3$)

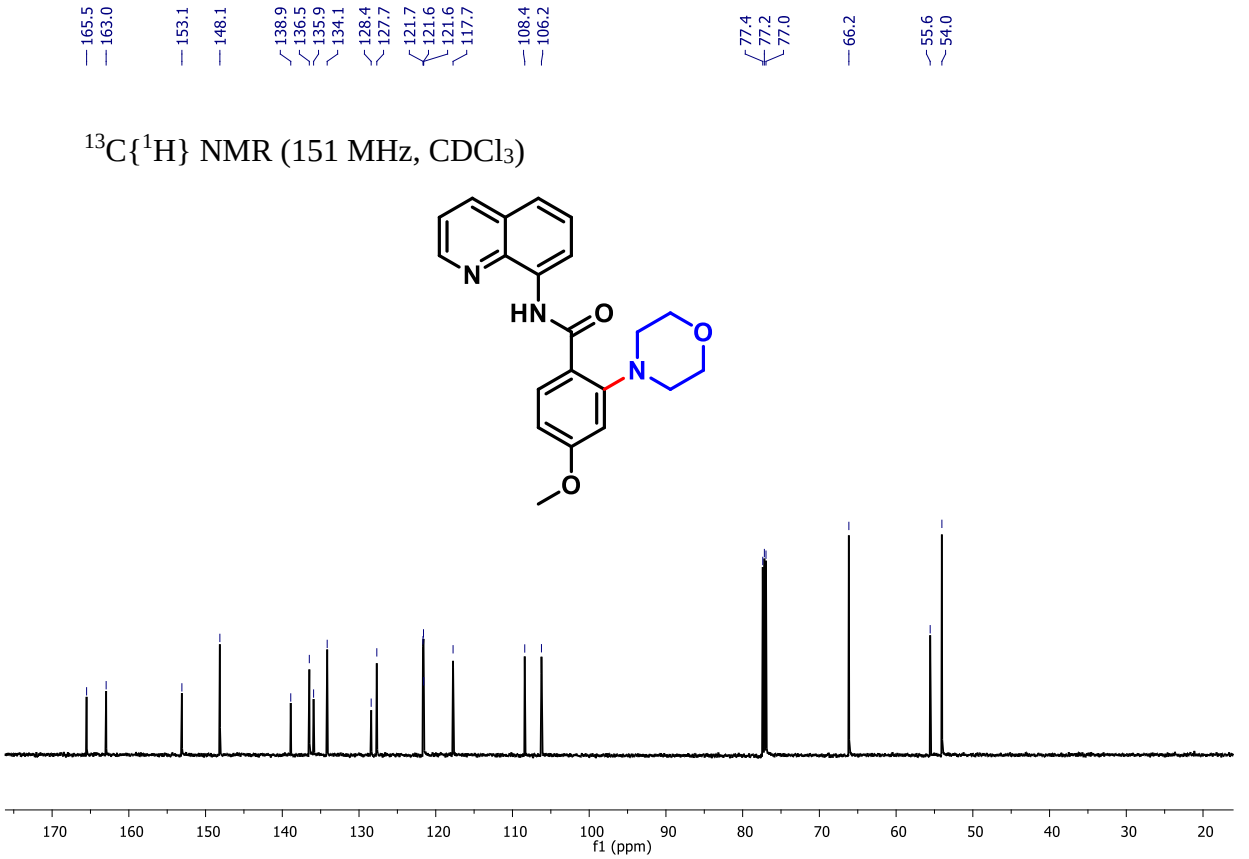

^{13}C{^{1}H} NMR (151 MHz, $CDCl_3$)

2-chloro-6-morpholino-4-nitro-N-(quinolin-8-yl)benzamide (5n):

^{1}H NMR (600 MHz, $CDCl_3$)

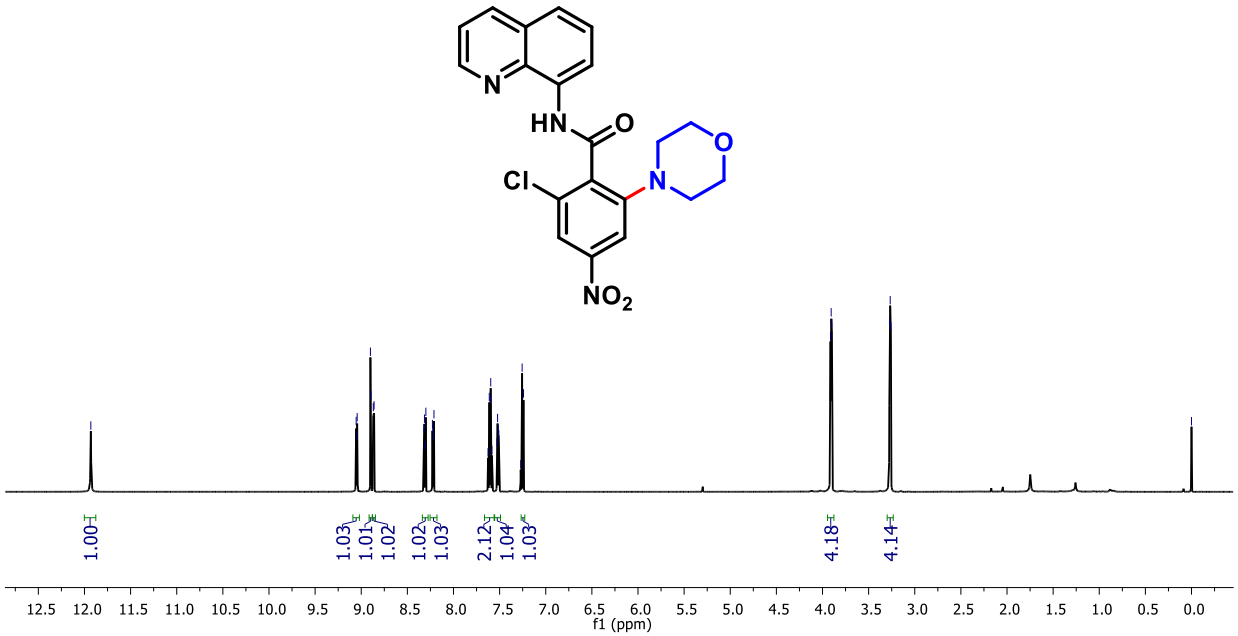

^{13}C{^{1}H} NMR (151 MHz, $CDCl_3$)

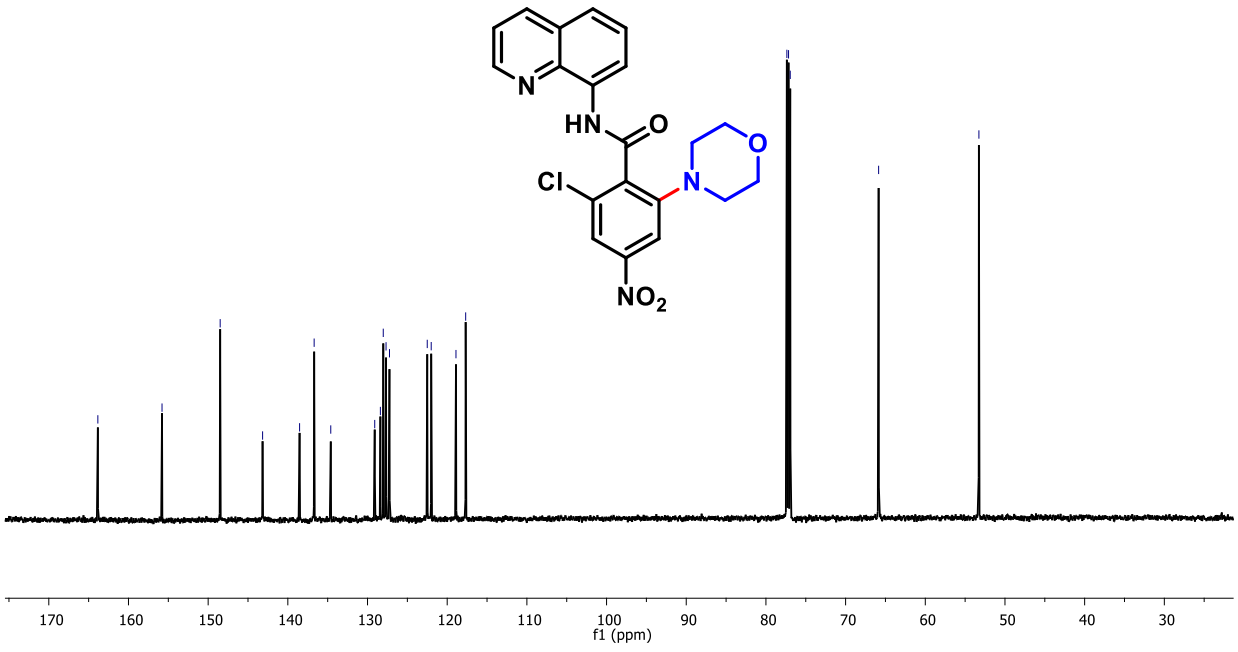

2-Morpholino-N-(quinolin-8-yl)-1-naphthamide (5o):

^{1}H NMR (600 MHz, $CDCl_3$)

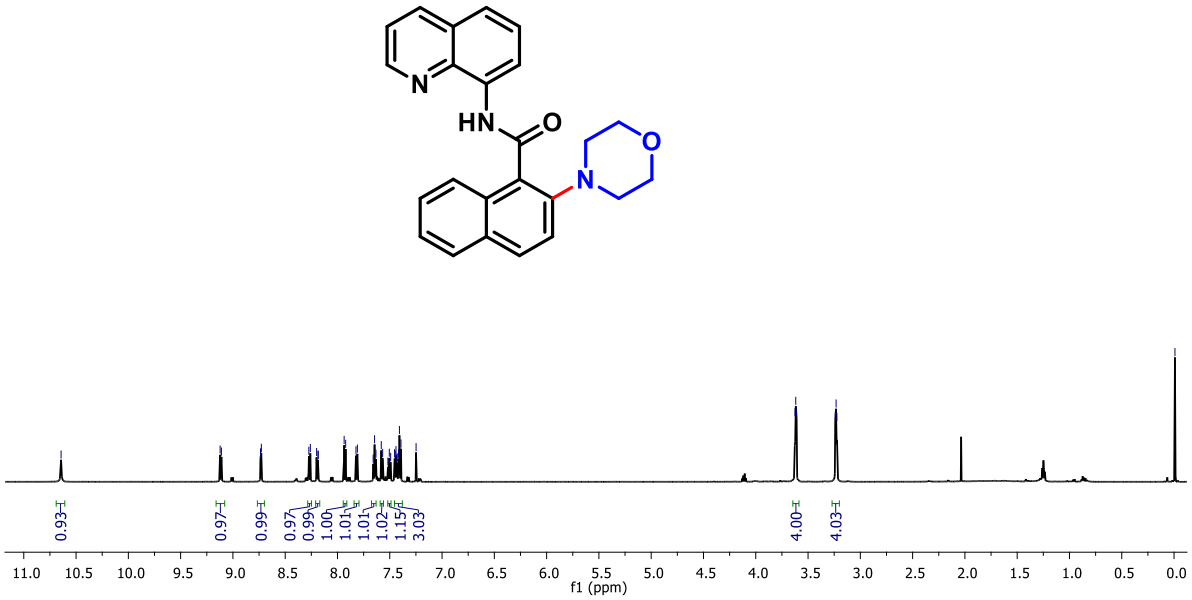

^{13}C{^{1}H} NMR (151 MHz, $CDCl_3$)

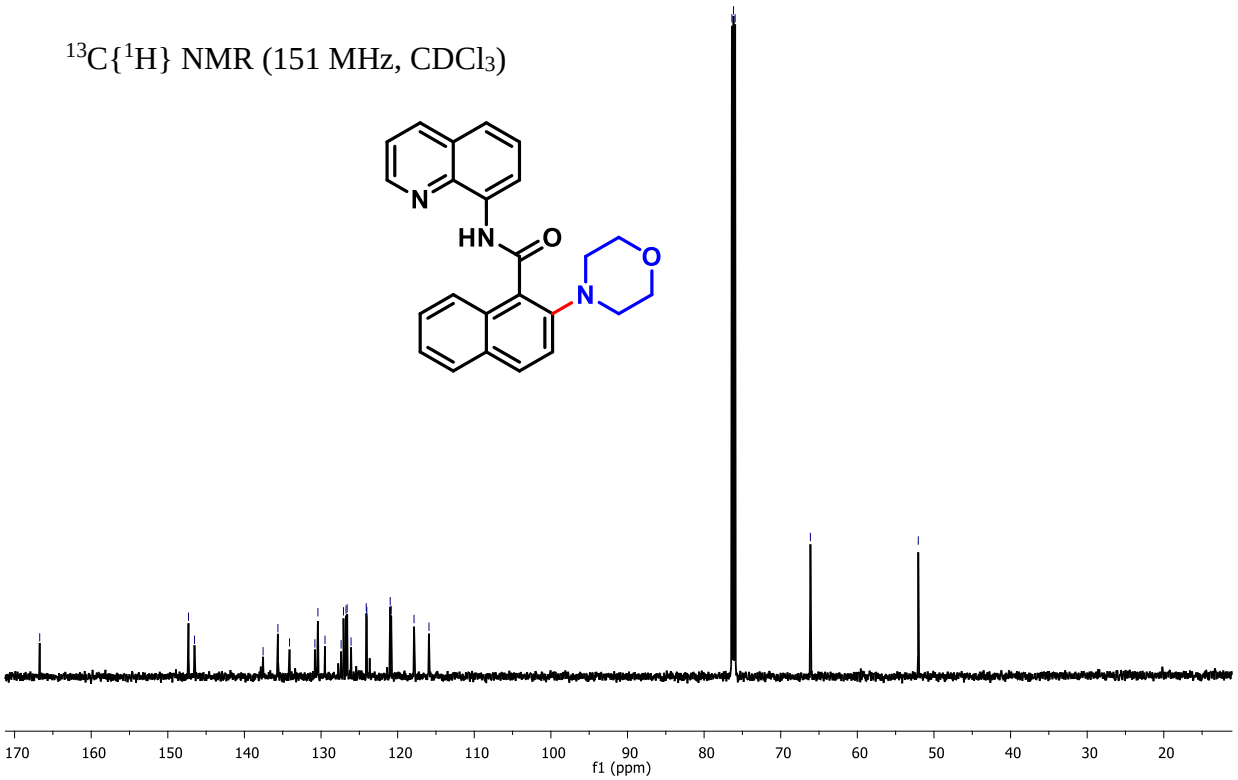

2-thiomorpholino-N-(quinolin-8-yl)naphthamide (5p):

^{1}H NMR (600 MHz, $CDCl_3$)

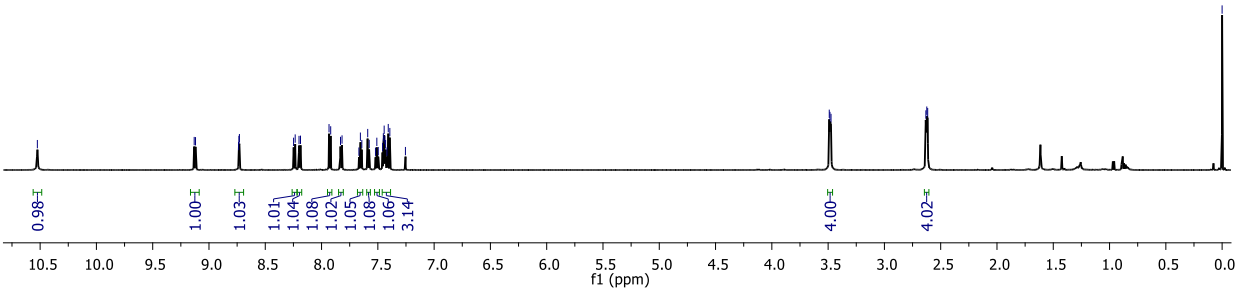

^{13}C{^{1}H} NMR (151 MHz, $CDCl_3$)

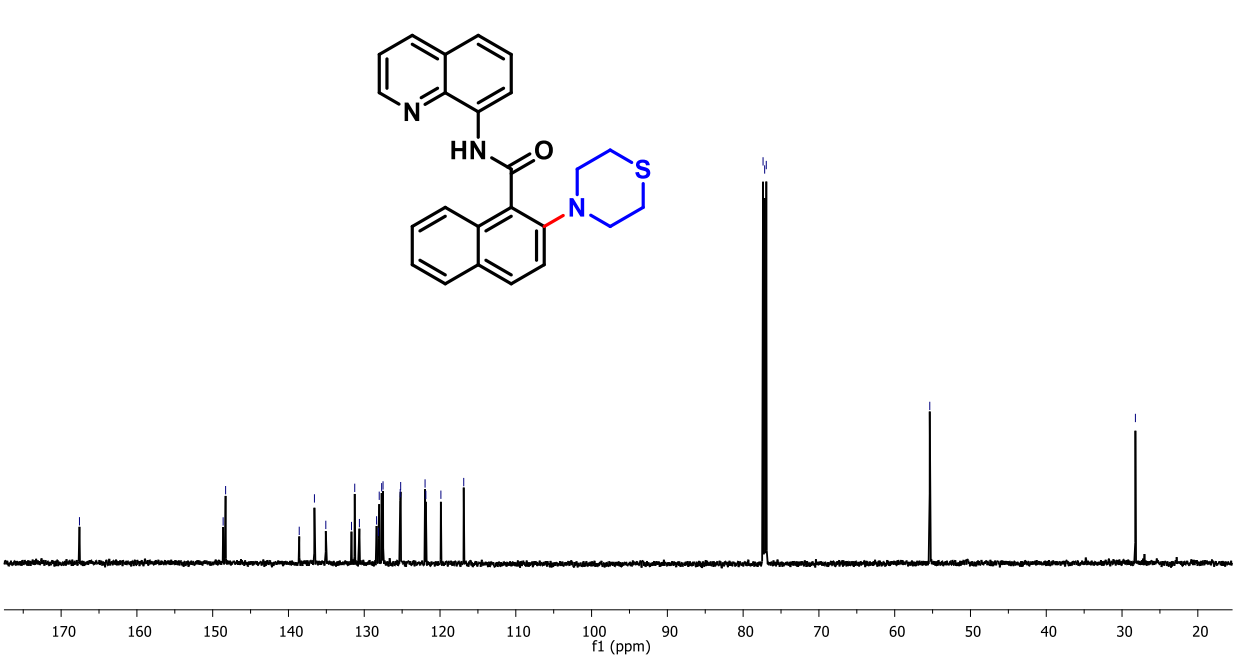

3-(Morpholino)-N-(quinolin-8-yl)thiophenecarboxamide (5q):

^{1}H NMR (500 MHz, $CDCl_3$)

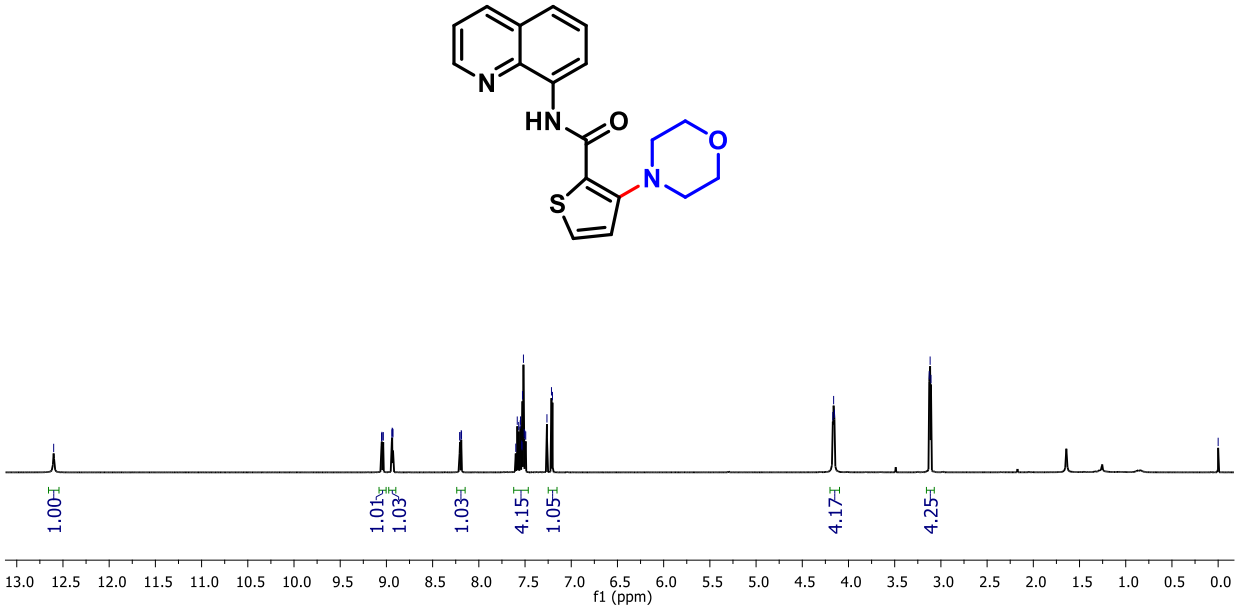

^{13}C{^{1}H} NMR (126 MHz, $CDCl_3$)

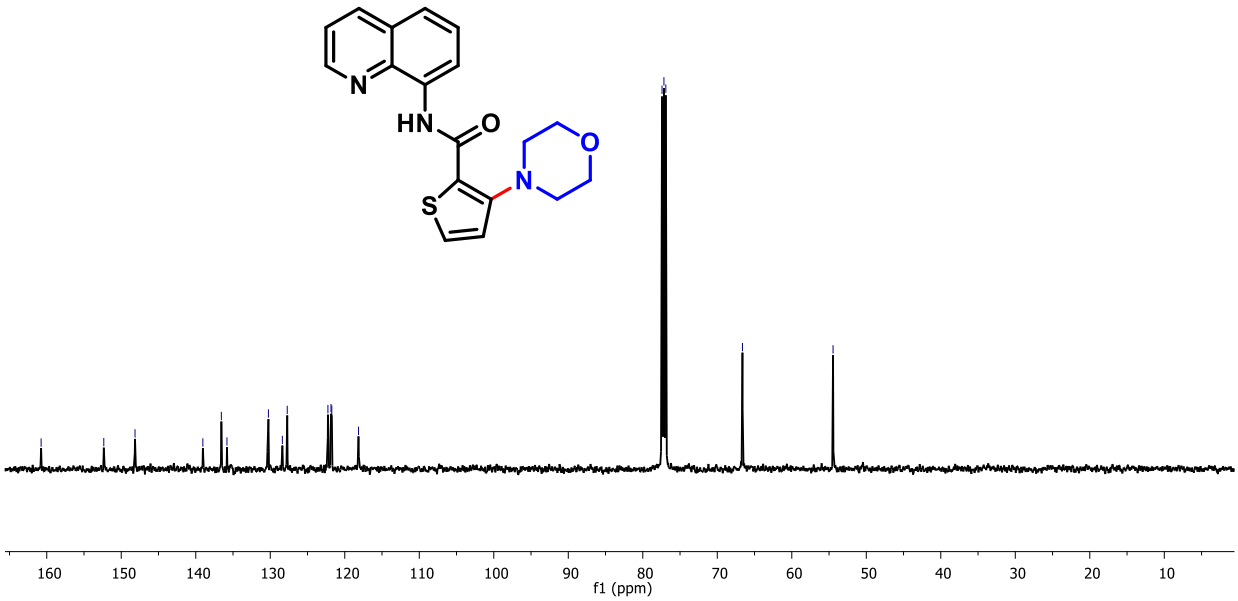

2-(3,4-dihydroisoquinolin-2(1H)-yl)-N-(quinolin-8-yl)benzamide (5r):

^{1}H NMR (600 MHz, $CDCl_3$)

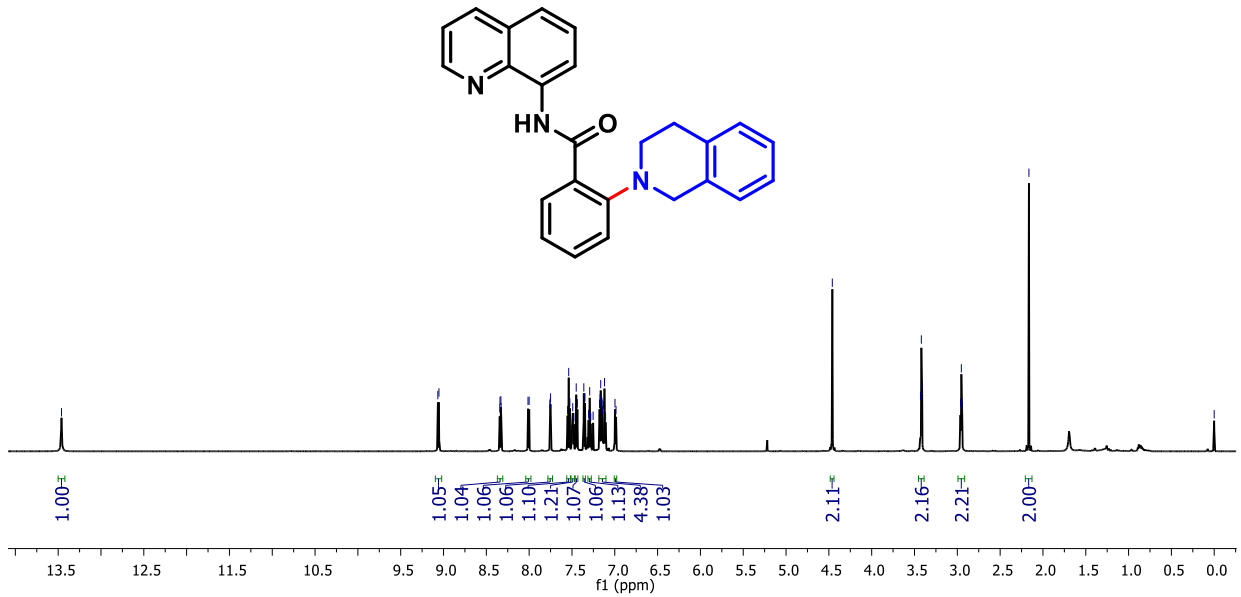

^{13}C{^{1}H} NMR (151 MHz, $CDCl_3$)

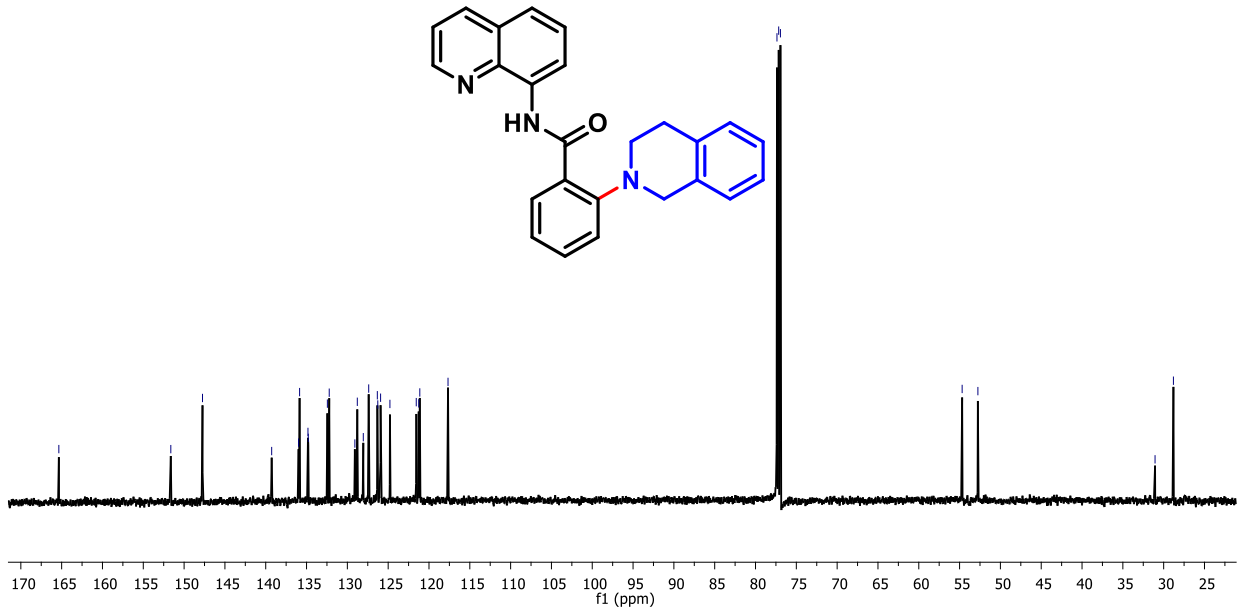

2-(4-methylpiperazin-1-yl)-N-(quinolin-8-yl)benzamide (5s):

^{1}H NMR (600 MHz, $CDCl_3$)

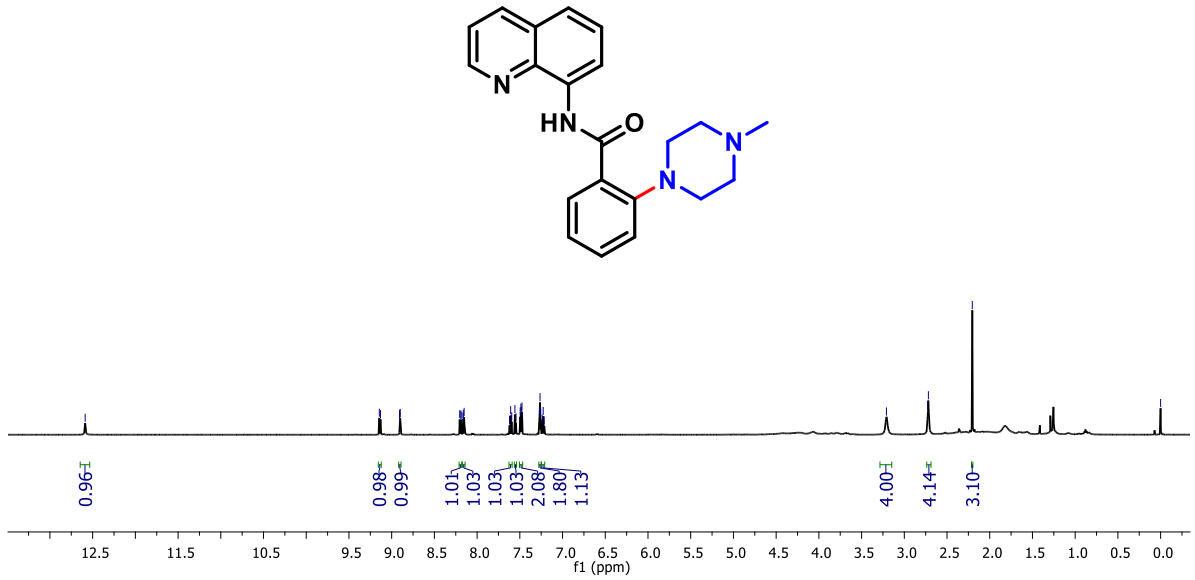

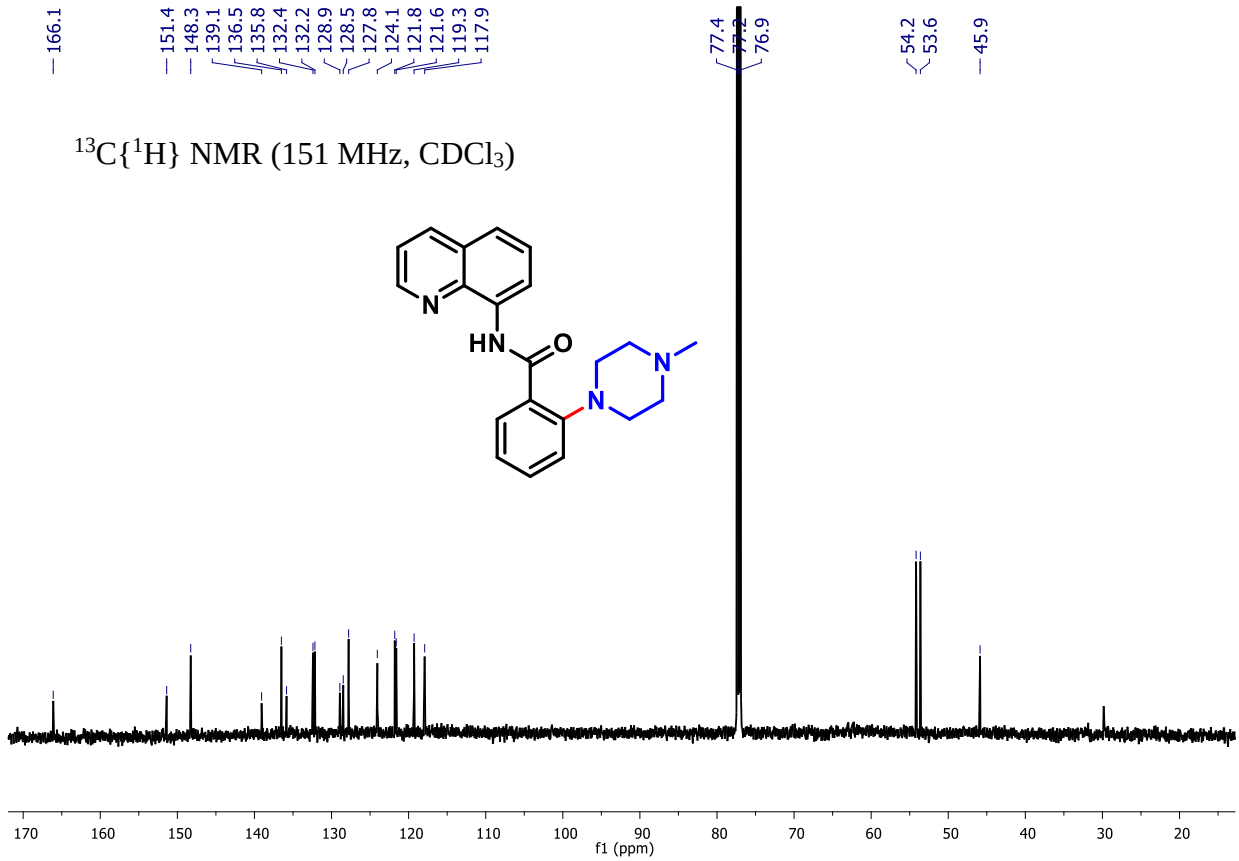

^{13}C{^{1}H} NMR (151 MHz, $CDCl_3$)

2-(benzyl)(methyl)amino-N-(quinolin-8-yl)benzamide (5s):

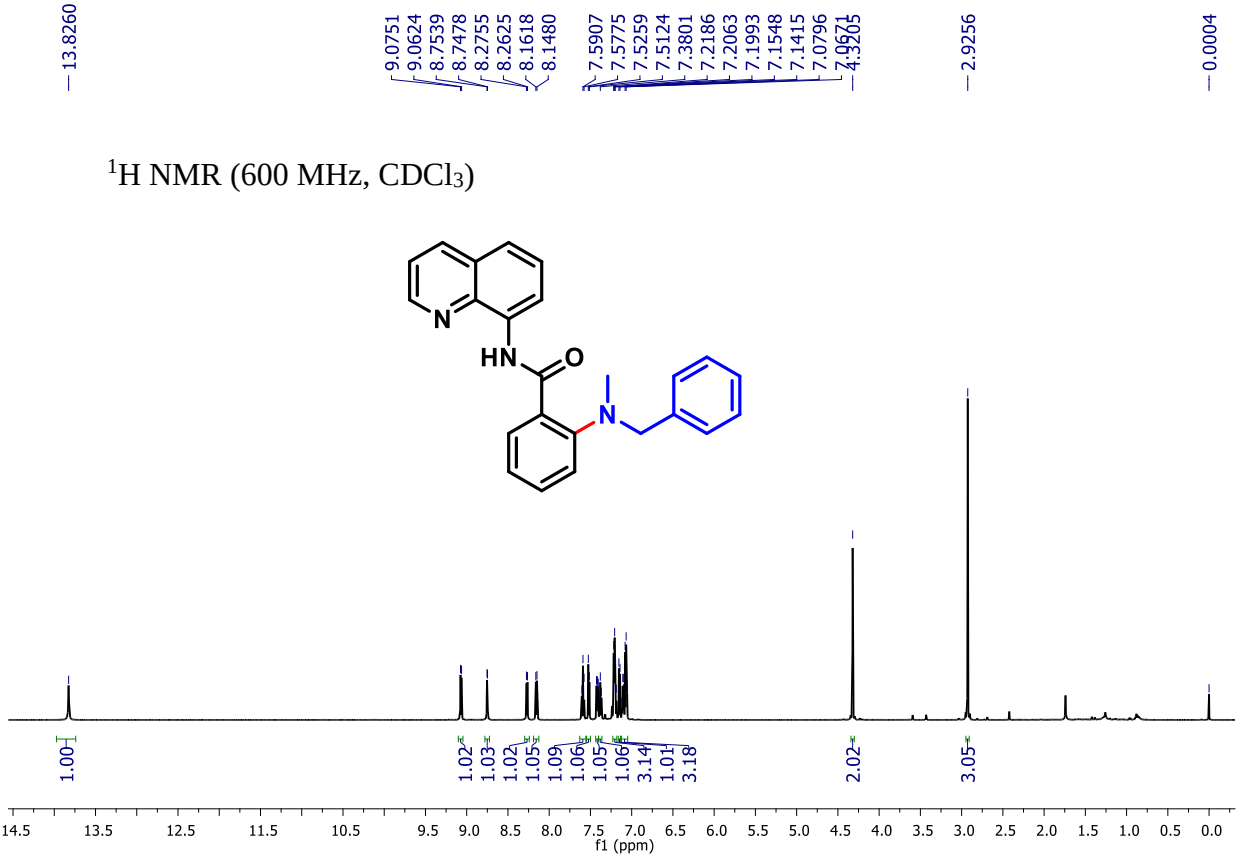

^{1}H NMR (600 MHz, $CDCl_3$)

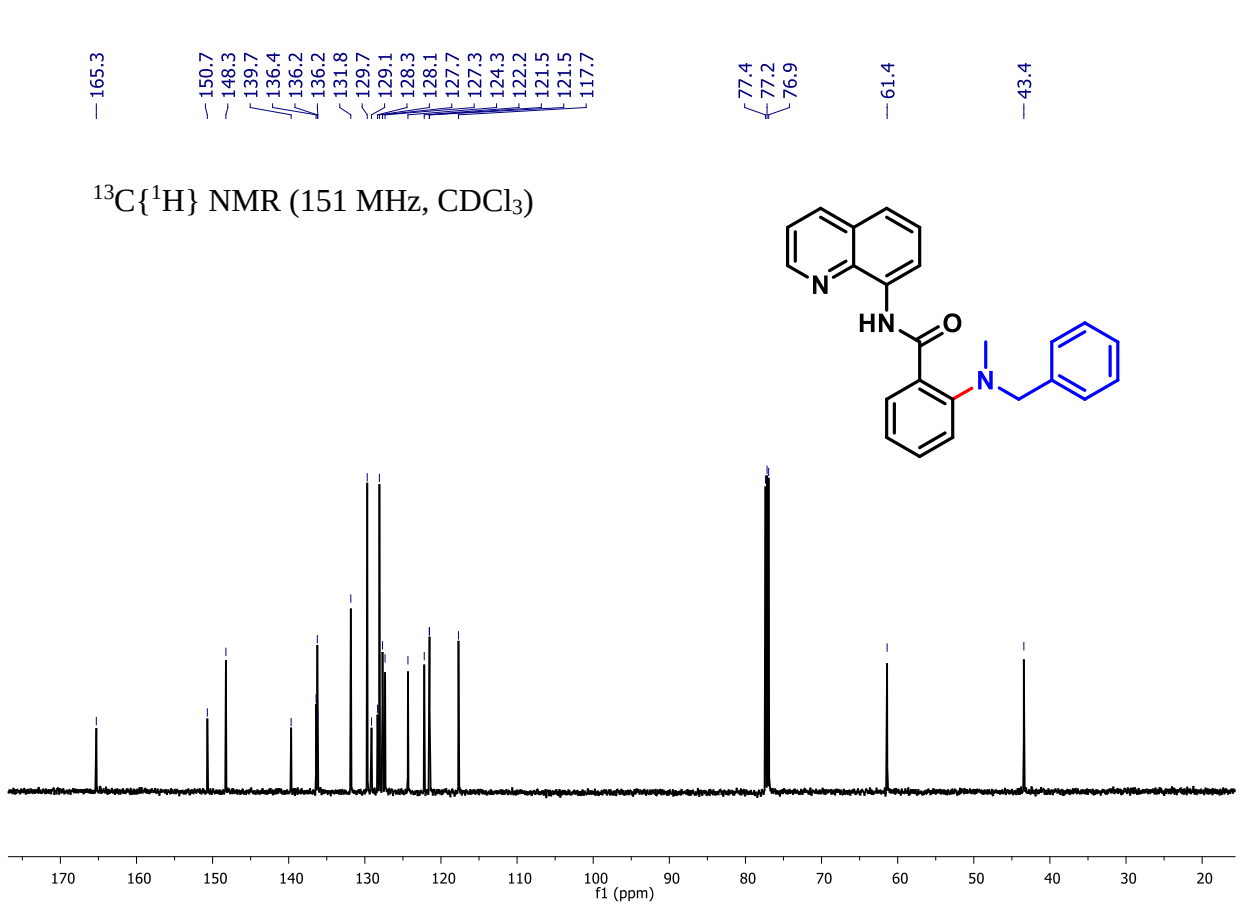

^{13}C{^{1}H} NMR (151 MHz, $CDCl_3$)

4. X-ray crystallographic data: Compound 3r (CCDC – 2034527)

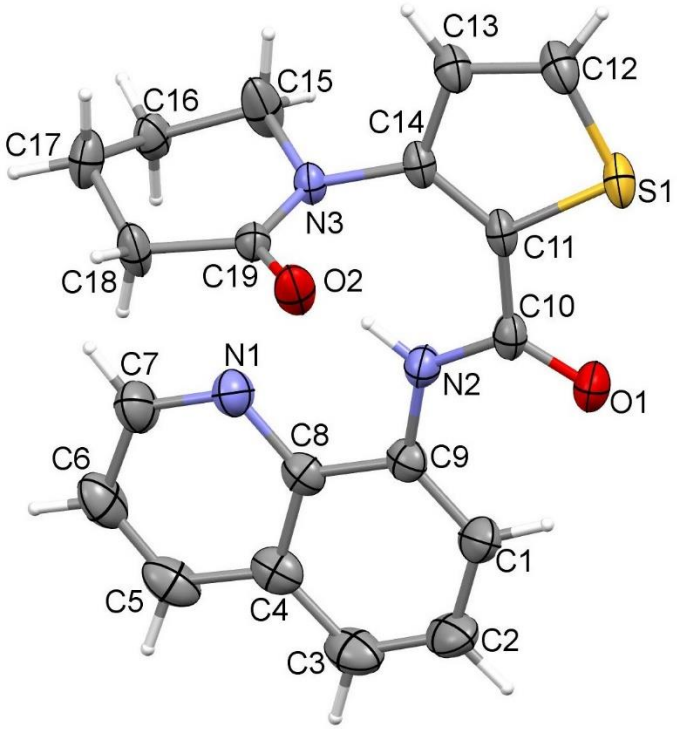

Figure S8. ORTEP diagram of the organic compound **3r** with atom numbering scheme (50% probability factor for the thermal ellipsoids). Crystal growth from mixed solvent ethyl acetate: hexane (50:50).

Table S2: Crystal data and structure refinement for 3r

Identification code	3r
Empirical formula	$C_{19}H_{17}N_3O_2S$
Formula weight	351.41
Temperature/K	180.(2)
Crystal system	orthorhombic
Space group	$P2_12_12_1$
a/Å	5.7640(2)
b/Å	16.4028(5)
c/Å	17.1645(5)
α/°	90
β/°	90
γ/°	90
Volume/Å^3	1622.83(9)
Z	4
ρ_{calc}g/cm^3	1.438
μ/mm^{-1}	0.218
F(000)	736.0
Crystal size/mm^3	0.412 × 0.089 × 0.050
Radiation	MoKα (λ = 0.71073)
2Θ range for data collection/°	4.74 to 61.02
Index ranges	$-8 \leq h \leq 8$, $-23 \leq k \leq 23$, $-24 \leq l \leq 24$
Reflections collected	46779
Independent reflections	4947 [R_{int} = 0.0692, R_{sigma} = 0.0428]
Data/restraints/parameters	4947/0/294
Goodness-of-fit on F^2	1.085
Final R indexes [I>=2σ (I)]	R_1 = 0.0427, wR_2 = 0.0806
Final R indexes [all data]	R_1 = 0.0696, wR_2 = 0.0926
Largest diff. peak/hole / e Å^{-3}	0.21/-0.28
Flack parameter	0.00(3)

X-ray crystallographic data: Compound 5d (CCDC – 2034528)

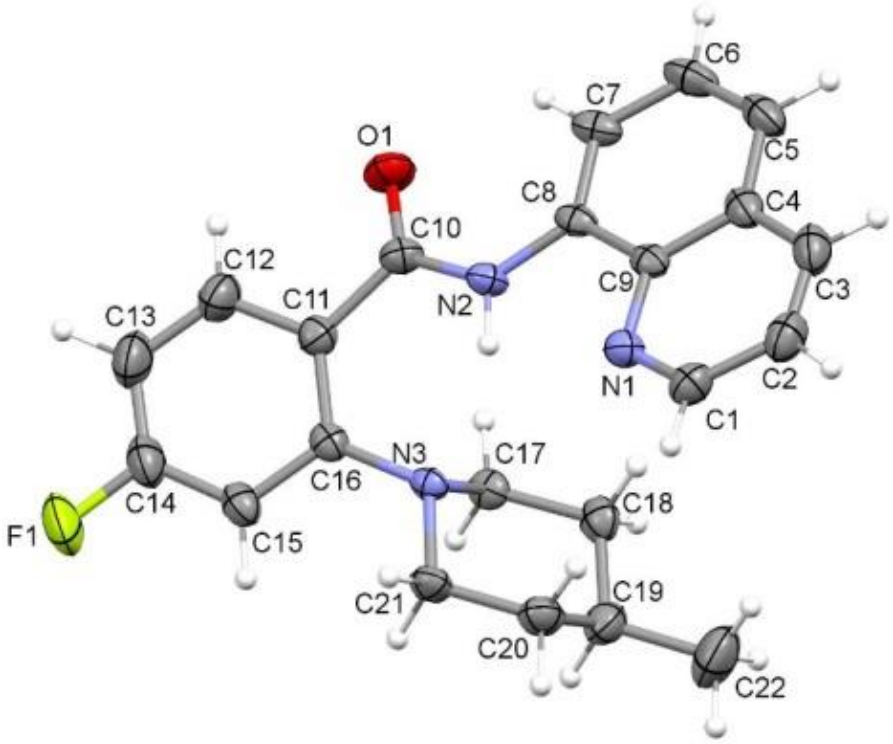

Figure S 9: ORTEP diagram of the organic compound **5d** with atom numbering scheme (50% probability factor for the thermal ellipsoids) Crystal growth from mixed solvent ethyl acetate: hexane (50:50).

Table S3: Crystal data and structure refinement for 5d

Identification code	5d
Empirical formula	$C_{22}H_{22}FN_3O$
Formula weight	363.42
Temperature/K	150.(2)
Crystal system	orthorhombic
Space group	Pbca
a/Å	14.956(3)
b/Å	12.299(3)
c/Å	20.468(4)
α/°	90
β/°	90
γ/°	90
Volume/Å^3	3765.0(13)
Z	8
ρ_{calc}g/cm^3	1.282
μ/mm^{-1}	0.087
F(000)	1536.0
Crystal size/mm^3	0.393 × 0.268 × 0.186
Radiation	MoKα (λ = 0.71073)
2Θ range for data collection/°	4.72 to 70
Index ranges	$-24 \leq h \leq 24$, $-19 \leq k \leq 19$, $-32 \leq l \leq 32$
Reflections collected	56279
Independent reflections	8245 [R_{int} = 0.0772, R_{sigma} = 0.0490]
Data/restraints/parameters	8245/0/332
Goodness-of-fit on F^2	1.038
Final R indexes [I>=2σ (I)]	R_1 = 0.0522, wR_2 = 0.1193
Final R indexes [all data]	R_1 = 0.1111, wR_2 = 0.1571
Largest diff. peak/hole / e Å^{-3}	0.33/-0.21

X-ray crystallographic data: Compound 5i (CCDC – 2034529)

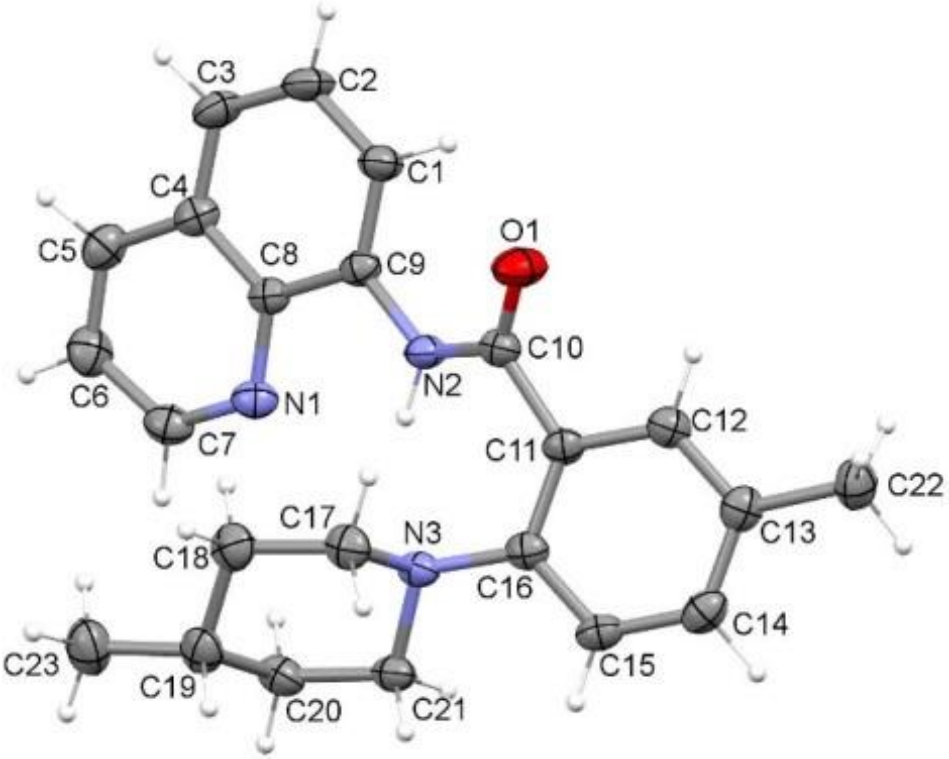

Figure S 10: ORTEP diagram of the organic compound **5i** with atom numbering scheme (50% probability factor for the thermal ellipsoids) Crystal growth from mixed solvent ethyl acetate: hexane (50:50).

Table S4: Crystal data and structure refinement for 5i.

Identification code	5i
Empirical formula	$C_{23}H_{25}N_3O$
Formula weight	359.46
Temperature/K	155.(2)
Crystal system	monoclinic
Space group	$P2_1$
a/Å	8.6945(16)
b/Å	7.7258(14)
c/Å	14.163(3)
α/°	90
β/°	97.573(5)
γ/°	90
Volume/Å^3	943.1(3)
Z	2
ρ_{calc}g/cm^3	1.266
μ/mm^{-1}	0.079
F(000)	384.0
Crystal size/mm^3	0.364 × 0.324 × 0.112
Radiation	MoKα (λ = 0.71073)
2Θ range for data collection/°	4.72 to 63.18
Index ranges	$-12 \leq h \leq 12$, $-11 \leq k \leq 11$, $-20 \leq l \leq 20$
Reflections collected	14071
Independent reflections	6231 [R_{int} = 0.0521, R_{sigma} = 0.0733]
Data/restraints/parameters	6231/1/344
Goodness-of-fit on F^2	1.054
Final R indexes [I>=2σ (I)]	R_1 = 0.0582, wR_2 = 0.1119
Final R indexes [all data]	R_1 = 0.0971, wR_2 = 0.1318
Largest diff. peak/hole / e Å^{-3}	0.23/-0.26
Flack parameter	0.3(10)